



Quantifying sediment sources of floodplain deposits in the lower Oroua River using sediment fingerprinting



August 2018

Horizons Report 2018/EXT/1612



Landcare Research
Manaaki Whenua

Prepared for:

Abby Matthews
Science & Innovation Manager

August 2018
Report No. 2018/EXT/1612
ISBN 978-1-98-853764-1

Prepared by:

Simon Vale
Manaaki Whenua – Landcare Research

Contract Report LC3287

CONTACT	24 hr Freephone 0508 800 800	help@horizons.govt.nz	www.horizons.govt.nz
SERVICE CENTRES	Kairanga Cnr Rongotea and Kairanga-Bunnythorpe Roads Palmerston North Marton Hammond Street	REGIONAL HOUSES	DEPOTS
		Taumarunui 34 Maata Street Palmerston North 11-15 Victoria Avenue Whanganui 181 Guyton Street	Levin 120–122 Hōkio Beach Road Taihape Torere Road Ohotu Woodville 116 Vogel Street
POSTAL ADDRESS	Horizons Regional Council, Private Bag 11025, Manawatū Mail Centre, Palmerston North 4442		F 06 9522 929



Manaaki Whenua
Landcare Research

Quantifying sediment sources of floodplain deposits in the lower Oroua River using sediment fingerprinting

Prepared for: Horizons Regional Council

August 2018



Quantifying sediment sources of floodplain deposits in the lower Oroua River using sediment fingerprinting

Contract Report: LC3287

Simon Vale

Manaaki Whenua – Landcare Research

Reviewed by:

Hugh Smith
Geomorphologist
Manaaki Whenua – Landcare Research

Approved for release by:

Chris Phillips
Portfolio Leader – Managing Land & Water
Manaaki Whenua – Landcare Research

Disclaimer

This report has been prepared by Manaaki Whenua – Landcare Research for Horizons Regional Council. If used by other parties, no warranty or representation is given as to its accuracy and no liability is accepted for loss or damage arising directly or indirectly from reliance on the information in it.

Contents

Summary.....	v
1 Introduction	1
2 Objectives	1
3 Background.....	2
4 Methods	3
4.1 Oroua River Sampling Strategy	3
4.2 Sediment Sample Analysis.....	5
4.3 Statistical Discrimination and Tracer Selection	6
4.4 Multivariate Mixing Model	6
4.5 Synthetic Mixtures	7
4.6 Sediment yield.....	8
5 Results.....	9
5.1 Particle Size Analysis.....	9
5.2 Geochemical Results	12
5.3 Statistical Discrimination and Tracer Selection	16
5.4 Mixing model Performance.....	27
5.5 Quantitative Sediment source contributions	34
6 Conclusion & Recommendations.....	40
7 Acknowledgements.....	41
8 References	42
Appendix 1: Geochemical range plot for size fraction: < 63 μm	45
Appendix 2: Geochemical range plot for size fraction: 125–300 μm	54
Appendix 3: Mineralogy Summary Outputs.....	63

Summary

Project and Client

Sediment source quantification of lower Oroua River floodplain deposition was investigated by Manaaki Whenua – Landcare Research for Horizons Regional Council in 2017/18. This involved an application of the sediment fingerprinting technique, which comprises (1) geochemical analysis and characterization of the main sediment sources in the catchment, (2) statistical discrimination of sources using selected geochemical tracers, and (3) quantitative apportionment of the relative contributions from catchment sources to floodplain sediment deposits.

Objectives

The objectives for the sediment fingerprinting investigation in the Oroua River Catchment were to:

- evaluate the particle size and mineralogy of the sediment sources in the Oroua River catchment
- geochemically characterize the dominant sediment sources in the Oroua River catchment based for two size fractions
- select appropriate tracers to geochemically differentiate sediment sources for quantitative determination of sediment proportions
- quantitatively determine relative proportions of sediment sources contributing to the Overbank deposits in the lower Oroua River catchment.

Results

- The dominant sediment sources contributing to Overbank sediment deposition in the Oroua River catchment for the total particle size distribution (both $<63\ \mu\text{m}$ and $125\text{--}300\ \mu\text{m}$) originates from Hill Subsurface (31–37%) and Unconsolidated sediment sources (26–27%). The remaining proportions comprise Mudstone (9–10%), Mountain Range (9–15%), and Hill Surface (7–8%) sediment sources, with a possible Channel Bank sediment contribution of up to 18%.
- The dominant sediment source for the $<63\text{-}\mu\text{m}$ -size fraction shows Unconsolidated sediment sources (36–41%) and Hill Subsurface (27–34%) are the dominant sources, followed by Mudstone (11–12%), Hill Surface (8–11%), and Mountain Range (3–4%) with Channel Bank possibly contributing up to 12%.
- The dominant sediment source for the $125\text{--}300\text{-}\mu\text{m}$ -size fraction shows Hill Subsurface (37–42%) and Mountain Range (17–32%) as the dominant sediment sources, followed by Unconsolidated (10–12%), Mudstone (10–12%), and Hill Surface (2–8%), with Channel Bank potentially contributing up to 27% to Overbank sediment deposits.
- The specific sediment yield includes lower and upper estimates based on the inclusion and exclusion of Channel Bank from the calculation. The highest specific sediment yield source originates from Unconsolidated ($1928\text{--}2151\ \text{t km}^{-2}\text{yr}^{-1}$) followed by Mudstone ($1131\text{--}1257\ \text{t km}^{-2}\text{yr}^{-1}$), Hill Subsurface ($953\text{--}1138\ \text{t km}^{-2}\text{yr}^{-1}$), and

Mountain Range (589–981 t km⁻² yr⁻¹). Hill Surface (52–60 t km⁻² yr⁻¹) displays a low specific yield due to the large potential spatial area and Channel Bank potentially is responsible for up to 220 t km⁻¹ y⁻¹ by length. This emphasizes that the Unconsolidated sources of sediment provide the greatest specific sediment yield; steep hill terrain also provides a significant total load but over a larger spatial area.

- Particle size analysis showed two distinct sediment size distributions. Mountain Range, Channel Bank, and Unconsolidated sediment exhibited coarser-size fractions evidenced by a D₅₀ range from ≈ 100 to 180 μm. Hill Surface, Mudstone, and Hill Subsurface sediment exhibited finer sediment-size fractions evidenced by D₅₀ values from ≈ 35 to 70 μm.
- The < 63-μm-size fraction represented most of the total particle-size fraction for Hill Surface (63%), Mudstone (63%), Hill Subsurface (52%), and Over Bank (42%), while the 125–300-μm-size fraction represented the larger component of Unconsolidated (31%), Channel Bank (48%), and Mountain Range (33%) sediment sources.
- Testing two different sets of tracers showed that the choice of tracers used in un-mixing sources influences the accuracy of source apportionment results when compared with known synthetic mixture combinations. Moreover, un-mixing performance differed between the < 63- and 125–300-μm-size fractions. The < 63-μm fraction deviation was generally < 5% from the synthetic percentage for both tracer sets and each source, although Channel Bank deviated from 5 to 13%. Removing Channel Bank as a source improved the synthetic mixture testing performance for both models in the < 63-μm-size fraction. The deviations for the 125–300-μm-size fraction were generally around 5–7% difference, while removal of the Channel Bank did not improve the accuracy of un-mixing compared with the synthetic mixtures.

Conclusions and Recommendations

- Sediment sources in the Oroua river catchment can be characterized and differentiated using a range of geochemical tracers. Tracers providing the best discrimination of sediment sources vary between the two size fractions. Reasonable source discrimination can be achieved through combinations of multiple tracers that capture a wide range of geochemical properties across sources.
- The main sediment sources related to land management areas are Hill Subsurface and Hill Surface, which collectively account for 38–45% of the total sediment source contribution. These areas are predominantly associated with steep hill country under agricultural production. Continuation of management initiatives to reduce erosion across this landscape is likely to achieve further reduction in sediment delivery to the lower Oroua.
- Channel Bank sediment sources present a challenge for statistical differentiation from other major sediment sources. This is because in addition to being a contemporary sediment source, banks may also represent historical depositional features comprising source material coming from other primary sediment sources in the catchment.
- Sediment originating from Mountain Range and Mudstone sources account for 18–25% and represent mostly natural erosion. Mountain Range sediment originates from the Ruahine Range under indigenous vegetation, while Mudstone sources primarily occur from lateral erosion of cliffs and incision of mudstone material in the upper Oroua catchment.

- Unconsolidated sediment sources account for 26–29% of the total fine sediment source. This source is typically associated with gully erosion but also delivers sediment through a range of erosion processes. It is evident that, alongside Hill Subsurface, unconsolidated sediment sources are significant in the catchment.

1 Introduction

Horizons Regional Council has a responsibility for maintaining protection from flood events in the Lower Oroua River. This is primarily achieved through levees built adjacent to the channel throughout the Lower Oroua River floodplain. The design of these levees is based on maintaining protection for an assigned flood capacity. Floodplain deposition of sediment between the levees in over-bank deposits compromises the flood capacity that the levees can contain. Characterising and understanding the source of this sediment provides information to better understand the catchment system and guide management activity to minimize sediment deposition in these locations.

Horizons Regional Council contracted Manaaki Whenua Landcare Research to undertake a sediment fingerprinting analysis to understand the proportions of sediment sources contributing to floodplain deposition in the lower Oroua River. To undertake this analysis, sediment sources underwent geochemical characterisation and were statistically discriminated using selected geochemical tracers, and quantitative contributions were determined for catchment sources to floodplain sediment deposits.

2 Objectives

The objectives relating to sediment fingerprinting investigation in the Oroua River Catchment were to:

- evaluate the particle size and mineralogy of the sediment sources in the Oroua River catchment
- geochemically characterize the dominant sediment sources in the Oroua River catchment based on two size fractions
- select appropriate tracers to geochemically differentiate sediment sources for determination of proportional sediment source contributions
- quantitatively determine relative proportions of sediment sources contributing to the Overbank deposits in the lower Oroua River catchment.

3 Background

Sediment fingerprinting provides a means of directly quantifying sediment contributions from sources within river catchments. This relies on several techniques: 1) sediment samples are taken throughout a catchment to represent the sources of sediment erosion in addition to the downstream samples to represent the suspended sediment, sediment deposition or sediment outflow from the catchment; 2) these sources are processed and characterized geochemically to differentiate the sources using a selection of physical properties or tracers; and 3) the sediment source signatures are related to the downstream sediment signature through quantitative mixing models to derive the source contributions.

A considerable range of tracers has been employed in historical sediment fingerprinting research including; mineralogy (e.g. Eberl 2004; Gingele & De Deckker 2005), mineral magnetic signatures (e.g. Caitcheon 1998; Blake et al. 2006; Pulley et al. 2017), bulk geochemical compositions (e.g. Collins et al. 1998; Hardy et al. 2010; Zhang et al. 2012; Collins et al. 2013; Lamba et al. 2015; Vale et al. 2016a), isotopic ratios (e.g. Douglas et al. 1995; Gingele & De Deckker 2005), radionuclides (e.g. Olley et al. 2013; Porto et al. 2013; Wilkinson et al. 2013), organic elements (Fox & Papanicolaou 2008; Evrard et al. 2013), and compound specific isotopes (e.g. Gibbs 2008; Blake et al. 2012; Hancock & Revill 2013).

The current state of sediment fingerprinting research relate to several areas of development and have drawn attention to variations in sediment mixing models (e.g. Haddadchi et al. 2014), tracer selection (e.g. Pulley et al. 2015), source classification and within-source geochemical variability (e.g. Collins et al. 2010). There is an increasing awareness of the need to better understand the relationships between erosion processes and geochemical signatures, and to select tracers that provide a level of redundancy and robustness against un-conservativeness behaviour (Belmont et al. 2014). Model selection used for quantitative determination of proportions has also received attention due to an increasing number of models available combined with increasing optimization parameters. While frequentist models, which rely on minimizing the sum of least squares, have traditionally been the dominant models used, Bayesian modelling is being increasingly used to better account for uncertainties associated with source and sediment mixture variability. The choice of model and optimisation technique can have a significant impact on sediment outputs, thus comparison and careful section is important to provide meaningful results (Haddadchi et al. 2014; Smith & Blake 2014).

4 Methods

4.1 Oroua River Sampling Strategy

The Oroua River drains the western side of the Ruahine Range through a generally south-west direction along ≈ 130 km before joining with the main stem of the Manawatu River ≈ 20 km from the coast. The catchment is sedimentary in geology. The Ruahine Range is dominated by greywacke rock, with widespread deposits of sandstone, loess, gravels, mudstone, and unconsolidated material found within the mid to lower reaches of the catchment. Alluvial deposits are also found near contemporary river channels (Fig. 1).

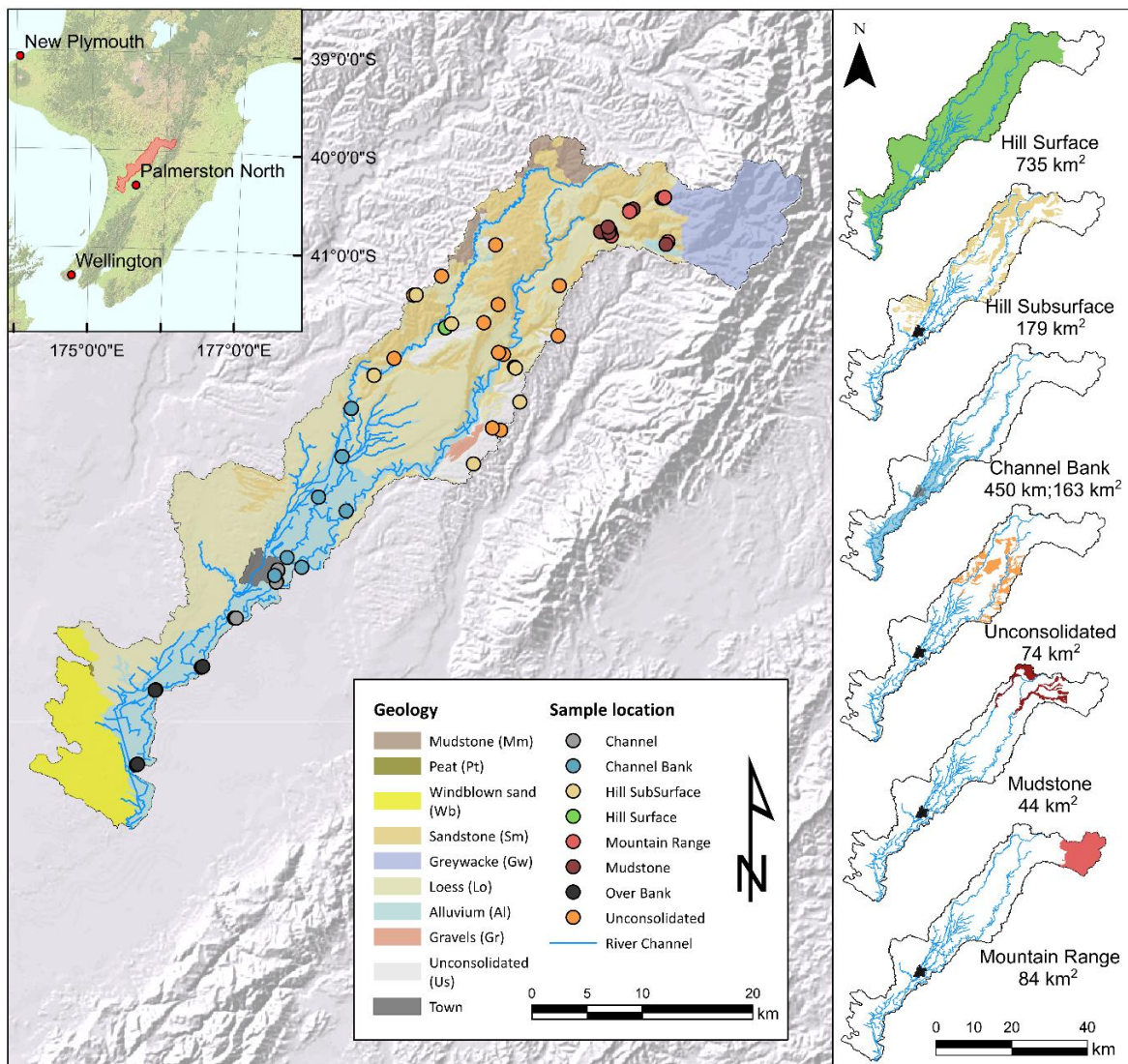


Figure 1. Oroua river catchment location and sediment sampling locations in the Oroua River with geology derived from top rock layer of NZLRI (left). Sediment source spatial extent is evaluated from NZLRI rock layer and manual interpretation of the area (right).

Sediment sampling is intended/designed to characterize the geomorphic units that are likely to have distinct geochemical signatures and can be related to the sediment erosion processes. The sampling comprised of 6 sediment sources with a minimum 8-sample

replication for each source (Table 1). The locations of these samples and the spatial extent of the sediment source groups are outlined in Figure 1. The sediment sink samples were collected from grab samples of Overbank sediment deposits in the lower Oroua River, and within-channel sediment deposits from the mid-Oroua River. In total, 69 initial sediment samples were used for analysis, comprising:

- Sediment source samples; Hillslope surface x 8, Hillslope sub-surface x 13, Channel-bank x 8, Mountain Range x 8, Mudstone sediment x 8, Unconsolidated x 8
- Sediment sink sample; Within-channel sediment x 8, Overbank sediment deposit x 8

Table 1. Sediment source characteristics from the Oroua River catchment

Sediment Source	Characteristic
Mountain Range (MR)	Mountain Range Sediment was sampled from the Ruahine Range to target landslide and debris avalanche material originating from the greywacke dominated terrain.
Mudstone (MS)	Mudstone samples were taken throughout the catchment typically from exposed mudstone cliffs.
Hill Subsurface (HSS)	Hill Subsurface samples were taken from subsurface scrapings of the steeper hill country terrain to represent a proxy for shallow translational landslide material.
Hill Surface (HS)	Hill Surface samples were taken from the upper 4 cm of the steeper hill country terrain to represent surface material originating from the steep slopes.
Unconsolidated (US)	Unconsolidated material was sampled from exposed material to represent gully erosion sources.
Channel Bank (CB)	Samples were collected from scrapes of subsurface sediment from channel banks proximate to active channel erosion and generally represent contemporary floodplain extent.

The spatial extents of the dominant sediment sources are further delineated in Figure 1. These are derived primarily from NZLRI layers in conjunction with the source descriptions in Table 1 to adequately convey the spatial origin of sediment sources. Mudstone and Mountain Range are derived directly from NZLRI rock layers. Unconsolidated was mapped according to NZLRI rock layers and updated in balance with Hill Subsurface. Hill Subsurface was limited to the steep hill terrain, while Hill Surface was expressed across all areas except those within the Ruahine Range and windblown sand. Channel Bank generally represents the area of alluvium from NZLRI, although as the spatial extent of this feature is limited, it is expressed as a length. The spatial extent of each source is: Hill Surface, 735 km²; Hill Subsurface, 179 km²; Mudstone, 44 km²; Unconsolidated, 74 km²; and Mountain Range, 44 km². Alluvial floodplain represents 163 km², while Channel Bank represents a channel length of 450 km.

4.2 Sediment Sample Analysis

4.2.1 Sample Preparation

A sub-sample of sediment was taken to be used for Particle Size Analysis (PSA). The remaining sediment samples were wet sieved to separate and collect two grain size fractions: the < 63- μm - and 125–300- μm -size fractions. These samples were dried at 40°C in plastic trays and subsequently scraped into sample containers for further analysis.

4.2.2 Geochemical Analysis

Bulk geochemical analysis

Samples were weighed into crucibles for XRF analysis and combusted at 850°C overnight to oxidize all elements and combust any organic material. Then 2 g of sample was mixed with 6 g of lithium tetraborate and fused into glass discs.

Geochemical analysis included analysis from two instruments. The glass discs were analysed using a Spectro X-LAB 2000 X-ray Fluorescence Spectrometer for SiO₂, TiO₂, Al₂O₃, Fe₂O₃, MnO, MgO, CaO, Na₂O, K₂O, P₂O₅, BaO, and SrO. The glass discs were retained and analysed using a Perkin-Elmer SCIEX ELAN DRC II Inductively Coupled Plasma-Mass Spectrometer with an attached Laser Ablation unit (LA-ICP-MS). LA-ICP-MS elements analysed included Na, Mg, Al, K, Ca, Sc, Ti, V, Cr, Mn, Fe, Co, Ni, Cu, Ga, Ge, Rb, Sr, Y, Zr, Nb, Cs, Ba, La, Ce, Pr, Nd, Sm, Eu, Gd, Tb, Dy, Ho, Er, Tm, Yb, Lu, Ta, Pb, Th, and U.

Radionuclides

Gamma spectroscopy was used to measure radionuclides, ⁷Be, ²¹⁰Pb, ¹³⁷Cs, ²²⁶Ra, and ²²⁸Ra. The concentration is calculated based on 1-day counts to a value above background at a level of confidence of 95%. The reported uncertainty is based on the combined standard uncertainty (u_c) multiplied by a coverage factor (k) = 2 (providing a level of confidence of 95%) as described by International Organization for Standardization Guide to the expression of uncertainty in measurement, ISO, Geneva (1995). Minimal detectable concentration was reported as a 'less than' where the value was consistent with a background measurement. The minimal detectable concentration with a level of confidence of 95% for both errors of the first and second kind is calculated according to ISO standard 11929 'Determination of the characteristic limits (decision threshold, detection limit and limits of confidence interval) for measurements of ionizing radiation – Fundamentals and application'.

Mineralogy

Mineralogy was analysed through X-Ray Diffraction as a non-destructive analysis using a Philips PW analytical diffractometer. Sediment samples were pressed into a powder mount for XRD analysis and major mineral assemblages reported.

4.3 Statistical Discrimination and Tracer Selection

Two approaches are used to select tracers for sediment source discrimination and subsequent apportionment through quantitative un-mixing:

- 1 The first approach deployed the widely applied method after Collins et al. (1998), which uses a two-step statistical approach for selecting appropriate tracers. First, a Kruskal-Wallis non-parametric test is used to statistically evaluate tracers that show significant differences for individual tracers between two or more source groups. This was carried out for each geochemical concentration relying on a 95% confidence interval or an α level of 0.05 for the critical p-value. Second, a multivariate stepwise Discriminant function analysis (DFA) through minimization of Wilk's lambda is applied to tracers that pass the first test to determine the most suitable subset of variables that can provide discrimination. DFA allows for prediction of group membership based on linear combinations of predictor variables and Wilk's lambda is a measure of the between-group variability to within-group variability, whereby minimizing the value increases between-group distance and reduces within-group distance.
- 2 The second approach selects tracers based on the technique following Smith et al. (2018), by which selected tracers are removed based on evidence of 'non-conservative' behaviour identified through tracer-particle size relationships and source mixing polygons. Source tracer data are plotted pairwise for all tracer combinations and minimum bounding polygons are fitted to these data. If downstream samples fall outside the plotted polygons, then these tracers are removed. Increasing specific surface area (SSA) associated with finer particle sizes can influence the geochemical behaviour of individual tracers, so non-conservative behaviour can also be partially identified if strong correlations exist between SSA and tracer concentration.

4.4 Multivariate Mixing Model

The selected elements were incorporated into multivariate mixing models to estimate the relative proportions of sediment source contributions to the sink sample. Frequentist models have been the traditional models used in sediment source un-mixing. In these models, the relative proportions of each source group are estimated through minimizing the sum of the residuals of the element concentrations through least squares. In this instance, the model selected is the mixing model after Collins et al. (1997), Owens et al. (1999), and Walling et al. (1999) shown in equation 1:

$$R_{es} = \sum_{i=1}^n \left(\frac{C_i - \sum_{j=1}^m X_j \bar{S}_{ij}}{C_i} \right)^2 \quad (1)$$

R_{es} = the sum of squares of the residuals

n = the number elements in the composite fingerprint

C_i = the concentration of element (i) in the sediment sink sample

m = the number of source groups (e.g. mudstone, hill surface, etc.)

X_j = the relative proportion from source group (j) to the sediment sink sample

\bar{S}_{ij} = the mean concentration of element (i) from the sample in source group (j)

The model adheres to two constraints that must be satisfied to produce realistic values. The first constrains each source group proportion to being a positive value between 0 and 1, expressed as:

$$0 \leq P_i \leq 1 \quad (2)$$

The second constrains the sum of all source group contributions to being equal to 1, expressed as:

$$\sum_{i=1}^n P_i = 1 \quad (3)$$

The model uses calculated values based on the mean and standard deviation of each source group to employ a Monte Carlo approach for the desired number of replications.

The optimization of these models was conducted using the solver extension on Microsoft Excel. The solving method employed 'Generalized Reduced Gradient (GRG) Nonlinear' as the solving method. The GRG-Nonlinear method was employed using the multi-start parameter to improve likelihood of a globally optimal solution. The multi-start method automatically runs repeated iterations using different random starting values for the decision variables, thereby providing a selection of locally optimal solutions of which the best can be selected as a likely globally optimal solution (Table 2).

Table 2. Parameters used in the mixing model optimization

Parameters	Mixing Model
Method	GRG nonlinear
Auto-scaling	Yes
Constraint Precision	0.01
Differencing	Central
Multi-start	Yes
Population size	200
Convergence	0.01
Random Seed	Yes
Iterations	5000

4.5 Synthetic Mixtures

The synthetic mixtures were used to assess the ability of the models to predict sediment source proportions for each of the models. Synthetic mixtures were created by generating random proportions of each source, and deriving calculated tracer values based on known proportions of each tracer value for the respective source groups. A Monte Carlo approach was used to derive 1000 tracer values for each synthetic mixture proportion and solved for each mixture to account for uncertainty.

Table 3. Synthetic mixture percentages used for each size fractions of 6-source and 5-source scenarios

Sediment Source	% of synthetic mixture								
	< 63- μm fraction				125–300- μm fraction				
	Mix 1	Mix 2	Mix 3	Mix 4	Mix 5	Mix 6	Mix 7	Mix 8	
6-source	Hill Surface	10	10	45	16	13	11	22	2
	Unconsolidated	13	12	9	20	14	12	22	12
	Mudstone	29	23	11	20	13	27	0	14
	Channel Bank	2	11	8	7	24	23	22	36
	Mountain Range	26	21	2	19	20	23	9	15
	Hill Subsurface	19	23	26	18	16	5	25	22
5-source	Hill Surface	10	11	48	17	17	14	28	3
	Unconsolidated	13	13	10	22	18	15	28	18
	Mudstone	30	26	12	22	17	35	0	22
	Mountain Range	27	24	2	20	26	29	12	23
	Hill Subsurface	20	26	28	19	21	6	32	34

4.6 Sediment yield

To derive the distribution of sediment yield throughout the catchment, the sediment source proportions are distributed according to each sediment source spatial area. Since there is no measured load for the total catchment, the total sediment yield for the catchment relied on the modelled SedNetNZ yield for the Oroua River catchment of 550,000 t yr⁻¹ (Dymond et al. 2014). This value was allocated according to the sediment fingerprinting source proportions, distributed across their respective spatial extents (Fig. 1) and then combined to express specific sediment yield patterns across the Oroua river catchment.

5 Results

5.1 Particle Size Analysis

Particle size analysis showed two distinct particle-size distributions. Coarser particle-size ranges were exhibited by Mountain Range, Channel Bank, and Unconsolidated sediment, while finer particle sizes were observed for Hill Surface, Mudstone, and Hill Subsurface. The coarser particle size exhibited D_{50} values from ≈ 100 to $180 \mu\text{m}$, while finer sources exhibited D_{50} values from ≈ 35 to $70 \mu\text{m}$ (Table 4).

Channel and Overbank sediment were more closely aligned to the coarser sediment samples, although Overbank sediment was somewhat finer than the Channel sediment. Channel sediment was lacking in fine sediment, likely being washed through the channel. Mountain Range displayed considerable variation in grain size between individual samples as evidenced by the standard error of the mean (Table 4). The distribution of the particle sizes was slightly skewed, possibly due to the loss of finer sediment during sample collection and processing, but also due to uncertainty associated with laser analysis (Fig. 2). Either way, it does not present a significant problem for the geochemical analysis since it is only the extreme fine sediment component.

Specific Surface Area increases with decreasing particle size, and commensurately Hill Surface sediment exhibits the greatest specific surface area ($1,017 \text{ m}^2/\text{kg}$), followed by Hill Subsurface ($659 \text{ m}^2/\text{kg}$), and Mudstone ($502 \text{ m}^2/\text{kg}$), while the remaining sediment sources exhibit lower specific surface areas $\approx 100 - 250 \text{ m}^2/\text{kg}$ (Table 4).

Table 4. Main particle size statistics for each of the sediment sources sampled

Source	D10		D50		D90		Specific Surface Area (m^2/kg)
	Mean	SE	Mean	SE	Mean	SE	Mean
Hill Surface	1.5	0.2	35.3	6.4	215.4	21.0	1017
Unconsolidated	34.3	7.3	99.9	12.0	199.4	24.2	121
Mudstone	2.7	0.5	38.8	6.1	146.8	9.7	502
Channel Bank	36.0	5.8	133.5	5.4	267.5	11.3	170
Mountain Range	34.2	11.0	179.0	50.4	508.5	148.9	164
Hill Subsurface	2.5	0.2	67.1	7.6	244.2	23.7	659
Channel	51.4	7.4	143.2	13.0	276.0	23.4	110
Over Bank	16.8	3.8	81.3	11.0	194.1	16.9	226

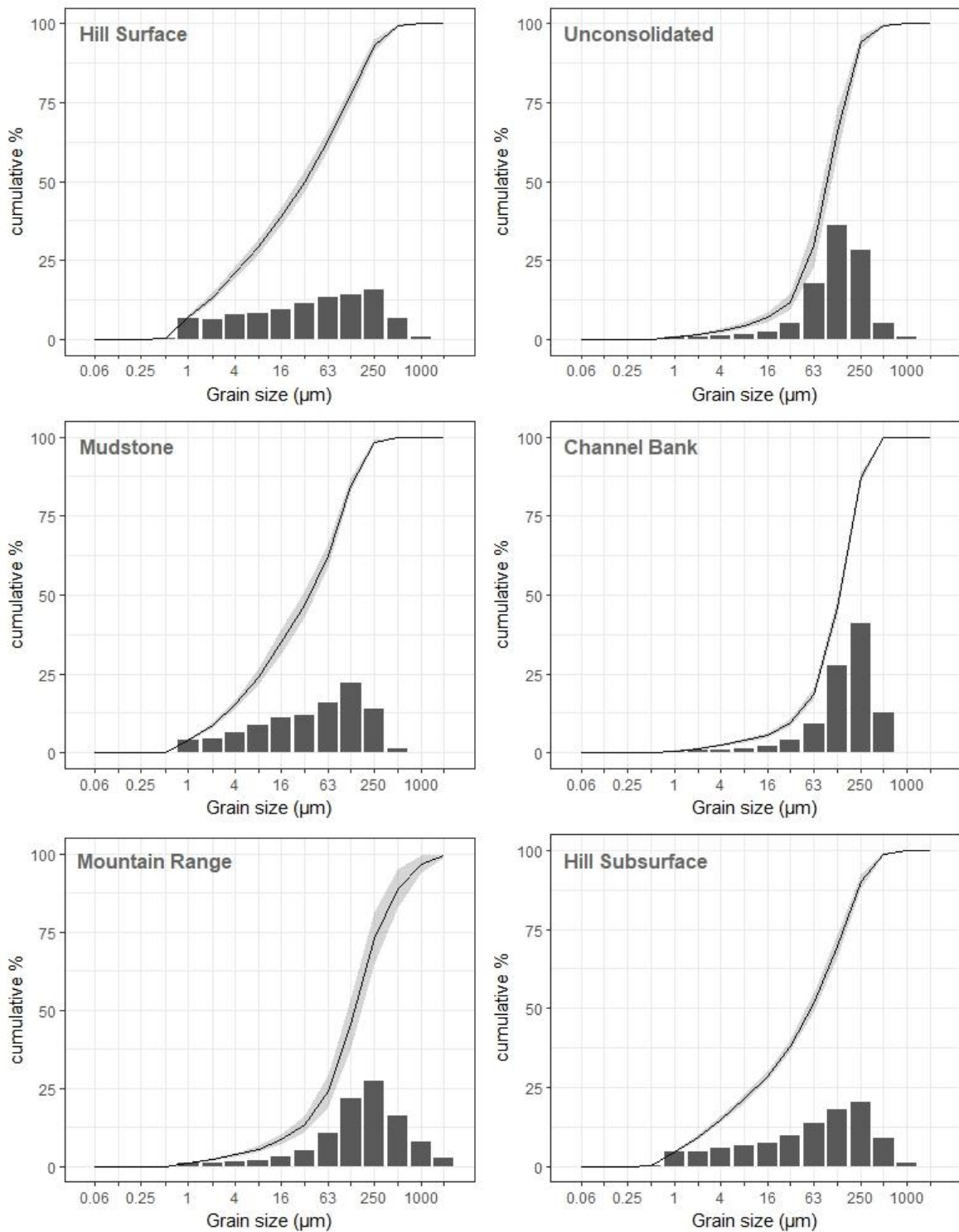


Figure 2. Grain size plots showing cumulative % (line) with standard error (shaded), and frequency (bar) of the sediment sources.

The particle-size fractions selected for geochemical analysis represent the majority of sediment from all sediment sources, with 57% at the lower end of representation and 82% at the higher end (Fig. 3). The < 63-μm-sediment-size fractions represent 52–64% of the sediment for Hill Surface, Hill Subsurface, and Mudstone sources, but only 20–30% for Channel Bank, Mountain Range, and Unconsolidated sources. The trend was reversed for the coarser sediment fraction: 125–300 μm represented 30–50% of Unconsolidated,

Mountain Range and Channel Bank, but represented only 15–25 % of Mudstone, Hill Surface, and Hill Subsurface sediment. Overbank sediment was represented more by the < 63- μm sediment size, while Channel sediment was better represented by the 125–300- μm fraction (Table 5).

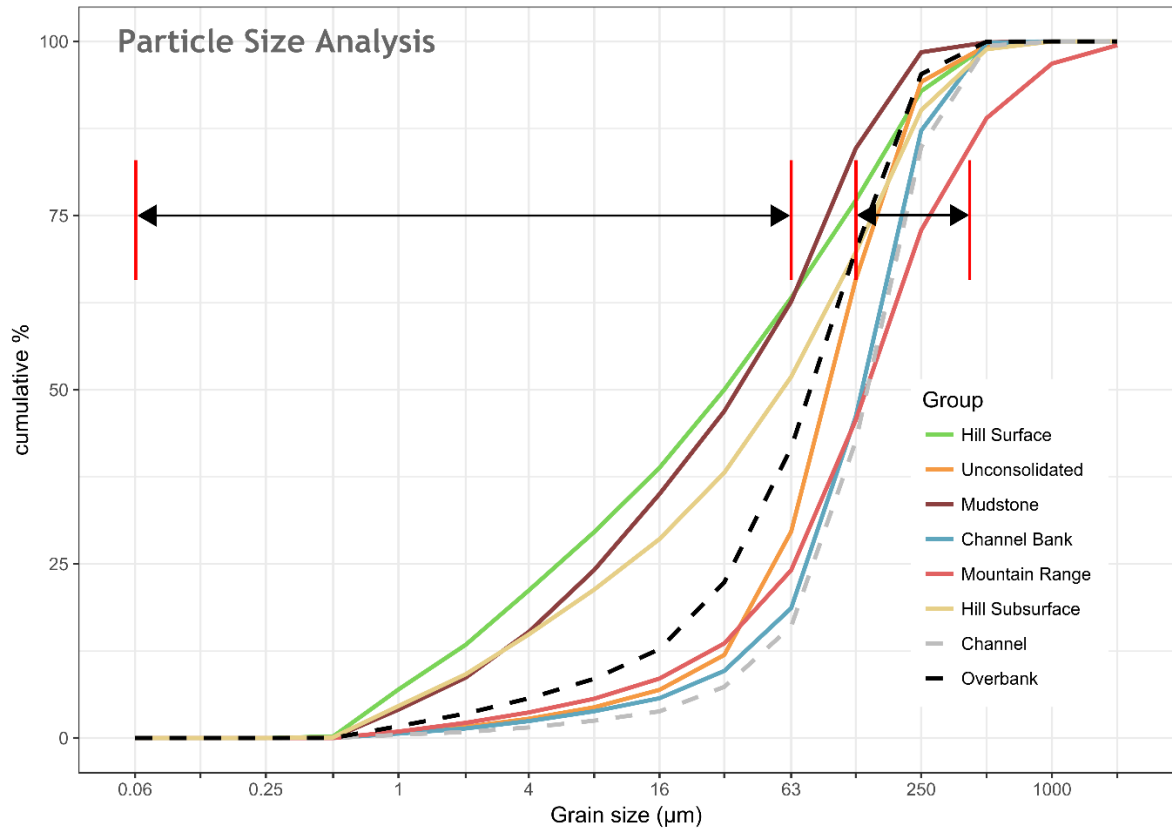


Figure 3. Grainsize of each sediment source and downstream deposits shown as a cumulative % with indication of the two grain size fractions.

Table 5. Grainsize % captured by each of the two grainsize fractions for each of the sediment sources

Sediment Group	Particle Size		Total
	< 63 μm	125–300 μm	
Hill Surface	63.1	18.6	81.8
Unconsolidated	29.6	31.1	60.8
Mudstone	62.7	14.7	77.4
Channel Bank	18.6	47.5	66.2
Mountain Range	24.1	32.7	56.8
Hill Subsurface	51.9	24.0	75.9
Channel	16.0	49.3	65.3
Over Bank	41.7	28.2	69.8

5.2 Geochemical Results

The geochemical results exhibit varying levels of differentiation between sources based on individual tracers for both size fractions analysed. Spider plots of trace and rare earth element geochemistry for both sediment size fractions are shown in Figure 4–7. Tracer values are reported for each individual tracer as a range plot based on source group, showing mean, upper, and lower values in Figures 23–40 (Appendices 1 and 2). These Figures also display Overbank sediment values overlaid on each plot to show the relationship with sources, which is shown for both sediment-size fractions.

The < 63- μm fraction displays the highest SiO_2 concentrations in Channel Bank, Hill Subsurface, and Unconsolidated. Al_2O_3 , TiO_2 , Fe_2O_3 , and MgO display higher concentrations for Hill Surface, Mountain Range, and Unconsolidated, while MnO and P_2O_5 show the highest concentrations in Hill Surface (Appendix 1). Trace elements and Rare Earth Elements (REEs) display higher concentrations in Mountain Range, Mudstone and Unconsolidated sources, and lower concentrations in the Hill Subsurface and Hill Surface sediments due to the effects of weathering (Figs 4 & 5). This is consistent with other studies (e.g. Vale et al. 2016a) where comparatively lower trace element concentrations are observed in Hill Surface and Hill Subsurface due to weathering, compared with less weather sediment sources. Concentrations of Large-Ion Lithophile (LIL) elements, Rb, Cs, K_2O , and Ba, are lowest in Hill Surface and Hill Subsurface sediments, and highest in the Mountain Range sediment. The High Field Strength Element (HFSE), Zr, is highest in the Unconsolidated, Channel Bank and Mudstone, while the remaining HFSE elements (Ta, U, Nb, and Y) are highest in the Mountain Range and Mudstone sediment with the exception of Y, which is highest in Unconsolidated. REE concentrations show light REE enrichment relative to heavy REE with Mountain Range, Unconsolidated, and Mudstone possessing higher concentrations than Hill Surface and Hill Subsurface. Unconsolidated sediment sources tend to have the highest concentrations of heavy REEs, whereas Mountain Range has the highest concentrations of lightest REEs (Fig. 5).

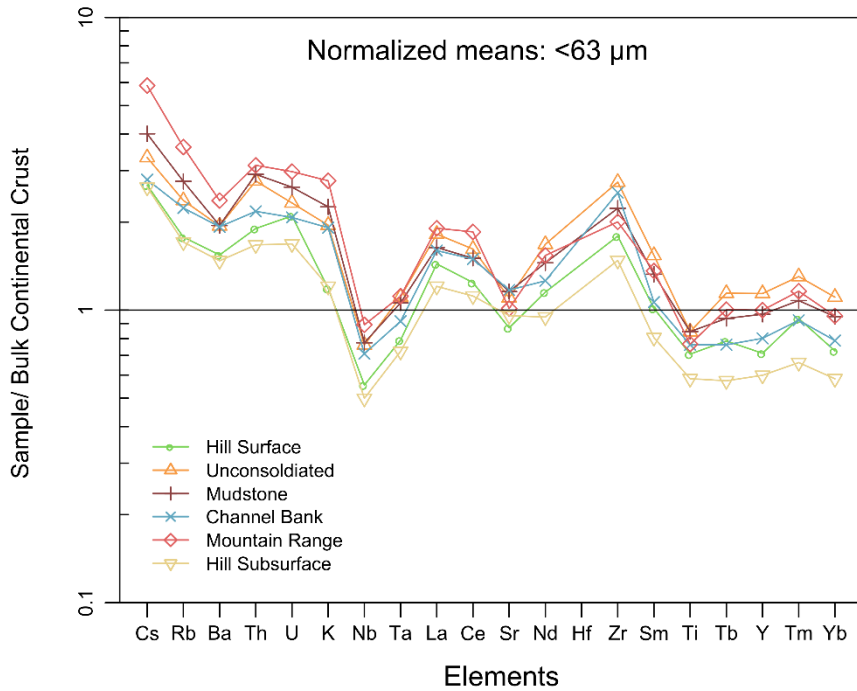


Figure 4. Normalized multi-element plot for <63- μ m-size fraction. Mobile elements are plotted to the left, while more immobile elements are plotted to the right. Normalized against Bulk Continental Crust after Taylor and McLennan (1995).

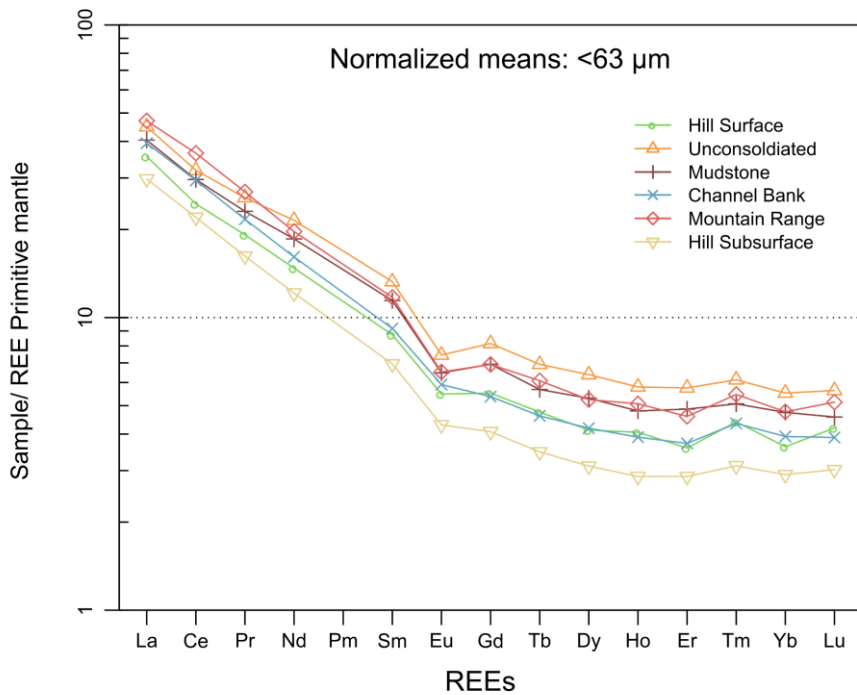


Figure 5. Normalized REE plot for <63- μ m-size fraction. Normalized against McDonough and Sun (1995).

The 125–300- μm fractions show much more variation, with the highest SiO_2 concentrations in Channel Bank, Hill Surface, Mountain Range, and a wide range for Unconsolidated. Al_2O_3 shows highest values in Hill Subsurface; TiO_2 , and Fe_2O_3 display highest concentrations for Hill Subsurface and Unconsolidated; MgO and CaO display highest values in Mudstone, K_2O highest in Mountain Range and Mudstone; and P_2O_5 displays highest in Hill Surface and Unconsolidated (Appendix 2). Similar to the < 63- μm -size fraction, trace elements and REEs display higher concentrations in Unconsolidated, Mountain Range, and Mudstone sources, and lower concentrations in the Hill Subsurface and Hill Surface sediments due to the effects of weathering (Figs 6 & 7). Concentrations of Large-Ion Lithophile (LIL) elements, Rb, Cs, K_2O , and Ba, are lowest in Hill Surface and Hill Subsurface sediments and highest in the Mountain Range sediment. High Field Strength Element (HFSE), Hf & Zr, are highest in the Unconsolidated, Channel Bank, and Mountain. Channel Bank shows particularly high values of Zr, which is likely associated with highly resistant zircon mineral enrichment as reported by Vale et al. (2016b). The remaining HFSE elements (Ta, U, Nb and Y) are highest in the Unconsolidated, Mudstone, and Mountain Range sediment (Fig. 6). REE concentrations show light REE enrichment relative to heavy REE with Unconsolidated, followed by Mountain Range and Mudstone, which possess higher concentrations than Hill Surface and Hill Subsurface. Unconsolidated tends to have the highest concentrations of light REEs, while Mudstone light REE concentrations increase for some of the heavier REEs (Fig. 7).

Radionuclide results for the < 63- μm -size fraction showed the highest values for ^{137}Cs in Hill Surface sediment, while ^{226}Ra and ^{228}Ra showed the highest values in Mountain Range, Mudstone, and Unconsolidated sediment. The same three sources, with the addition of Hill Surface, also had the highest ^{210}Pb values, while Channel Bank had the lowest values of ^7Be (Appendix 1). The 125–300- μm -size fraction showed similar patterns with respect to ^{137}Cs and Hill Surface, whereas ^7Be showed the highest concentrations in Mountain Range and Channel Bank; although the ^7Be results may be unreliable due to detection limits and time between sample collection and analysis. ^{226}Ra and ^{228}Ra showed the lowest values for Hill Surface sediment, with Hill Subsurface showing low values of ^{226}Ra but not ^{228}Ra . Hill Subsurface possessed the lowest values of ^{210}Pb (Appendix 2).

The mineralogy analysis gave an indication of some of the major mineral assemblages but did not provide much beneficial information regarding the nature of the geochemistry observed in the sediment sources. The XRD outputs are reported in Appendix 3. As expected, Silicon Oxide in the form of quartz was the major mineral identified in all samples. Plagioclase minerals such as Albite and Andesine (Sodium Aluminium Silicate or Albite) were identified, along with minerals of the chlorite and muscovite groups. Glauconite (Potassium Sodium Iron Aluminium Magnesium Silicate Hydroxide), which is related to marine depositional environments, was identified in Mudstone samples. A considerable amount of further analysis could be undertaken on the XRD outputs to resolve further mineral assemblages; however, this would be beyond the scope of these sediment fingerprinting objectives.

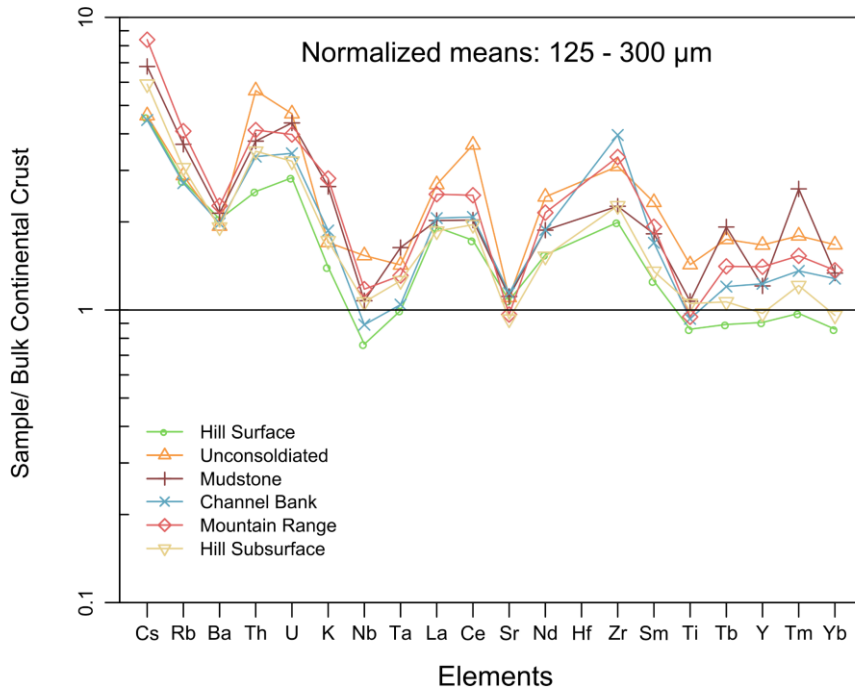


Figure 6. Normalized multi-element plot for 125–300-µm-size fraction. Mobile elements are plotted to the left, while more immobile elements are plotted to the right. Normalized against Bulk Continental Crust after Taylor and McLennan (1995).

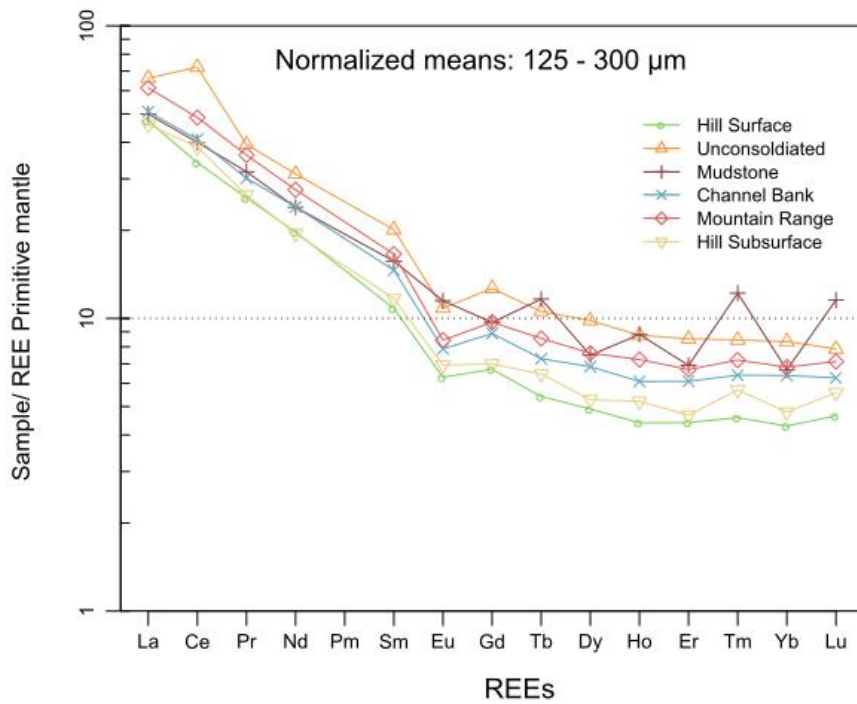


Figure 7. Normalized REE plot for 125–300-µm-size fraction. Normalized against McDonough and Sun (1995).

5.3 Statistical Discrimination and Tracer Selection

5.3.1 Model 1: Size fraction < 63 µm

Unsuccessful tracers in the Kruskal-Wallis test were TiO₂ and ¹³⁷Cs (Table 6). It is not geochemically clear why these two specific tracers do not pass the test; however, the large number of successful elements likely reflects the relatively large number of sediment sources. In combination with well-defined geochemical sediment sources at several of the sources, this increases the likelihood of distinct geochemistry.

Table 6. Model 1 Kruskal-Wallis results showing successful and unsuccessful tracers for < 63-µm-size fraction

Kruskal-Wallis test	
Successful	Unsuccessful
SiO ₂ , Al ₂ O ₃ , MnO, Fe ₂ O ₃ , MgO, CaO, Na ₂ O, K ₂ O, P ₂ O ₅ , SrO, BaO, Sc, V, Cr, Co, Ni, Cu, Ga, Ge, Rb, Y, Zr, Nb, Cs, La, Ce, Pr, Nd, Sm, Eu, Gd, Tb, Dy, Ho, Er, Tm, Yb, Lu, Ta, Pb ²⁰⁶ , Pb ²⁰⁷ , Pb ²⁰⁸ , Th, U, ⁷ Be, ²¹⁰ Pb, ²²⁶ Ra, ²²⁸ Ra	TiO ₂ , ¹³⁷ Cs

Stepwise-Discriminant Function Analysis (DFA) produced a 14-element solution that included, in order of the tracers entered into the function, K₂O, Cr, Er, Ce, MgO, Na₂O, ²¹⁰Pb, Cs, V, BaO, Ho, Fe₂O₃, SiO₂, and P₂O₅. The tracers represent various geochemical groups, with major, trace, and rare earth elements included. Five functions were used in the analysis and through the 14 variables, Wilk's lambda was minimized to 0.0001. The first function accounted for 55.5% of the variance, followed by 22.1% in the second function, which cumulatively accounted for 78% of the total variance from the first two functions (Table 7). This indicates most of the variance is being accounted for (Figs 8 & 9). While Mountain Range, Hill Subsurface, and Hill Surface differentiate well, Unconsolidated and Mudstone sources do not appear to be well differentiated from Overbank and Channel Bank sediment. The highest coefficients for LD1 are P₂O₅, Ho & MgO (4.8, 4.7 & -3.61,) which provide differentiation of Mountain Range and Hill Surface (Table 7). Hill Subsurface and Mudstone are differentiated through LD2 coefficients for P₂O₅, Ho, and K₂O in the positive direction (12.50, 9.33, and 4.02), while Fe₂O₃ and Na₂O provide differentiation in the negative (-6.02, and -4.61). LD3 appears primarily to provide discrimination of Hill Surface and Unconsolidated through positive coefficients for Ho and P₂O₅ (9.89 & 5.58) and negative coefficients of Er (-8.99). The Channel Bank sediment plots centrally and overlaps slightly with Unconsolidated and Hill Subsurface.

Table 7. Model 1 results of stepwise discriminant function analysis showing coefficients for each of the linear discriminants and Wilks lambda for < 63- μ m-size fraction

Stepwise DFA Variables entered			Coefficients of linear discriminants:				
Step	Entered	λ Statistic	LD1	LD2	LD3	LD4	LD5
1	K ₂ O	0.2516	1.07	4.02	-0.25	-0.33	-2.94
2	Cr	0.0918	0.08	0.01	0.00	-0.05	-0.03
3	Er	0.0370	-2.07	0.30	-8.99	1.91	3.38
4	Ce	0.0180	0.12	-0.23	0.08	-0.04	0.05
5	MgO	0.0089	-3.61	3.47	3.13	-3.43	4.56
6	Na ₂ O	0.0058	-2.39	-4.61	1.47	-0.98	-3.13
7	²¹⁰ Pb	0.0039	-0.19	-0.04	0.07	0.00	0.02
8	Cs	0.0027	3.20	-1.88	-0.20	1.86	0.84
9	V	0.0014	-0.13	0.14	0.03	-0.02	-0.05
10	BaO	0.0008	-0.02	0.02	0.01	-0.01	-0.02
11	Ho	0.0005	4.69	9.33	9.89	1.38	-11.40
12	Fe ₂ O ₃	0.0003	-0.39	-6.02	-0.89	2.05	-1.35
13	SiO ₂	0.0002	-0.07	-0.98	0.05	0.78	-0.79
14	P ₂ O ₅	0.0001	4.78	12.50	5.58	10.90	-15.86
% of variance			55.5	22.1	10.6	7.4	4.4

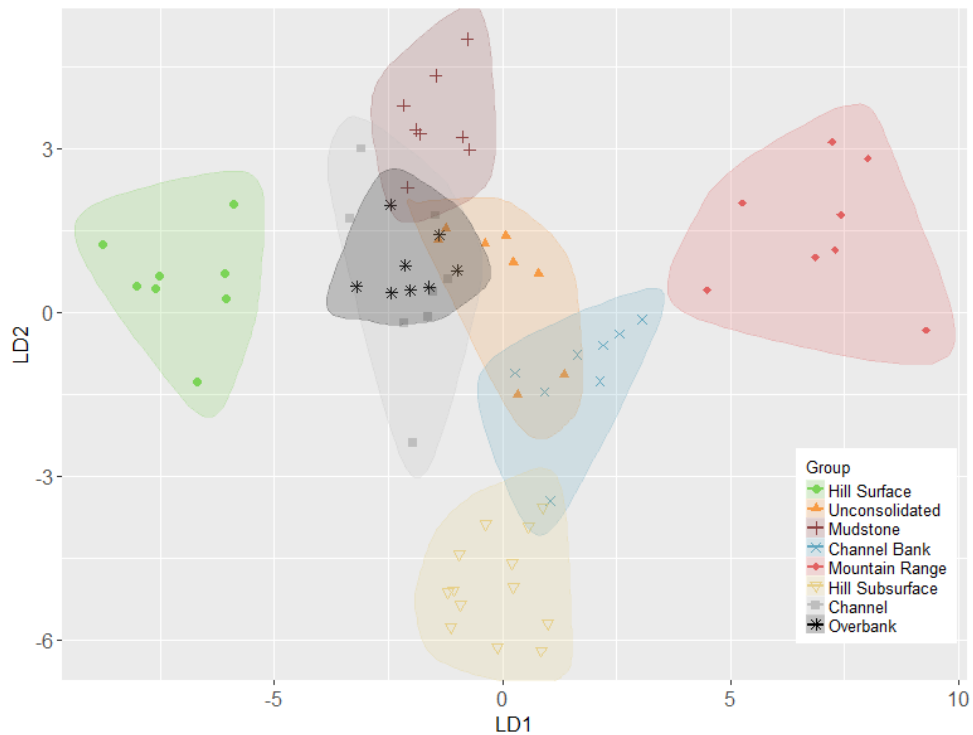


Figure 8. Model 1 plot of LD1 and LD2 from the stepwise discriminant function analysis for each sediment source for <63- μ m-size fraction. DFA results include SiO₂, Fe₂O₃, MgO, Na₂O, K₂O, P₂O₅, BaO, V, Cr, Cs, Ce, Ho, Er, ²¹⁰Pb.

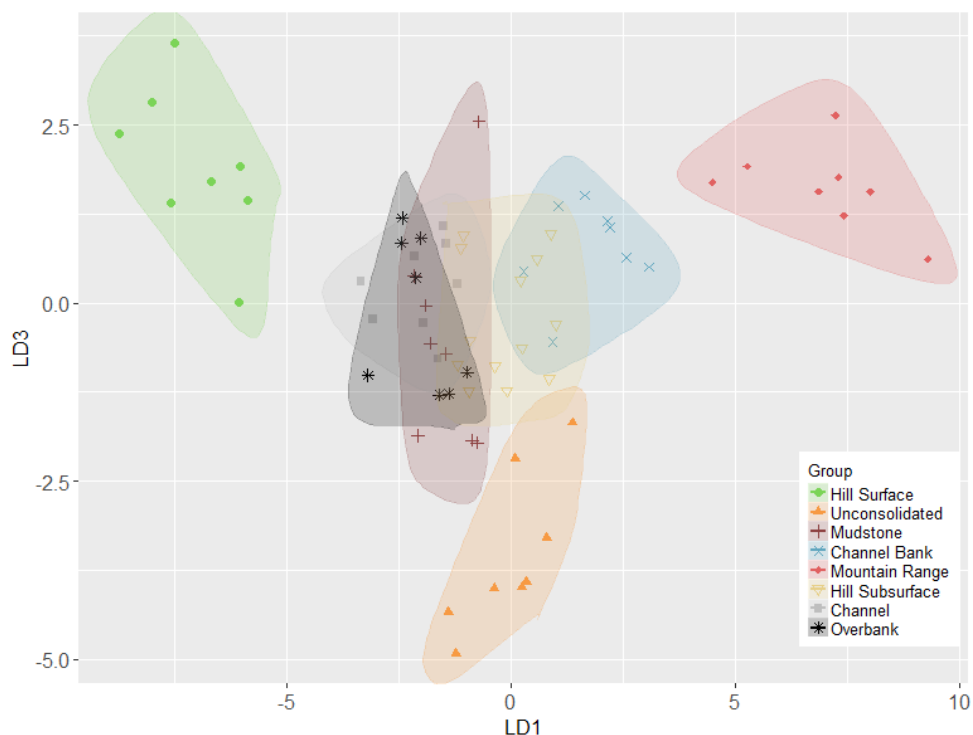


Figure 9 Model 1 plot of LD1 and LD3 from the stepwise discriminant function analysis for each sediment source for <63- μ m-size fraction. DFA results include SiO₂, Fe₂O₃, MgO, Na₂O, K₂O, P₂O₅, BaO, V, Cr, Cs, Ce, Ho, Er, ²¹⁰Pb.

5.3.2 Model 1: Size fraction 125–300 μ m

Unsuccessful tracers produced from the Kruskal-Wallis test were TiO₂, MnO, BaO, Sc, Co, and Cu (Table 8). Similar to the fine sediment fraction, the large number of successful elements likely reflect the large number of geochemically distinct sediment sources.

Table 8. Model 1 Kruskal-Wallis results showing successful and unsuccessful tracers for 125–300- μ m-size fraction

Kruskal-Wallis test	
Successful	Unsuccessful
SiO ₂ , Al ₂ O ₃ , Fe ₂ O ₃ , MgO, CaO, Na ₂ O, K ₂ O, P ₂ O ₅ , SrO, V, Cr, Ni, Ga, Ge, Rb, Y, Zr, Nb, Cs, La, Ce, Pr, Nd, Sm, Eu, Gd, Tb, Dy, Ho, Er, Tm, Yb, Lu, Ta, Pb ²⁰⁶ , Pb ²⁰⁷ , Pb ²⁰⁸ , Th, U, ⁷ Be, ²¹⁰ Pb, ¹³⁷ Cs, ²²⁶ Ra, ²²⁸ Ra	TiO ₂ , MnO, BaO, Sc, Co, Cu

Stepwise-DFA produced a 12-element solution that included, in order of the elements entered into the function, K₂O, MgO, Y, Pr, P₂O₅, Fe₂O₃, Dy, La, V, Zr, ²²⁶Ra, and SrO. These tracers represent a mix of geochemical groups, including major, minor, trace, rare earth, and radionuclide geochemistry. Five functions were used in the analysis and through the 12 variables, Wilk's lambda was minimized to 0.0002. The first function accounted for 59.1% of the variance, followed by 18.0% of the variance for the second function. Cumulatively, this amounts to 77% of variance across the first two functions (Table 9). The

tracer selection provides good visual discrimination between several sources. Unconsolidated and Mountain Range sources are clearly separated from the remaining sources in the first two discriminant functions (Fig. 10). The highest coefficient in LD1 relate to Dy (3.7), which correlates to Unconsolidated sediment, whereas Mountain Range, Mudstone, Hill Surface, and Hill Subsurface relate mostly to the negative LD1 coefficients of P₂O₅, K₂O, and Pr (-8.8, -6.0, and -5.8) (Table 9). Due to the similar parent geochemistry, Hill Surface and Hill Subsurface group together in LD1 and LD2 and slightly overlap with Mudstone sediment sources, which separates further within in LD3 (Fig. 11). LD4 allows for differentiation of the Hill Surface and Subsurface attributed to different P₂O₅ concentrations reflected in the high LD4 coefficient (20.4). The Channel Bank sediment plots to a similar position to Channel and Overbank sediment sources.

Table 9. Model 1 results of stepwise discriminant function analysis showing coefficients for each of the linear discriminants and Wilks lambda for 125–300- μ m-size fraction

Stepwise DFA Variables entered			Coefficients of linear discriminants:				
Step	Entered	λ Statistic	LD1	LD2	LD3	LD4	LD5
1	K ₂ O	0.3096	-6.036	-4.147	1.277	-0.146	0.324
2	MgO	0.1327	1.121	6.460	2.241	-0.594	-1.319
3	Y	0.0471	0.698	-0.244	0.007	0.045	0.343
4	Pr	0.0195	-5.789	0.060	-1.138	0.298	0.366
5	P ₂ O ₅	0.0094	-8.811	-5.943	3.635	20.446	-3.044
6	Fe ₂ O ₃	0.0046	0.140	-0.080	-1.793	-1.110	-0.128
7	Dy	0.0022	3.698	1.647	1.804	-0.019	-0.993
8	La	0.0013	0.748	-0.100	0.082	-0.131	-0.115
9	V	0.0008	-0.061	0.019	0.064	0.036	0.024
10	Zr	0.0005	-0.011	-0.007	0.002	-0.007	-0.009
11	²²⁶ Ra	0.0003	0.140	0.030	0.022	0.017	-0.002
12	SrO	0.0002	0.012	0.020	0.000	-0.007	-0.007
% of variance			59.1	18.0	16.5	5.1	1.3

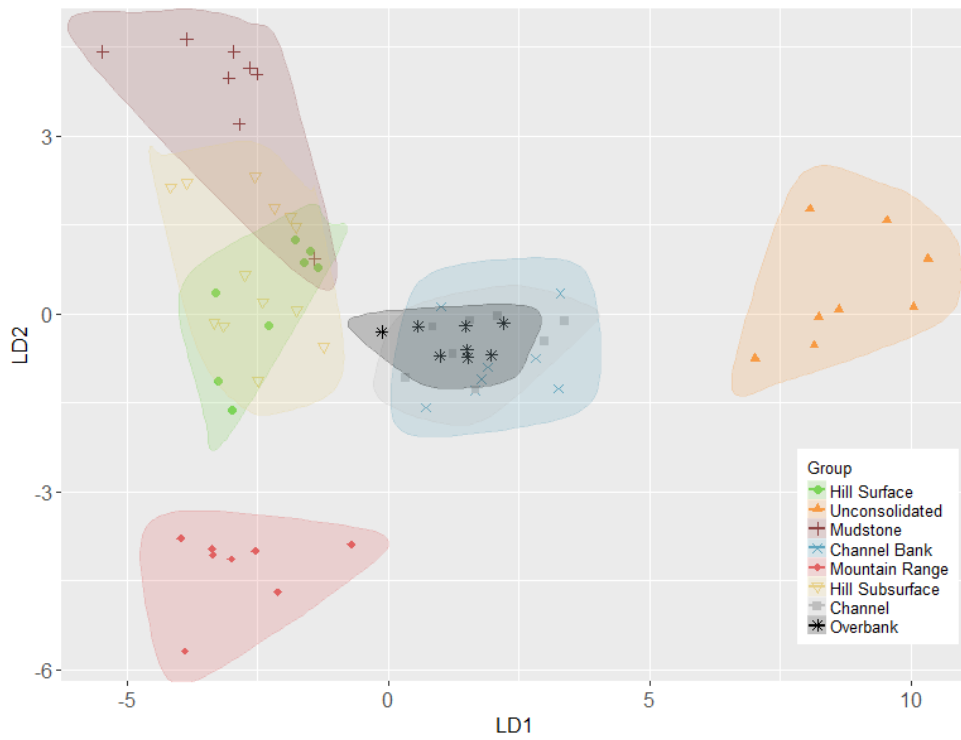


Figure 10. Model 1 plot of LD1 and LD2 from the stepwise discriminant function analysis for each sediment source for 125–300- μ m-size fraction. DFA results include K₂O, MgO, Y, Pr, P₂O₅, Fe₂O₃, Dy, La, V, Zr, ²²⁶Ra, SrO.



Figure 11. Model 1 plot of LD1 and LD3 from the stepwise discriminant function analysis for each sediment source for 125–300- μ m-size fraction. DFA results include K₂O, MgO, Y, Pr, P₂O₅, Fe₂O₃, Dy, La, V, Zr, ²²⁶Ra, SrO.

5.3.3 Model 2: Size fraction < 63 µm

The tracers selected after excluding those tracers that were found to exhibit 'non-conservative' behaviour according to the procedure outlined by Smith et al. (2018) were: SiO₂, CaO, K₂O, SrO, V, Y, Zr, Nb, La, Ce, Pr, Nd, Sm, Eu, Lu, Ta, Pb²⁰⁷, Th, ¹³⁷Cs and ²²⁶Ra (Table 10).

Table 10. Model 2 'Non-conservative' Behaviour results showing successful and unsuccessful tracers for < 63-µm-size fraction

'Non-conservativeness' Behaviour	
Successful	Unsuccessful
SiO ₂ , CaO, K ₂ O, SrO, V, Y, Zr, Nb, La, Ce, Pr, Nd, Sm, Eu, Lu, Ta, Pb ²⁰⁷ , Th, ¹³⁷ Cs, ²²⁶ Ra	Al ₂ O ₃ , TiO ₂ , MnO, Fe ₂ O ₃ , MgO, Na ₂ O, P ₂ O ₅ , BaO, Sc, Cr, Co, Ni, Cu, Ga, Ge, Rb, Cs, Gd, Tb, Dy, Ho, Er, Tm, Yb, Pb ²⁰⁶ , Pb ²⁰⁸ , U, ⁷ Be, ²¹⁰ Pb, ²²⁸ Ra

DFA was applied to the entire 20 element solution which included in order of the significance in the function; K₂O, Lu, SiO₂, Y, Ce, Pb²⁰⁷, V, Nb, Th, CaO, SrO, Eu, Zr, ²²⁶Ra, Sm, Pr, Nd, La, Ta, ¹³⁷Cs. DFA was not used stepwise to select the tracer, as with Model 1, but rather so that coefficients and tracer significance could be compared. Five functions were used in the analysis and through the 20 variables; Wilk's lambda was minimized to 0.004. The first function accounted for 37.5% of the variance followed by 36.1% of the variance for the second function, cumulatively accounting for 73.6 % of variance across the first two functions (Table 11). The sources appear well discriminated visually as shown by the linear discriminant plots (Figs 12 & 13). Hill Surface and Hill Subsurface are well discriminated, and although Channel Bank plots close to Overbank and Channel sediment, it appears to have better discrimination than Model 1. This is attributed to a larger array of tracers in general, which decrease the effect of an individual tracer. In this instance, K₂O, Eu, Lu, CaO, and Pr all appear to have strong positive correlation with LD1 coefficients (6.3, 5.3, 4.6, 3.9, and 2.2 respectively). This relates predominantly to the Mountain Range values, although it correlates negatively to Hill Surface and Subsurface. Similarly, Lu, K₂O, and CaO, have positive coefficients (6.1, 3.8, and 2.4), which relate to Hill Surface, Mudstone and Unconsolidated, while Pr and Ta have strong negative coefficients (-8.6 & -7.8) for LD2, relating to Hill Subsurface, Mountain Range and Channel Bank sediment. LD3 provides further discrimination between Mudstone and Unconsolidated sediment, mostly due to Lu, Pr, and Eu values.

Table 11. Model 2 results of stepwise discriminant function analysis showing coefficients for each of the linear discriminants and Wilks lambda for < 63- μ m-size fraction

DFA Variables			Coefficients of linear discriminants:				
Step	Entered	λ Statistic	LD1	LD2	LD3	LD4	LD5
1	K ₂ O	0.2516	6.28	2.82	3.84	3.05	3.98
2	Lu	0.1410	4.57	6.14	6.64	23.63	-13.13
3	SiO ₂	0.0871	0.66	0.61	-0.29	-0.20	-0.04
4	Y	0.0471	0.55	0.53	-0.79	0.48	-0.09
5	Ce	0.0220	-0.09	-0.13	-0.02	0.13	-0.04
6	Pb ²⁰⁷	0.0146	-0.07	-0.72	-0.52	-0.19	-0.33
7	V	0.0092	0.08	0.20	0.05	0.03	0.04
8	Nb	0.0058	-1.46	-0.69	-1.04	-1.32	0.00
9	Th	0.0042	0.72	0.97	1.05	-1.14	-0.18
10	CaO	0.0033	3.89	2.43	0.53	-0.21	-0.62
11	SrO	0.0016	-0.07	-0.02	-0.02	-0.02	0.02
12	Eu	0.0014	5.32	1.89	3.01	4.54	8.00
13	Zr	0.0012	0.01	-0.01	0.00	0.01	0.01
14	²²⁶ Ra	0.0010	-0.15	0.21	-0.03	-0.19	-0.05
15	Sm	0.0009	-0.32	-0.78	2.48	-1.78	0.43
16	Pr	0.0008	2.19	-8.60	5.02	1.36	-0.53
17	Nd	0.0005	-0.51	1.42	-1.21	-0.56	-0.56
18	La	0.0004	-0.17	0.58	-0.34	-0.06	0.42
19	Ta	0.0004	-0.29	-7.78	-0.85	8.39	0.65
20	¹³⁷ Cs	0.0004	-0.17	-0.57	-0.27	0.57	-0.88
% of variance			37.5	36.1	16.4	6.7	3.4

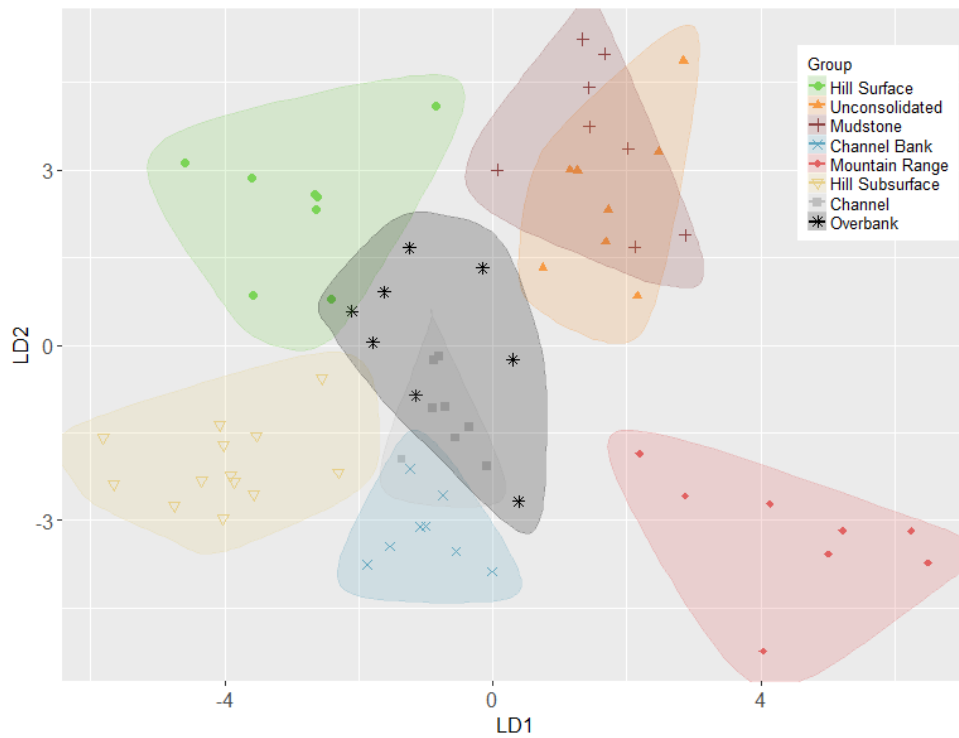


Figure 12. Model 2 plot of LD1 and LD2 from the stepwise discriminant function analysis for each sediment source for < 63- μ m-size fraction. DFA results include K2O, Lu, SiO₂, Y, Ce, Pb207, V, Nb, Th, CaO, SrO, Eu, Zr, 226Ra, Sm, Pr, Nd, La, Ta, 137Cs.

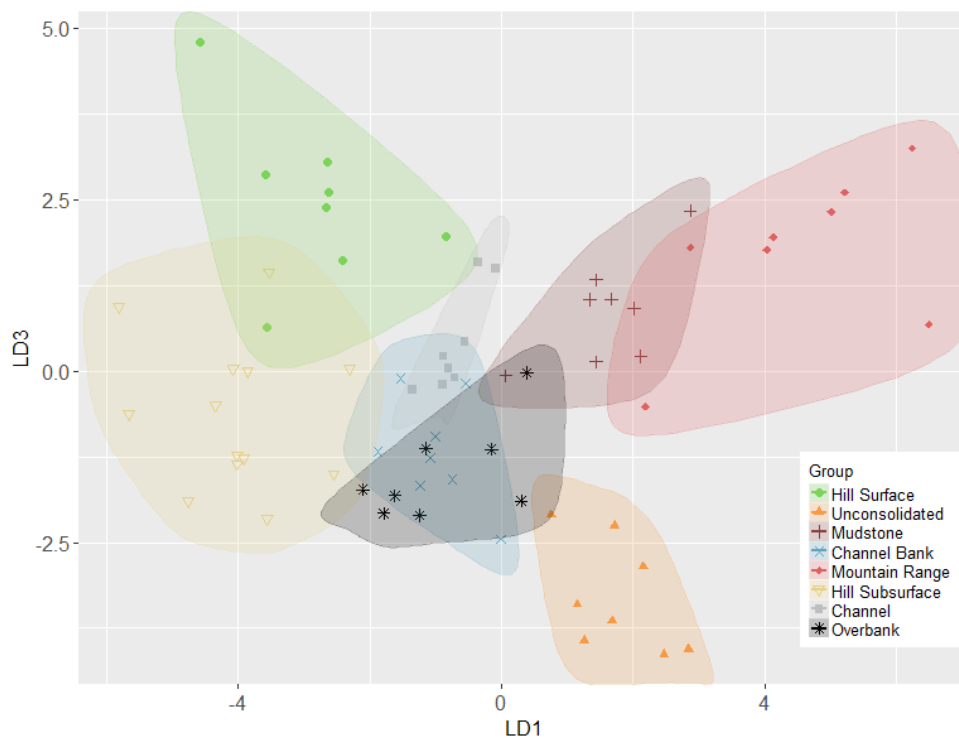


Figure 13. Model 2 plot of LD1 and LD3 from the stepwise discriminant function analysis for each sediment source for < 63- μ m-size fraction. DFA results include K2O, Lu, SiO₂, Y, Ce, Pb207, V, Nb, Th, CaO, SrO, Eu, Zr, 226Ra, Sm, Pr, Nd, La, Ta, 137Cs.

5.3.4 Model 2: Size fraction 125–300 µm

The tracers selected based on geochemical appraisal of 'non-conservative' behaviour according to Smith et al. (2018) were: Al₂O₃, MnO, MgO, K₂O, P₂O₅, Y, Zr, Nb, La, Ce, Pr, Nd, Sm, Eu, Dy, Er, Tm, Yb, Lu, Pb²⁰⁷, ¹³⁷Cs, ²²⁶Ra, and ²²⁸Ra (Table 12).

Table 12. Model 2 'Non-conservativeness' Behaviour results showing successful and unsuccessful tracers for < 63-µm-size fraction

'Non-conservativeness' Behaviour	
Successful	Unsuccessful
Al ₂ O ₃ , MnO, MgO, K ₂ O, P ₂ O ₅ , Y, Zr, Nb, La, Ce, Pr, Nd, Sm, Eu, Dy, Er, Tm, Yb, Lu, Pb ²⁰⁷ , ¹³⁷ Cs, ²²⁶ Ra, and ²²⁸ Ra	SiO ₂ , TiO ₂ , Fe ₂ O ₃ , CaO, Na ₂ O, SrO, BaO, Sc, V, Cr, Co, Ni, Cu, Ga, Ge, Rb, Cs, Gd, Tb, Ho, Ta, Pb ²⁰⁶ , Pb ²⁰⁸ , Th, U, ⁷ Be, and ²¹⁰ Pb

Discriminant Function Analysis (DFA) was applied to the entire 23 element solution, which included, in order of the tracer significance in the function, K₂O, Er, Ce, P₂O₅, MgO, La, ²²⁶Ra, Zr, Nb, Pr, Pb²⁰⁷, Al₂O₃, Dy, Sm, Y, Lu, MnO, Tm, ²²⁸Ra, Nd, Yb, Eu, ¹³⁷Cs. Five functions were used in the analysis and through the 23 variables, Wilk's lambda was minimized to 0.004. The first function accounted for 62.0% of the variance followed by 15.6% of the variance for the second function, cumulatively accounting for 77.6% of variance across the first two functions (Table 13). The sources discriminate well visibly as shown by the linear discriminant plots (Figs 14 & 15). Mountain Range and Unconsolidated sediment sources are differentiated the clearest from Hill Surface, Hill Subsurface and Mudstone sources. The largest LD1 positive coefficients relate to Tm and Dr (7.9 & 6.5) and are associated with Unconsolidated, while the largest negative coefficients are from Eu, P₂O₅, K₂O and MgO (-11.0, -6.0, -5.2, & -3.8), which are associated with Mudstone, Hill Surface, Hill Subsurface. LD2 provides discrimination of Mountain Range sediment through correlations with MnO, Lu, P₂O₅, & K₂O coefficients (-19.1, -14.3, -6.2, & -6.1). LD3 provides discrimination of Mudstone sediment from Hill Surface and Hill Subsurface through positive coefficients of MnO and Tm (10.7 & 6.9) and negative coefficients of P₂O₅ & Eu (-11.3 & -7.9).

Table 13. Model 2 results of stepwise discriminant function analysis showing coefficients for each of the linear discriminants and Wilks lambda for < 63- μ m-size fraction

DFA Variables			Coefficients of linear discriminants:				
Step	Entered	λ Statistic	LD1	LD2	LD3	LD4	LD5
1	K ₂ O	0.2516	-5.25	-6.05	-0.65	-0.25	-0.44
2	Er	0.1148	1.93	-0.59	-0.72	1.17	2.51
3	Ce	0.0515	-0.01	0.07	0.08	0.12	0.01
4	P ₂ O ₅	0.0213	-5.98	-6.21	-11.25	-17.56	-3.27
5	MgO	0.0128	-3.77	8.39	-1.58	0.69	1.56
6	La	0.0090	0.56	0.30	-0.02	0.00	0.04
7	²²⁶ Ra	0.0065	0.09	0.04	-0.06	-0.10	0.05
8	Zr	0.0041	-0.01	-0.01	-0.01	0.01	-0.01
9	Nb	0.0029	-0.11	-0.51	0.28	-0.89	0.55
10	Pr	0.0023	-3.81	-0.78	0.40	1.97	2.15
11	Pb ²⁰⁷	0.0019	-0.11	-0.04	-0.25	-0.02	-0.24
12	Al ₂ O ₃	0.0016	-0.44	-0.17	0.20	0.57	-0.12
13	Dy	0.0014	6.45	-0.92	-2.86	-1.71	0.14
14	Sm	0.0011	0.79	0.56	1.82	2.55	0.77
15	Y	0.0009	0.35	-0.19	-0.12	-0.27	0.04
16	Lu	0.0008	-1.21	-14.34	0.83	-28.14	10.30
17	MnO	0.0007	-1.85	-19.09	10.72	9.08	-12.54
18	Tm	0.0006	7.96	1.59	6.88	21.04	-3.61
19	²²⁸ Ra	0.0006	0.15	0.06	0.02	0.21	-0.09
20	Nd	0.0005	-0.24	-0.53	0.08	-0.94	-0.59
21	Yb	0.0005	-2.08	4.21	1.91	1.83	-0.67
22	Eu	0.0004	-11.01	9.69	-7.89	0.23	-9.17
23	¹³⁷ Cs	0.0004	-0.60	0.62	1.63	0.10	-0.89
% of variance			62.0	15.6	12.7	6.1	3.6

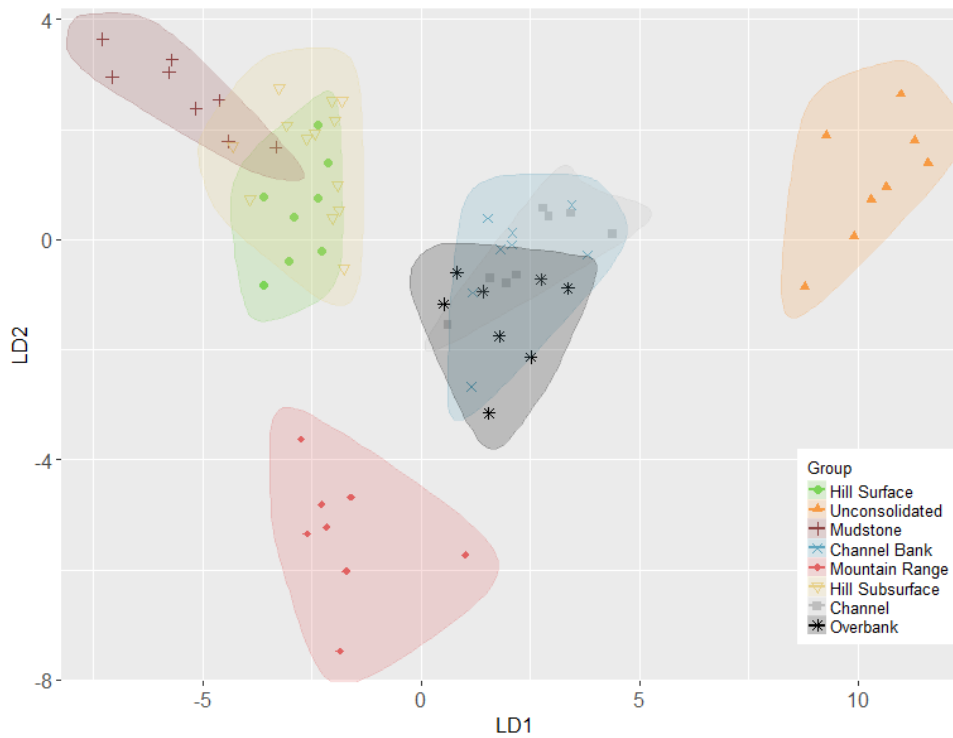


Figure 14. Model 2 plot of LD1 and LD2 from the stepwise discriminant function analysis for each sediment source for 125–300- μ m-size fraction. DFA results include Al_2O_3 , MnO , MgO , K_2O , P_2O_5 , Y , Zr , Nb , La , Ce , Pr , Nd , Sm , Eu , Dy , Er , Tm , Yb , Lu , Pb_{207} , ^{137}Cs , ^{226}Ra , and ^{228}Ra .

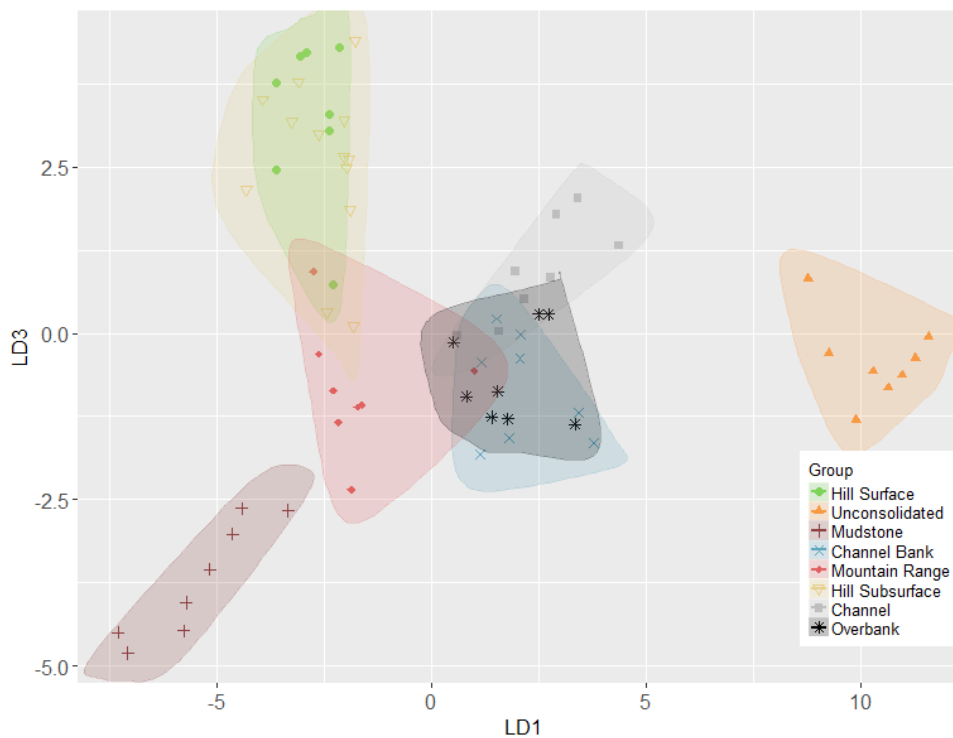


Figure 15. Model 2 plot of LD1 and LD3 from the stepwise discriminant function analysis for each sediment source for 125–300- μ m-size fraction. DFA results include Al_2O_3 , MnO , MgO , K_2O , P_2O_5 , Y , Zr , Nb , La , Ce , Pr , Nd , Sm , Eu , Dy , Er , Tm , Yb , Lu , Pb_{207} , ^{137}Cs , ^{226}Ra , and ^{228}Ra .

5.4 Mixing model Performance

5.4.1 Size fraction: < 63 µm

Model Estimates

The models generally show good agreement between major sediment source contributions although they do show a large range of estimates for several sediment sources. The initial model scenarios attribute 10–11% of sediment to Hill Surface sediment, < 3% to Mountain Range, 1–11% to Mudstone, and similar estimates for Unconsolidated and Hill Subsurface, ranging from 36–38 and 27–30% respectively (Fig. 16 & Table 14). These scenarios include Channel Bank, with an estimate of 12–21%. However, Channel Bank sediment is a secondary source that presents a challenge for the models to differentiate clearly from primary sediment sources. This is shown particularly well with Model 1, which shows a 21% contribution from Channel Bank, but the distribution is not normally distributed, and comparison with Model 2 DFA plots (Figs 8, 9, 12, & 13) is less effective at differentiating the Channel Bank. Removing the Channel Bank source from the models provides a much clearer depiction of the sediment source contributions.

On removal of the Channel Bank source from the model scenarios, the relative proportions change to attribute 8% of sediment to Hill Surface sediment, < 4% to Mountain Range, 2–12% to Mudstone, and 41–49 and 34–42 % to Unconsolidated and Hill Subsurface range respectively (Fig. 16 & Table 14). Both models benefit significantly from removing the Channel Bank source from the source apportionment, with frequency plots showing much more consistent distributions (Fig. 16); evidentially Hill Subsurface and Unconsolidated material receive the bulk of the Channel Bank sediment source portion. Standard deviation is high for most of the sources and reflects the inherent variability in geochemical data. It appears to be reduced for the major sources on removal of Channel Bank, reflecting the challenge Channel Bank provides to differentiation from sediment sources.

Table 14. Percentage of each sediment source for <63 µm size fraction for Model 1 and Model 2

<63 µm Sources	Model 1				Model 2			
	6-Source		5-source		6-source		5-source	
	Mean %	S.D.						
Hill Surface	10	6.3	8	5.6	11	5.6	8	4.7
Unconsolidated	38	7.9	49	6.6	36	8.2	41	7.3
Mudstone	1	2.5	2	3.5	11	8.4	12	9.4
Channel Bank	21	9.7	-	-	12	12.1	-	-
Mountain Range	0	0.9	0	1.2	3	3.6	4	4.2
Hill Subsurface	30	7.6	42	5.3	27	7.6	34	4.4

Model Output Frequency Distributions for < 63 micron size fraction

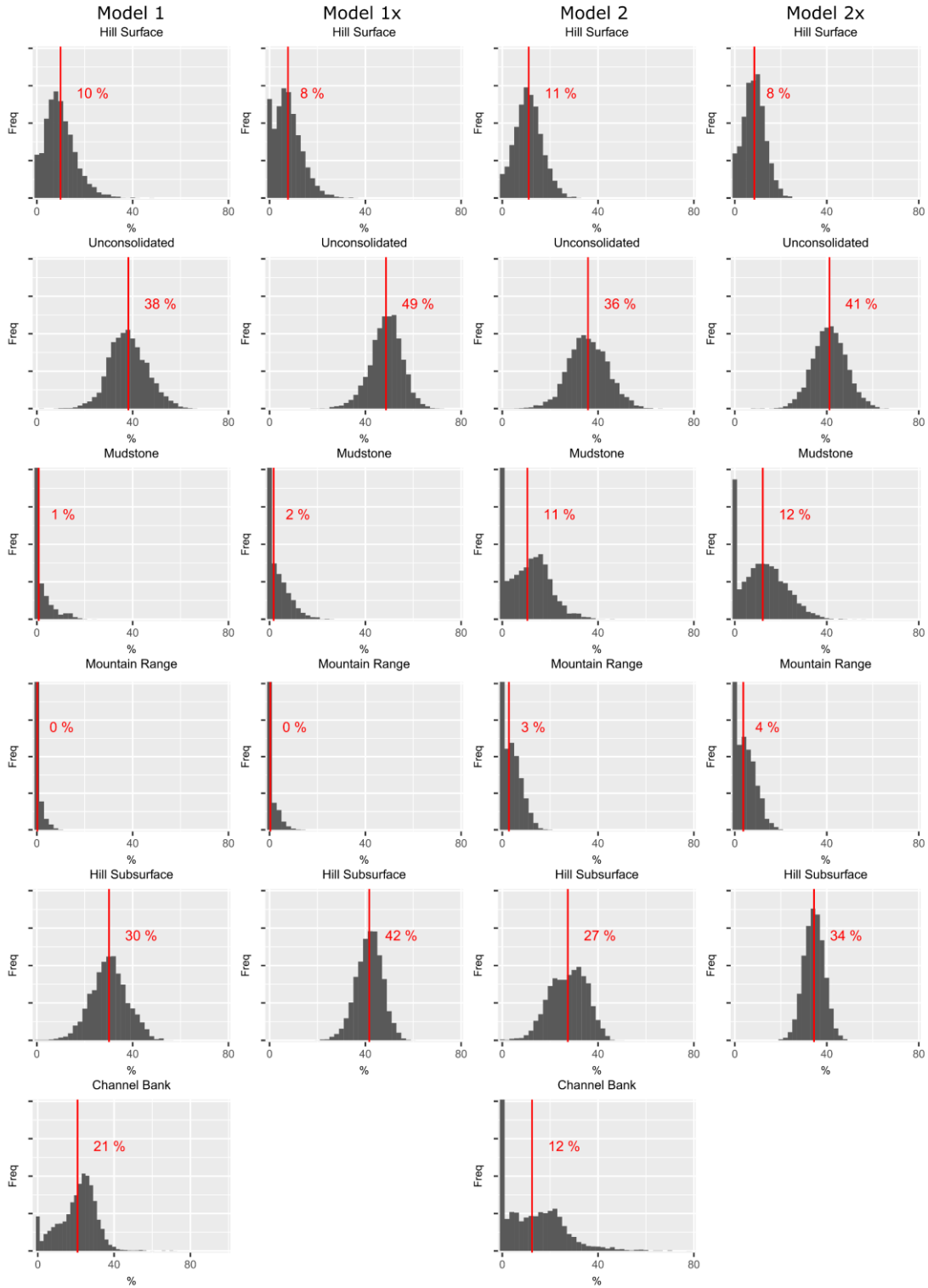


Figure 16. Frequency plots for Model 1, Model 1x (5-source), Model 2, and Model 2x (5-source) for the < 63- μ m fraction. Mean value indicated in red.

Synthetic Mixture Comparison

The synthetic mixtures (Table 3) were compared with the modelled output for each of the models. Both models produced comparable results to the synthetic mixtures, which indicates the models generally derive appropriate proportions of sediment sources; although synthetic mixture do not address potential measurement error or issues of tracer non-conservative behaviour during transport.

The models deviate the most from synthetic mixtures proportions for Channel Bank sources, with 5.5, 2.5, 1.0, and 3.8% difference for Model 1 (Table 15) and 13.3, 8.9, 9.0, and 12.5% difference for Model 2 (Table 16). This is quite significant for apportionment of that source and highlights the challenge of differentiation of channel bank sediment that is itself derived from primary sediment sources. Despite the Channel Bank challenge, the remaining sediment sources are all relatively consistent with the synthetic mixtures, although Hill Surface sediment seems to present a problem for 'Mix 3' in both Model 1 and Model 2. Removing Channel Bank sediment generally improves the model estimates, resulting in lower deviations from the synthetic mixtures of around 1–3% difference (Table 15), with the exception of 'Mix 3' for Model 1, although the two higher values in 'Mix 3' relate to Hill Surface (–8.6 %) and Hill Subsurface (6.2 %) differences, which pertain to large proportions (39.7 & 34%) so are not unreasonable values. Model 2 values display a slightly higher difference for some sources and synthetic mixtures once Channel Bank is removed. The difference in these values is generally < 5%, although 'Mix 3' presents higher difference for Hill Surface and Hill Subsurface (Table 16).

Table 15. Model 1 < 63- μ m-size fraction outputs for 4 synthetic mixtures for 6-source (upper) and 5-source (lower) scenarios with Mean Absolute Fit (MAF) displayed for each output

Model 1 < 63 μm		Mix 1		Mix 2		Mix 3		Mix 4	
		Mean %	Diff						
6-Source	Hill Surface	10.8	0.5	10.0	–0.3	38.5	–6.0	14.7	–1.2
	Unconsolidated	12.7	0.1	12.0	0.3	11.2	1.8	18.8	–0.9
	Mudstone	26.1	–3.1	22.0	–0.9	9.3	–1.4	20.3	0.1
	Channel Bank	7.8	5.5	13.8	2.5	8.8	1.0	11.2	3.8
	Mountain Range	25.3	–1.1	19.8	–1.1	2.9	1.1	17.6	–0.9
	Hill Subsurface	17.3	–1.9	22.4	–0.5	29.1	3.5	17.4	–0.9
MAF		96.7		98.4		96.8		96.6	
5-Source	Hill Surface	10.2	–0.4	11.1	–0.5	39.7	–8.6	15.6	–1.6
	Unconsolidated	14.4	1.5	14.7	1.5	12.8	2.5	21.1	–0.2
	Mudstone	28.9	–1.0	25.5	–0.3	10.2	–1.5	23.5	1.7
	Mountain Range	25.8	–1.2	22.2	–1.4	3.3	1.4	18.7	–1.4
	Hill Subsurface	20.6	1.0	26.5	0.7	34.0	6.2	21.1	1.4
	MAF		98.9		99.2		96.7		99.0

Table 16. Model 2 < 63- μ m-size fraction outputs for 4 synthetic mixtures for 6-source (upper) and 5-source (lower) scenarios with Mean Absolute Fit (MAF) displayed for each output

Model 2 < 63 μ m		Mix 1		Mix 2		Mix 3		Mix 4	
		Mean %	Diff						
6-Source	Hill Surface	9.2	-1.1	8.3	-2.0	27.9	-16.7	11.6	-4.3
	Unconsolidated	10.2	-2.4	9.9	-1.9	7.9	-1.6	15.0	-4.8
	Mudstone	21.3	-7.9	19.9	-2.9	9.9	-0.9	19.5	-0.6
	Channel Bank	15.6	13.3	20.2	8.9	16.8	9.0	19.9	12.5
	Mountain Range	26.6	0.3	20.0	-0.9	2.1	0.3	16.9	-1.7
	Hill Subsurface	17.0	-2.2	21.7	-1.2	35.5	9.8	17.1	-1.1
MAF		95.5		97.0		93.6		95.8	
5-Source	Hill Surface	9.7	-0.9	10.8	-0.8	30.6	-17.7	13.7	-3.4
	Unconsolidated	14.9	2.0	13.9	0.6	11.6	1.3	20.5	-0.8
	Mudstone	24.8	-5.1	23.0	-2.8	12.9	1.2	22.4	0.6
	Mountain Range	27.9	0.9	23.9	0.3	2.6	0.7	19.8	-0.2
	Hill Subsurface	22.8	3.1	28.4	2.6	42.3	14.5	23.5	3.8
	MAF		97.6		98.6		94.1		98.2

5.4.2 Size fraction: 125–300 μ m

Model Estimates

The models generally show good agreement between most of the sediment source contributions, although they exhibit significant differences for Hill Surface and Hill Subsurface sources. The initial scenarios of model 1 and 2 attribute 2–22% of sediment to Hill Surface, Mountain Range 13–17%, Mudstone 7–11%, Unconsolidated 10% and Hill Subsurface 11–37%, and Channel Bank 27–34% (Fig. 17 & Table 17). As with the finer < 63- μ m fraction, Channel Bank presents a challenge for the model to differentiate from the primary sediment sources as shown by the DFA plots (Figs 10, 11, 14, & 15). Unlike the < 63- μ m sediment, the Channel Bank distribution tends towards a normal distribution with a single peak indicating the models solve the coarser discrimination with greater consistency.

Removing the Channel Bank source changes the relative proportions of Hill Surface, Mountain Range, and Hill Subsurface sediment the most, but still produces different proportions of Hill Surface and Hill Subsurface sediment, displaying Hill Surface values of 8–29%, Unconsolidated 10–12%, Mudstone 2–6%, Mountain Range 32–42%, and Hill Subsurface 17–42% of sediment across (Fig. 17). Mountain Range sources increase most dramatically once Channel Bank is removed, indicating the possible masking effect Channel Bank has on the Mountain Range sediment. The standard deviations are generally

lower in Model 2 than Model 1, with the 5 source Model 2 estimates providing the lowest standard deviations.

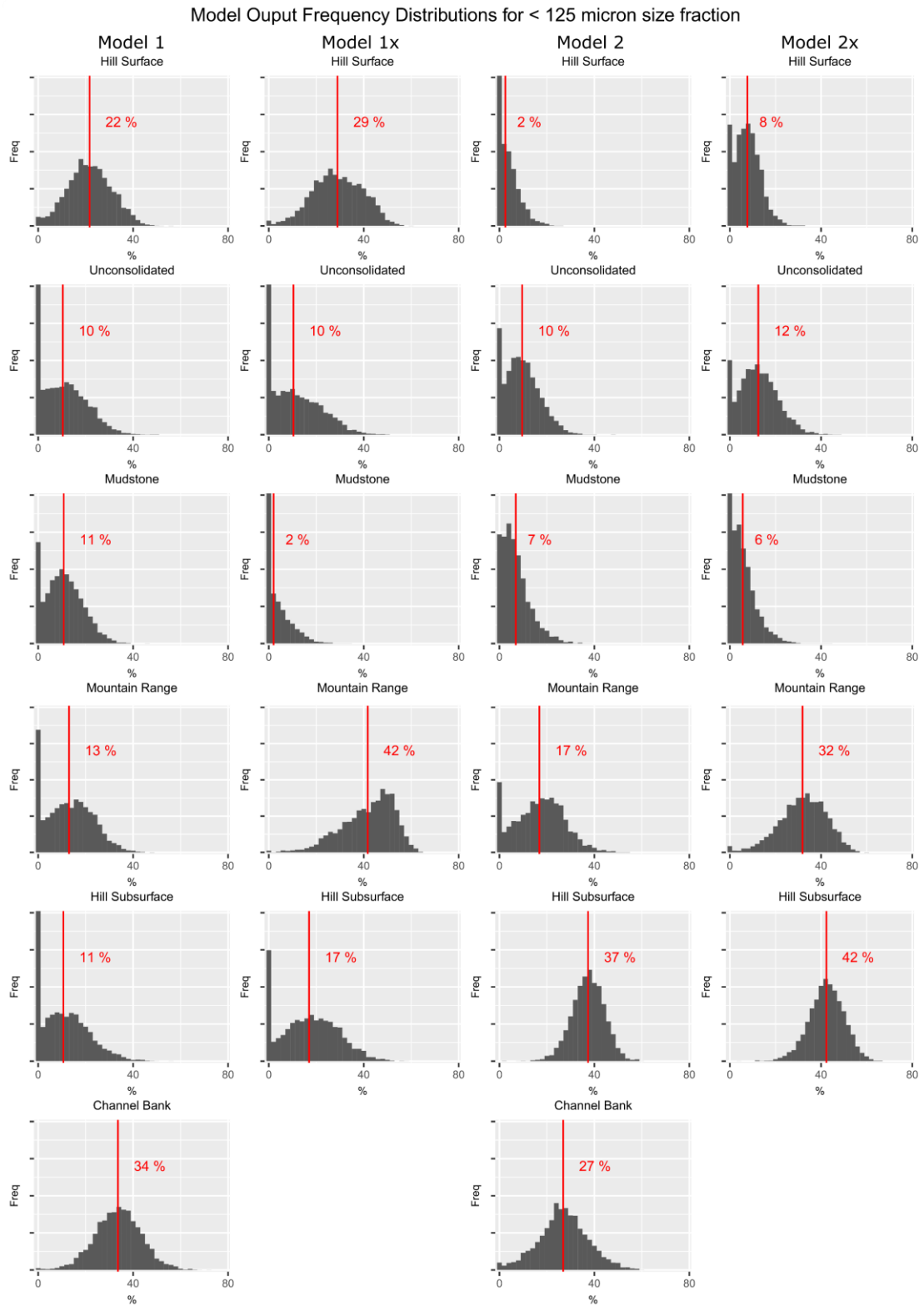


Figure 17. Frequency plots for Model 1, Model 1x (5-source), Model 2, and Model 2x (5-source) for the 125–300- μ m fraction. Mean value indicated in red.

Table 17. Percentage of each sediment source for 125–300- μm -size fraction for Model 1 and Model 2

125–300 μm Sources	Model 1				Model 2			
	6-Source		5-Source		6-Source		5-Source	
	Mean %	S.D.						
Hill Surface	22	9.2	29	10.6	2	3.8	8	5.4
Unconsolidated	10	9.2	10	10.2	10	7	12	8.3
Mudstone	11	7.6	2	4.2	7	5.9	6	5.5
Channel Bank	34	9.8	-		27	10.4	-	
Mountain Range	13	9.6	42	11.0	17	10.3	32	10.3
Hill Subsurface	11	9.8	17	11.8	37	6.9	42	7.6

Synthetic Mixture Comparison

The synthetic mixtures (Table 3) were compared to the modelled output for each of the models for the 125–300- μm -size fraction. Both models produced comparable results to the synthetic mixtures for most sources, although there are variations for several of the source materials. Unlike the < 63- μm -size fraction, Channel Bank did not seem to present as much of a challenge for the initial models to differentiate and produce similar proportions to the synthetic mixtures. Model 1 source proportions from the 6-source scenario produce differences as much as 5–6%. Model 2 results in a wider range of % difference, with most of the differences being with 6–7% although a few values exceeded 10%, e.g. Mudstone and Hill Subsurface (–14.7 & 11.8) from ‘Mix 6’, and Unconsolidated (–11.3) from ‘Mix 7’ (Table 18). Model 2 shows significant differences once Channel Bank is removed, with many values approaching 9–10% difference and larger differences occurring in Mudstone and Hill Subsurface (–20.1 & 16.2%) from ‘Mix 6’ and Unconsolidated (–14.3%) from ‘Mix 7’ (Table 19).

Table 18. Model 1 125–300- μm -size fraction outputs for 4 synthetic mixtures for 6-source (upper) and 5-source (lower) scenarios with Mean Absolute Fit (MAF) displayed for each output

Model 1 125–300 μm		Mix 5		Mix 6		Mix 7		Mix 8	
		Mean %	Diff						
6-Source	Hill Surface	14.8	1.8	11.3	0.1	22.8	0.7	7.1	5.6
	Unconsolidated	9.3	-5.0	8.0	-3.6	13.8	-7.8	8.0	-4.5
	Mudstone	13.1	-0.3	21.2	-5.5	4.8	4.5	12.8	-0.8
	Channel Bank	25.2	1.3	21.7	-1.1	25.3	3.7	33.8	-2.1
	Mountain Range	22.1	2.4	27.6	5.0	11.0	1.7	19.7	5.2
	Hill Subsurface	15.5	-0.1	10.2	5.2	22.3	-2.8	18.6	-3.4
MAF		98.2		96.6		96.5		96.4	
5-Source	Hill Surface	19.2	2.0	13.7	-0.8	30.0	1.7	9.5	7.1
	Unconsolidated	11.7	-7.0	10.1	-4.9	17.1	-10.4	11.0	-8.4
	Mudstone	16.3	-1.5	29.4	-5.3	5.7	5.2	21.2	0.0
	Mountain Range	31.1	5.3	33.7	4.5	16.6	4.7	28.4	5.7
	Hill Subsurface	21.7	1.2	13.1	6.6	30.7	-1.3	29.9	-4.4
	MAF		97.2		95.6		96.1		94.9

Table 19. Model 2 125–300- μm -size fraction outputs for 4 synthetic mixtures for 6-source (upper) and 5-source (lower) scenarios with Goodness of Fit (GOF) and Mean Absolute Fit (MAF) displayed for each output

Model 2 125–300 μm		Mix 5		Mix 6		Mix 7		Mix 8	
		Mean %	Diff						
6-Source	Hill Surface	13.4	0.3	13.4	2.2	20.3	-1.8	5.3	3.7
	Unconsolidated	7.2	-7.0	5.2	-6.5	10.2	-11.3	6.3	-6.1
	Mudstone	6.8	-6.6	12.0	-14.7	2.6	2.2	6.4	-7.2
	Channel Bank	26.4	2.5	23.7	0.9	27.5	5.9	32.9	-3.0
	Mountain Range	25.2	5.5	29.0	6.4	12.6	3.4	23.8	9.2
	Hill Subsurface	21.0	5.4	16.8	11.8	26.7	1.6	25.4	3.4
MAF		95.4		92.9		95.6		94.5	
5-Source	Hill Surface	18.1	0.9	18.9	4.4	28.8	0.6	7.5	5.1
	Unconsolidated	8.9	-9.9	6.9	-8.2	13.1	-14.3	8.4	-11.0
	Mudstone	8.0	-9.7	14.6	-20.1	3.2	2.8	10.6	-10.6
	Mountain Range	34.9	9.1	36.9	7.7	20.0	8.1	33.5	10.7
	Hill Subsurface	30.1	9.6	22.7	16.2	34.8	2.9	40.0	5.8
	MAF		93.5		88.7		95.2		91.4

5.5 Quantitative Sediment source contributions

Overall, Unconsolidated material and Hill Subsurface material are the dominant sources contributing sediment to Overbank deposits in the lower Oroua floodplain. Model 2 is considered more reliable for the < 63- μm -size fraction and a 5-source solution likely provides a more accurate picture of the relative source contributions. There is an argument for relying on Model 1 for the 125–300- μm -size fraction based on the synthetic mixture results; however, the frequency plots display larger distributions for Model 1 outcomes, while Model 2 incorporates a larger tracer selection that can account for variability and non-conservativeness more sufficiently than Model 1, thus Model 2 is the preferred option.

Table 20. Summary of model output % for each model and sediment fraction, extrapolated for total sediment size fraction based on particle size distribution

Sources	%					
	< 63 μm		125–300 μm		Total Combined	
	6-source	5-source	6-source	5-source	6-source	5-source
Hill Surface	11	8	2	8	7	8
Unconsolidated	36	41	10	12	26	29
Mudstone	11	12	7	6	9	10
Channel Bank	12	-	27	-	18	-
Mountain Range	3	4	17	32	9	15
Hill Subsurface	27	34	37	42	31	37

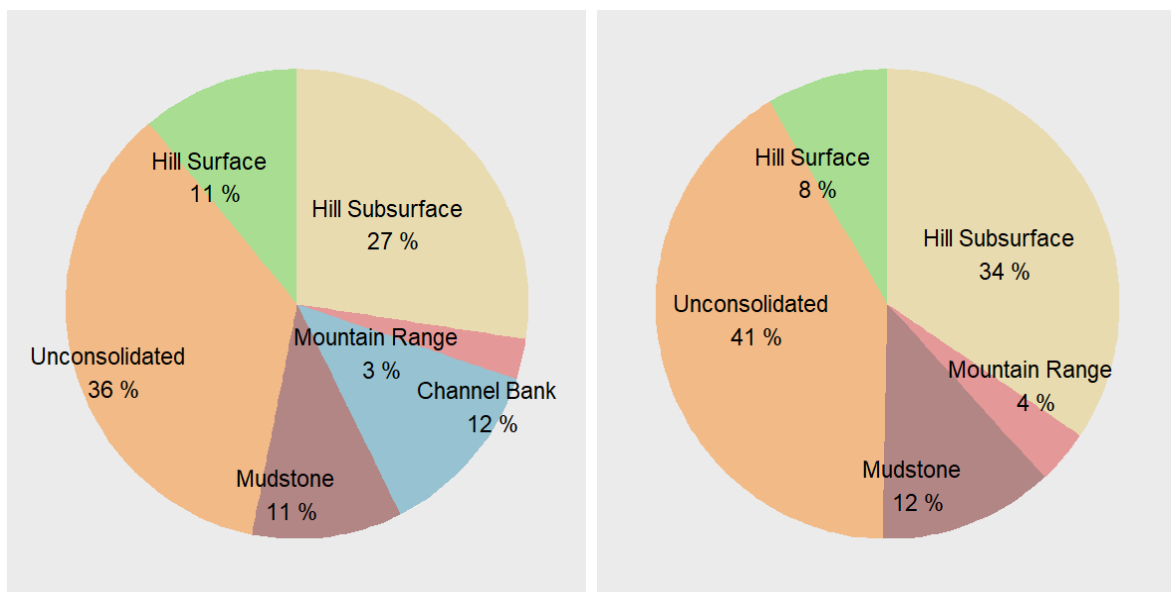


Figure 18. Pie graph of relative sediment source contributions from Model 2 for both 6-source (left) and 5-source (right) for the < 63- μm sediment fraction.

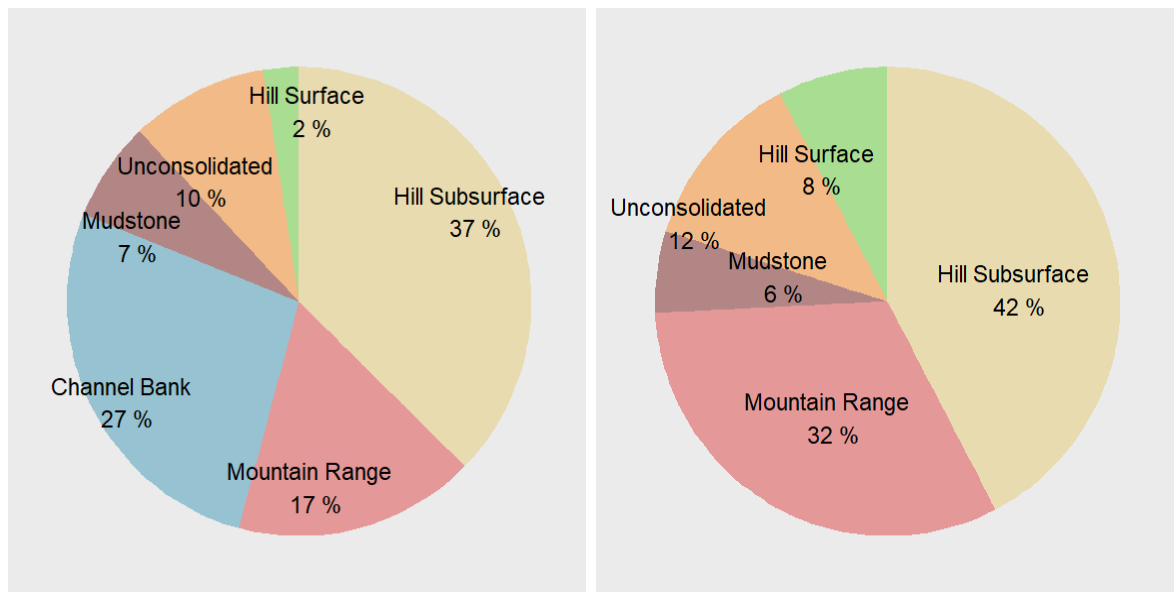


Figure 19. Pie graph of relative sediment source contributions from Model 2 for both 6-source (left) and 5-source (right) for the 125–300-µm sediment fraction.

Mean sediment source estimates based on Model 2 for < 63-µm-size fraction show Unconsolidated sediment sources provide 36–41% of the fine sediment, followed by Hill Subsurface (27–34%), Mudstone (11–12%), Hill Surface (8–11%) and Mountain Range (3–4%) (Table 20 & Fig. 18). Channel Bank sediment potentially provides up to 12% of sediment, although this is difficult to know definitively due to the previously mentioned discrimination issues associated with Channel Bank sources. It is likely that this value represents a maximum value for Channel Bank sediment source and the true value lies somewhere between 0 and 12%. The 125–300-µm-size fraction exhibits a slightly different order of sediment source contributions, with Hill Subsurface providing the greater contribution (37–42%), followed by Mountain Range (17–32%), Unconsolidated (10–12%), Mudstone (10–12%), and Hill Surface (2–8%). As with the fine sediment fraction, Channel Bank potentially provides up to 27% of the coarser material but there is potential uncertainty associated with the Channel Bank measurement. It is likely Channel Bank sediment provides a greater contribution to the coarser fraction due to the nature of the particle-size contribution, representing a preferential deposition. To assess the Channel Bank and its primary source assumptions, the un-mixing model was also run with Channel Bank as the target sediment. The source apportionment of the Channel Bank is generally consistent with the OverBank deposits, with both comprising relatively similar proportions of source sediment (Table 21). The Channel Bank sediment potentially represents a longer timescale of sediment sources within the catchment. Hill Subsurface still represents the dominant source contribution, followed by the Unconsolidated, while Hill Surface appears to be significantly higher in the coarse component. Mountain Range sediment represents a much higher proportion of the Channel Bank sediment, especially in the coarser component, while Mudstone, although displaying similar values for the total combined, is significantly higher in the fine component, and almost no contribution for the coarse component. This is consistent with the source contribution changes upon removing Channel Bank as a source.

Table 21. Summary of model output % contribution of sources to Channel Bank sediment

Sources	%		Total Combined source contribution for Channel Bank
	< 63 μm	125-300 μm	
Hill Surface	7	26	15
Unconsolidated	25	29	25
Mudstone	27	0	8
Mountain Range	2	31	23
Hill Subsurface	39	14	30

The total combined sediment contributions (Table 20) based on the two particle size distributions attribute Hill Subsurface to be the largest sediment source (31–37%), followed by Unconsolidated (26–27%), Mudstone (9–10%), Mountain Range (9–15%), and Hill Surface (7–8%) sediment, with a possible Channel Bank sediment proportion of up to 18% (Table 20, Figs 20 & 21). The highest specific sediment yields, based on total grain size distribution and both including and excluding Channel Bank sediment as a source, originate from the Unconsolidated sources ($1\,928\text{--}2\,151\text{ t km}^{-2}\text{ yr}^{-1}$), followed by Mudstone ($1\,131\text{--}1\,257\text{ t km}^{-2}\text{ yr}^{-1}$) and Hill Subsurface ($953\text{--}1,138\text{ t km}^{-2}\text{ yr}^{-1}$). These sources all reflect quite varying spatial extents: Mudstone comprises a low proportion of sediment (9–10%) from a low spatial extent (44 km^2) resulting in a high yield; Unconsolidated comprises the second largest contribution (26–29%) on the second lowest spatial extent (74 km^2); and Hill Subsurface contributes the largest proportion (31–37%) originating from 179 km^2 of the catchment. Sediment from the Mountain Range exhibits a comparatively low yield ($589\text{--}981\text{ t km}^{-2}\text{ yr}^{-1}$), although it is significantly higher with the exclusion of Channel Bank source, supporting the theory of Channel Bank sediment not being completely geochemically distinct from primary sediment sources. Hill Surface displays a very low value due to the low overall contribution and very large potential spatial area ($52\text{--}60\text{ t km}^{-2}\text{ yr}^{-1}$). Channel Bank sediment yield is estimated to be somewhere up to $99,000\text{ t yr}^{-1}$, or $220\text{ t km}^{-1}\text{ y}^{-1}$ by channel length.

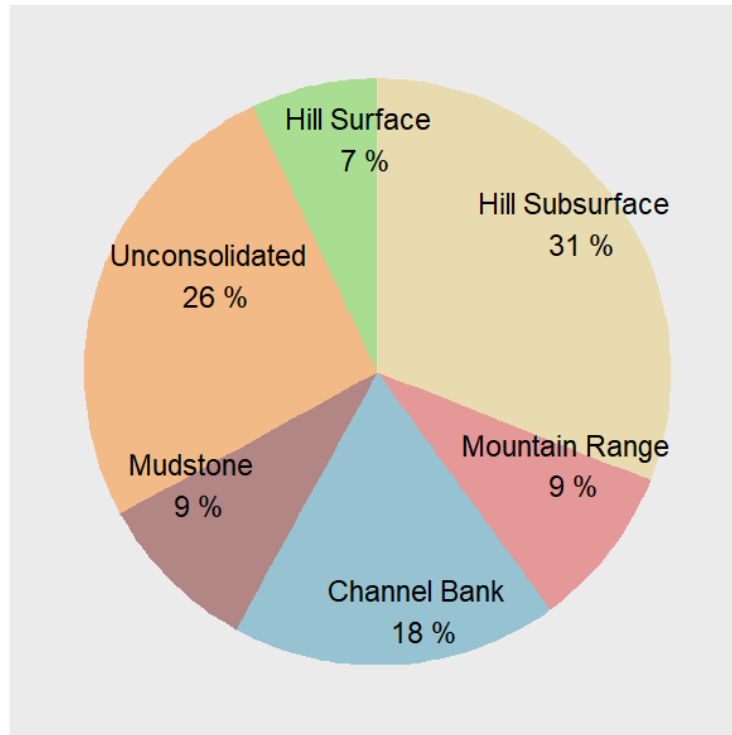


Figure 20. Pie graph of relative sediment source contributions for combined sediment size fraction estimates derived from Model 2 using 6-source.

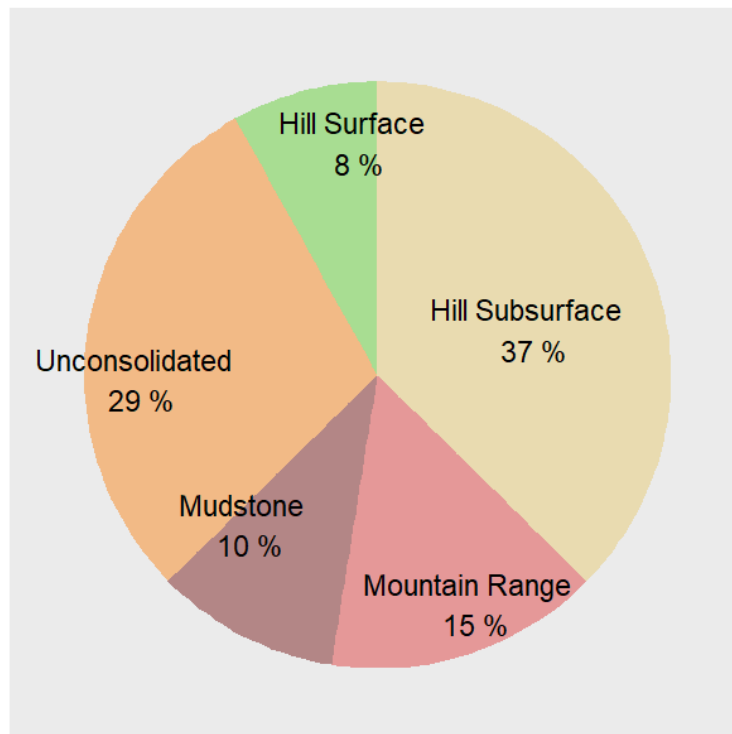


Figure 21. Pie graph of relative sediment source contributions for combined sediment size fraction estimates derived from Model 2 using 5-source.

Table 22. Sediment yield and spatial values for each of the sediment sources. The Range in value relates to the 6-source solution (including Channel Bank) and 5-source solution (excluding Channel Bank)

Sources	Spatial Area (%)	Spatial Area (km²)	Sediment contribution* (%)	Yield* (t yr⁻¹)	Specific yield* (t km⁻² yr⁻¹)
Hill Surface	82	735	7–8	38,500 – 44,000	52–60
Unconsolidated	8	74	26–29	143,000–159,500	1,928–2,151
Mudstone	5	44	9–10	49,500–55,000	1,131–1,257
Mountain Range	9	84	9–15	49,500–82,500	589–981
Hill Subsurface	20	179	31–37	170,500–203,500	953–1,138
		Length (km)			t km⁻¹ y⁻¹
Channel Bank	-	450	18	99,000	220

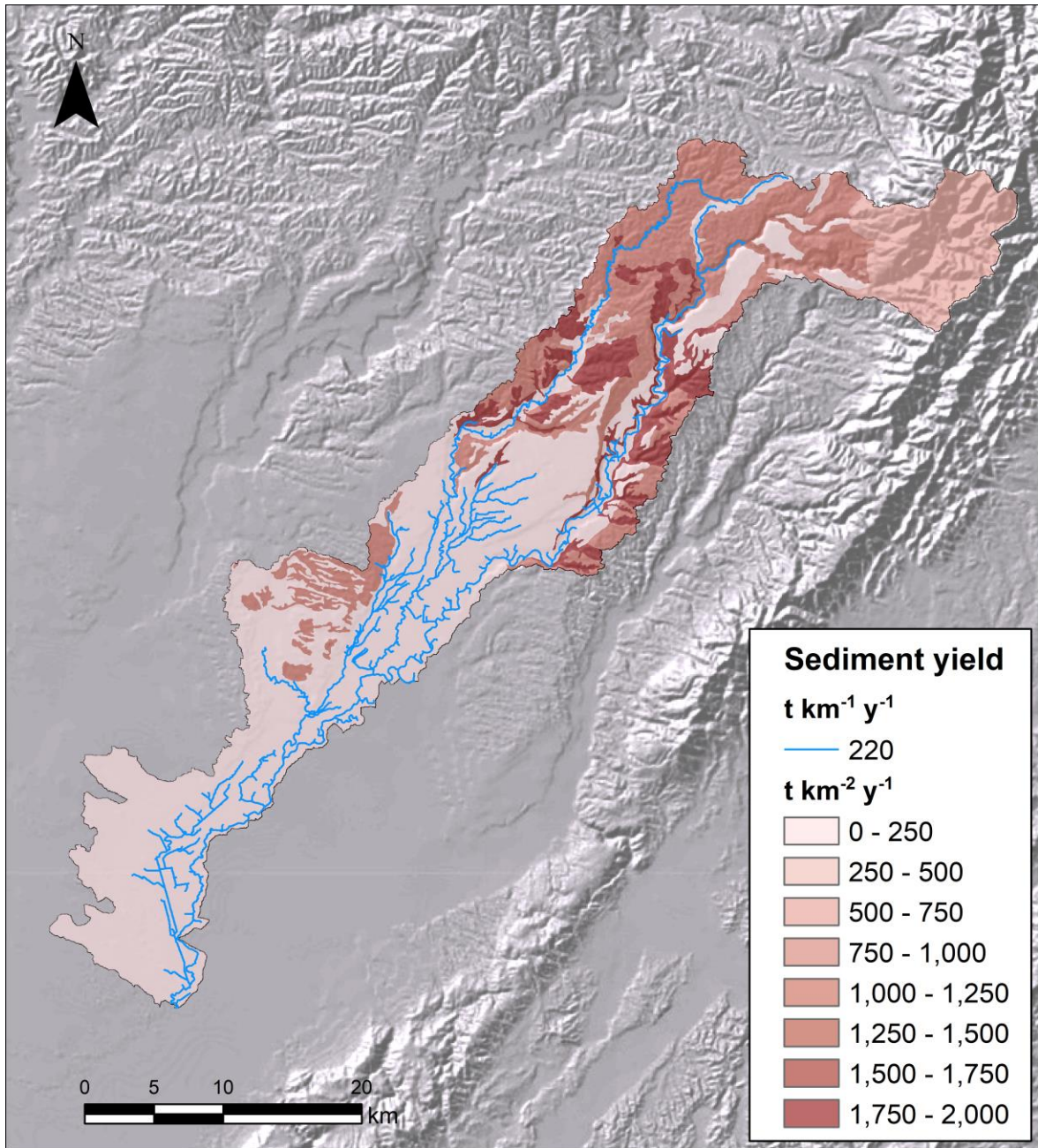


Figure 22. Total specific sediment yield derived from sediment fingerprinting proportions distributed across spatial extent of source material based on Model 2 6-source solution.

6 Conclusion & Recommendations

The dominant sediment source for the < 63- μm -size fraction shows Unconsolidated sediment sources (36–41%) and Hill Subsurface (27–34%) are the dominant sources, followed by Mudstone (11–12%), Hill Surface (8–11%), and Mountain Range (3–4%), with Channel Bank contributing up to 12%. The dominant sediment source for the 125–300- μm -size fraction shows Hill Subsurface (37–42%) and Mountain Range (17–32%) as the dominant sediment sources, followed by Unconsolidated (10–12%), Mudstone (10–12%), and Hill Surface (2–8%), with Channel Bank contributing up to 27% of the Overbank sediment deposits for the 125–300- μm -size fraction. These contributions are combined to provide a dominant sediment source for the total particle size distribution. This combination suggests the dominant contributions come from Hill Subsurface (31–37%) and Unconsolidated sediment sources (26–27%). The remaining contributions are comprised of Mudstone (9–10%), Mountain Range (9–15%), and Hill Surface (7–8%) sediment sources, with a possible Channel Bank sediment contribution of up to 18%.

Sediment source discrimination in the Oroua river catchment can be geochemically characterized and differentiated using a range of geochemical tracers. Tracers providing the best discrimination of sediment sources vary between the two size fractions, but source discrimination is typically achieved through a combination of tracers that capture a range of geochemical properties across sediment sources. Channel Bank sediment provides a challenge for both models to differentiate geochemically from the other sediment sources. This is shown in the DFA plots (Figs 8, 9, 10, & 11) whereby Channel Bank sources plot more centrally or overlap with other sediment sources and sinks. This is because in addition to being a contemporary sediment source, Channel Bank sediment is also a recent historical depositional feature comprising source material originating from other primary sediment sources included in the model and subsequently is not as geochemically distinct as other sediment sources. This is supported by running the model with Channel Bank as the targeted sediment sink, which identified that source proportions to Channel Bank material are relatively consistent with Over Bank deposits, although it should be acknowledged that Mountain Range contributes a significantly larger component. This issue has been identified in previous sediment fingerprinting research: Vale et al. (2016a), for instance, found this challenge within the wider Manawatu river catchment and sediment fingerprinting research has not discovered a definitive solution to address this issue.

Testing two different sets of tracers from each model showed that the selection of tracers used in sediment un-mixing influences the accuracy of source apportionment results when compared with synthetic mixture combinations. Moreover, un-mixing performance differed between the < 63- and 125–300- μm -size fractions. The < 63- μm -size fraction deviation was generally < 5% from the synthetic percentage for both tracer sets and each sediment source, with the exception of Channel Bank, which deviated between 5 and 13%. Removing Channel Bank as a source improved the synthetic mixture testing performance for both models in the < 63- μm -size fraction. The deviations for the 125–300- μm -size fraction was generally between 5 and 7%, while removal of the Channel Bank did not improve the accuracy of un-mixing compared with the synthetic mixtures in this coarser fraction.

Sediment originating from Mountain Range and Mudstone sources accounts for 18–25% of the Over Bank deposition, and represents mostly natural erosion and the highest specific sediment yields. Mountain Range sediment originates from the Ruahine Range under native vegetation, while Mudstone sources primarily occur from the erosion of cliffs and the incision of mudstone in the upper Oroua catchment. The main sediment sources related to land management areas are Hill Subsurface and Hill Surface, which collectively account for 38–45% of the total sediment source contribution. These areas are predominantly associated with steep hill country under agricultural production. Continuation of management initiatives to reduce erosion on this landscape is likely to achieve further reduction in sediment delivery to the lower Oroua over-bank deposits. Unconsolidated sediment sources account for 26–29% of total fine sediment source that represent gully erosion sources but also deliver sediment through a range of erosion processes, with Unconsolidated material found throughout the mid to upper Oroua catchment. It is evident that while unconsolidated sediment sources are significant in the catchment they are not the exclusive source of sediment.

The specific sediment yield includes lower and upper estimates based on the inclusion and exclusion of Channel Bank from the calculation. The highest specific sediment yield source originates from Unconsolidated ($1,928\text{--}2,151\text{ t km}^{-2}\text{ yr}^{-1}$) followed by Mudstone ($1,131\text{--}1,257\text{ t km}^{-2}\text{ yr}^{-1}$), Hill Subsurface ($953\text{--}1,138\text{ t km}^{-2}\text{ yr}^{-1}$) and Mountain Range ($589\text{--}981\text{ t km}^{-2}\text{ yr}^{-1}$). Hill Surface ($52\text{--}60\text{ t km}^{-2}\text{ yr}^{-1}$) displays a low specific yield due to the large potential spatial area, and Channel Bank potentially is responsible for up to $220\text{ t km}^{-1}\text{ y}^{-1}$ by length. This emphasizes that the Unconsolidated sources of sediment provide the greatest specific sediment yield, although steep hill terrain also provides a significant total load but over a larger spatial area.

This research presents a comprehensive geochemical characterization of the sediment transported through the Oroua catchment and provides a useful reference dataset to utilize and build on in future research. This could be particularly useful for temporal analysis of storm-event source discrimination and historical investigation of sediment source changes over time to see how such sources are changing from season to season and over longer periods. This research could also be combined with other techniques and new developments within sediment fingerprinting to further improve the spatial resolution of sediment source determination.

7 Acknowledgements

We thank Horizons Regional Council for initiating this work and providing feedback and review of an earlier draft of this report.

8 References

- Belmont P, Willenbring J, Schottler S, Marquard J, Kumarasamy K, Hemmis J 2014. Toward generalizable sediment fingerprinting with tracers that are conservative and nonconservative over sediment routing timescales. *Journal of Soils and Sediments* 14(8): 1479–1492.
- Blake WH, Wallbrink PJ, Doerr SH, Shakesby RA, Humphreys GS 2006. Magnetic enhancement in wildfire-affected soil and its potential for sediment-source ascription. *Earth Surface Processes and Landforms* 31(2): 249–264.
- Blake WH, Ficken KJ, Taylor P, Russell MA, Walling DE 2012. Tracing crop-specific sediment sources in agricultural catchments. *Geomorphology* 139/140: 322–329.
- Caitcheon GG 1998. The significance of various sediment magnetic mineral fractions for tracing sediment sources in Killimicat Creek. *Catena* 32(2): 131–142.
- Collins AL, Walling DE, Leeks GJL 1998. Use of composite fingerprints to determine the provenance of the contemporary suspended sediment load transported by rivers. *Earth Surface Processes and Landforms* 23(1): 31–52.
- Collins AL, Walling DE, Webb L, King P 2010. Apportioning catchment scale sediment sources using a modified composite fingerprinting technique incorporating property weightings and prior information. *Geoderma* 155(3-4): 249–261.
- Collins AL, Zhang YS, Duethmann D, Walling DE, Black KS 2013. Using a novel tracing-tracking framework to source fine-grained sediment loss to watercourses at sub-catchment scale. *Hydrological Processes* 27(6): 959–974.
- Douglas GB, Gray CM, Hart BT, Beckett R 1995. A Strontium Isotopic Investigation of the Origin of Suspended Particulate Matter (SPM) in The Murray-Darling River System, Australia. *Geochimica et Cosmochimica Acta* 59(18): 3799–3815.
- Dymond J, Herzig A, Ausseil A-G 2014. Using SedNetNZ to assess the impact of the Sustainable Land Use Initiative in the Manawatu-Wanganui region on river sediment loads Landcare Research Contract Report prepared for Horizons Regional Council 2014/EXT/1367.
- Eberl DD 2004. Quantitative mineralogy of the Yukon River system: Changes with reach and season, and determining sediment provenance. *American Mineralogist* 89(11-12): 1784–1794.
- Evrard O, Poulénard J, Némery J, Ayrault S, Gratiot N, Duvert C, Prat C, Lefèvre I, Bonté P, Esteves M 2013. Tracing sediment sources in a tropical highland catchment of central Mexico by using conventional and alternative fingerprinting methods. *Hydrological Processes* 27(6): 911–922.
- Fox JF, Papanicolaou AN 2008. Application of the spatial distribution of nitrogen stable isotopes for sediment tracing at the watershed scale. *Journal of Hydrology* 358(1-2): 46–55.
- Gibbs MM 2008. Identifying source soils in contemporary estuarine sediments: A new compound-specific isotope method. *Estuaries and Coasts* 31(2): 344–359.

- Gingele FX, De Deckker P 2005. Clay mineral, geochemical and Sr-Nd isotopic fingerprinting of sediments in the Murray-Darling fluvial system, southeast Australia. *Australian Journal of Earth Sciences* 52(6): 965–974.
- Haddadchi A, Olley J, Laceby P 2014. Accuracy of mixing models in predicting sediment source contributions. *Science of The Total Environment* 497–498(0): 139–152.
- Hancock GJ, Revill AT 2013. Erosion source discrimination in a rural Australian catchment using compound-specific isotope analysis (CSIA). *Hydrological Processes* 27(6): 923–932.
- Hardy F, Bariteau L, Lorrain S, Theriault I, Gagnon G, Messier D, Rougerie JF 2010. Geochemical tracing and spatial evolution of the sediment bed load of the Romaine River, Quebec, Canada. *Catena* 81(1): 66–76.
- Lamba J, Karthikeyan KG, Thompson AM 2015. Apportionment of suspended sediment sources in an agricultural watershed using sediment fingerprinting. *Geoderma* 239–240(0): 25–33.
- McDonough WF, Sun Ss 1995. The composition of the Earth. *Chemical Geology* 120(3–4): 223–253.
- Olley J, Burton J, Smolders K, Pantus F, Pietsch T 2013. The application of fallout radionuclides to determine the dominant erosion process in water supply catchments of subtropical South-east Queensland, Australia. *Hydrological Processes* 27(6): 885–895.
- Porto P, Walling DE, Callegari G 2013. Using ^{137}Cs and $^{210}\text{Pb}_{\text{ex}}$ measurements to investigate the sediment budget of a small forested catchment in southern Italy. *Hydrological Processes* 27(6): 795–806.
- Pulley S, Foster I, Antunes P 2015. The uncertainties associated with sediment fingerprinting suspended and recently deposited fluvial sediment in the Nene river basin. *Geomorphology* 228(0): 303–319.
- Pulley S, Foster I, Collins AL 2017. The impact of catchment source group classification on the accuracy of sediment fingerprinting outputs. *Journal of Environmental Management* 194: 16–26.
- Smith HG, Blake WH 2014. Sediment fingerprinting in agricultural catchments: A critical re-examination of source discrimination and data corrections. *Geomorphology* 204(0): 177–191.
- Smith HG, Karam DS, Lennard AT 2018. Evaluating tracer selection for catchment sediment fingerprinting. *Journal of Soils and Sediments* (in press).
- Taylor SR, McLennan SM 1995. The geochemical evolution of the continental crust. *Reviews of Geophysics* 33(2): 241–265.
- Vale SS, Fuller IC, Procter JN, Basher LR, Smith IE 2016a. Characterization and quantification of suspended sediment sources to the Manawatu River, New Zealand. *Science of the Total Environment* 543(Pt A): 171–186.
- Vale SS, Fuller IC, Procter JN, Basher LR, Smith IE 2016b. Application of a confluence-based sediment-fingerprinting approach to a dynamic sedimentary catchment, New Zealand. *Hydrological Processes* 30: 812–829.

- Wilkinson SN, Hancock GJ, Bartley R, Hawdon AA, Keen RJ 2013. Using sediment tracing to assess processes and spatial patterns of erosion in grazed rangelands, Burdekin River basin, Australia. *Agriculture, Ecosystems & Environment* 180(0): 90–102.
- Zhang YS, Collins AL, Horowitz AJ 2012. A preliminary assessment of the spatial sources of contemporary suspended sediment in the Ohio River basin, United States, using water quality data from the NASQAN programme in a source tracing procedure. *Hydrological Processes* 26(3): 326–334.

Appendix 1: Geochemical range plot for size fraction: < 63 μm

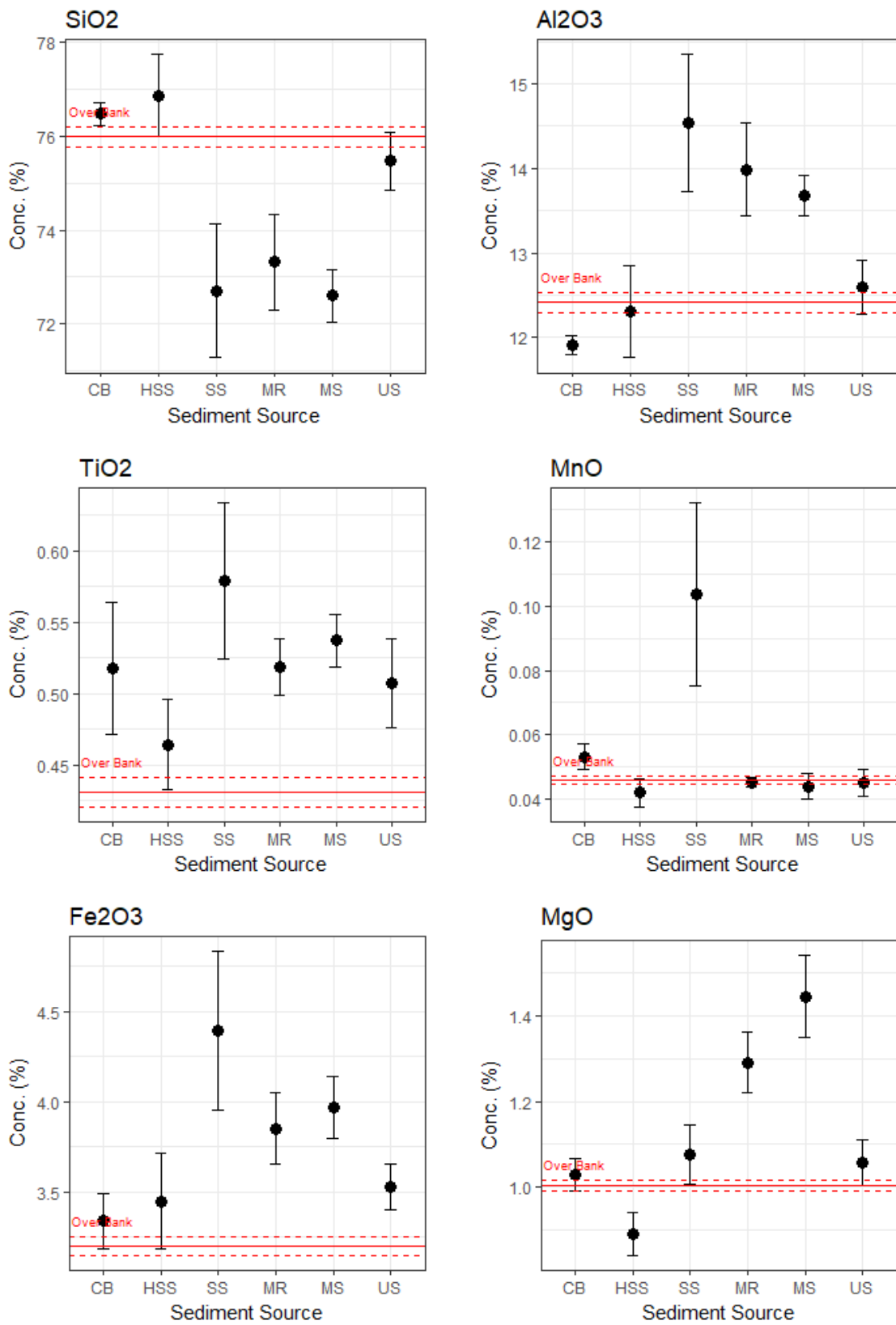


Figure 23. Geochemical plots of mean, minimum and maximum values for each sediment source group by individual tracer with Over Bank deposits overlaid in red for <63- μm -size fraction.

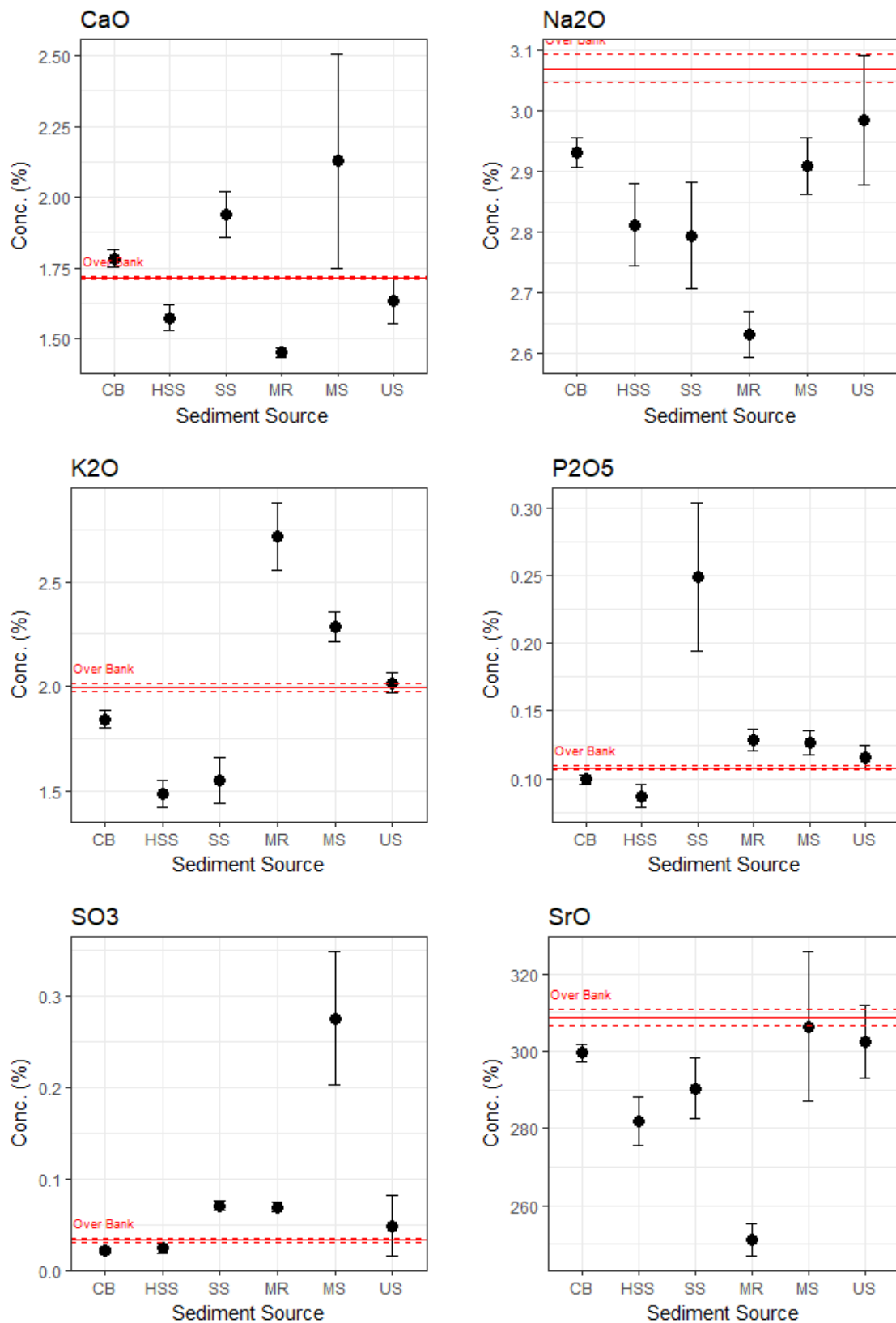


Figure 24. Geochemical plots of mean, minimum and maximum values for each sediment source group by individual tracer with Over Bank deposits overlaid in red for <63- μ m-size fraction.

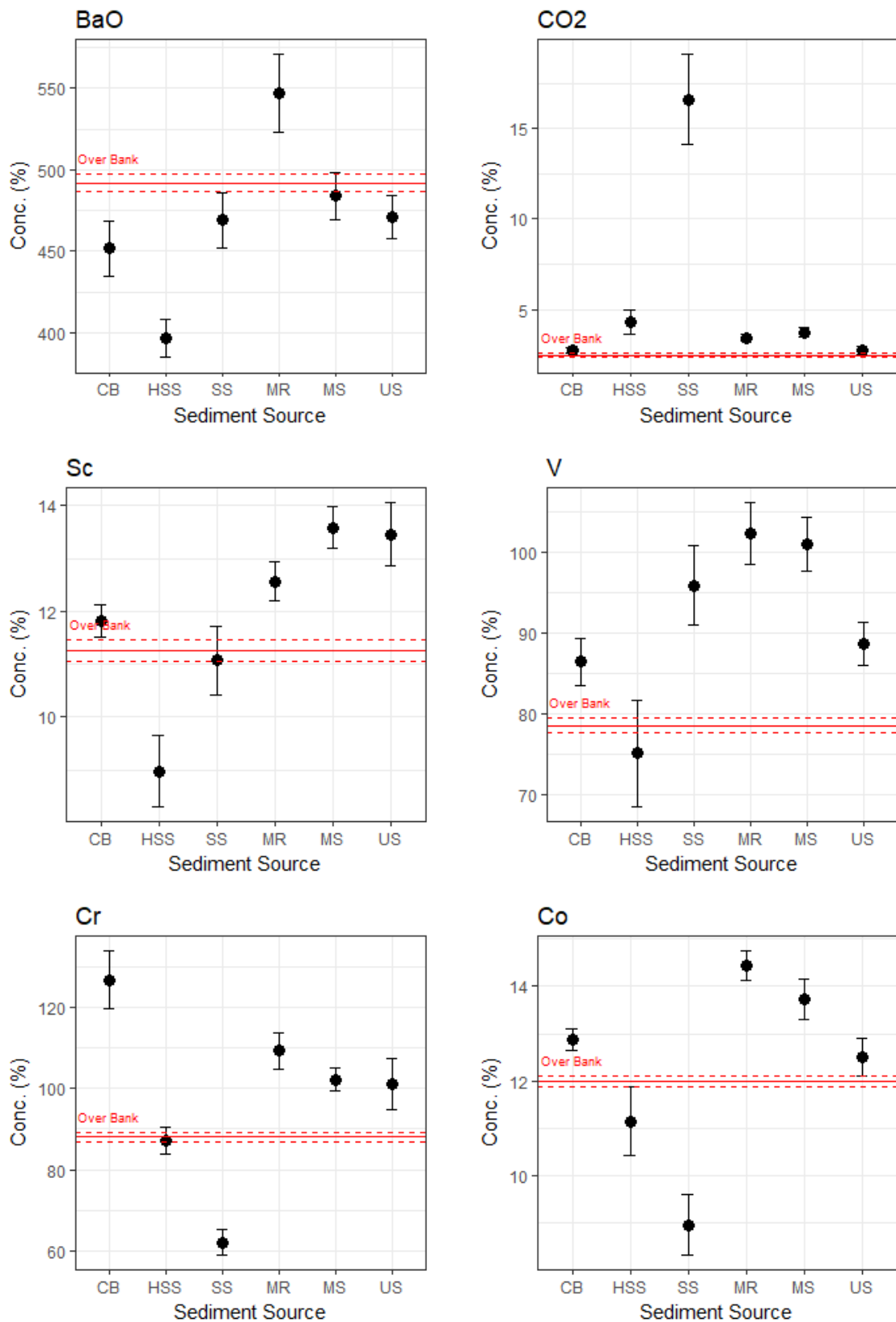


Figure 25. Geochemical plots of mean, minimum and maximum values for each sediment source group by individual tracer with Over Bank deposits overlaid in red for <63- μ m-size fraction.

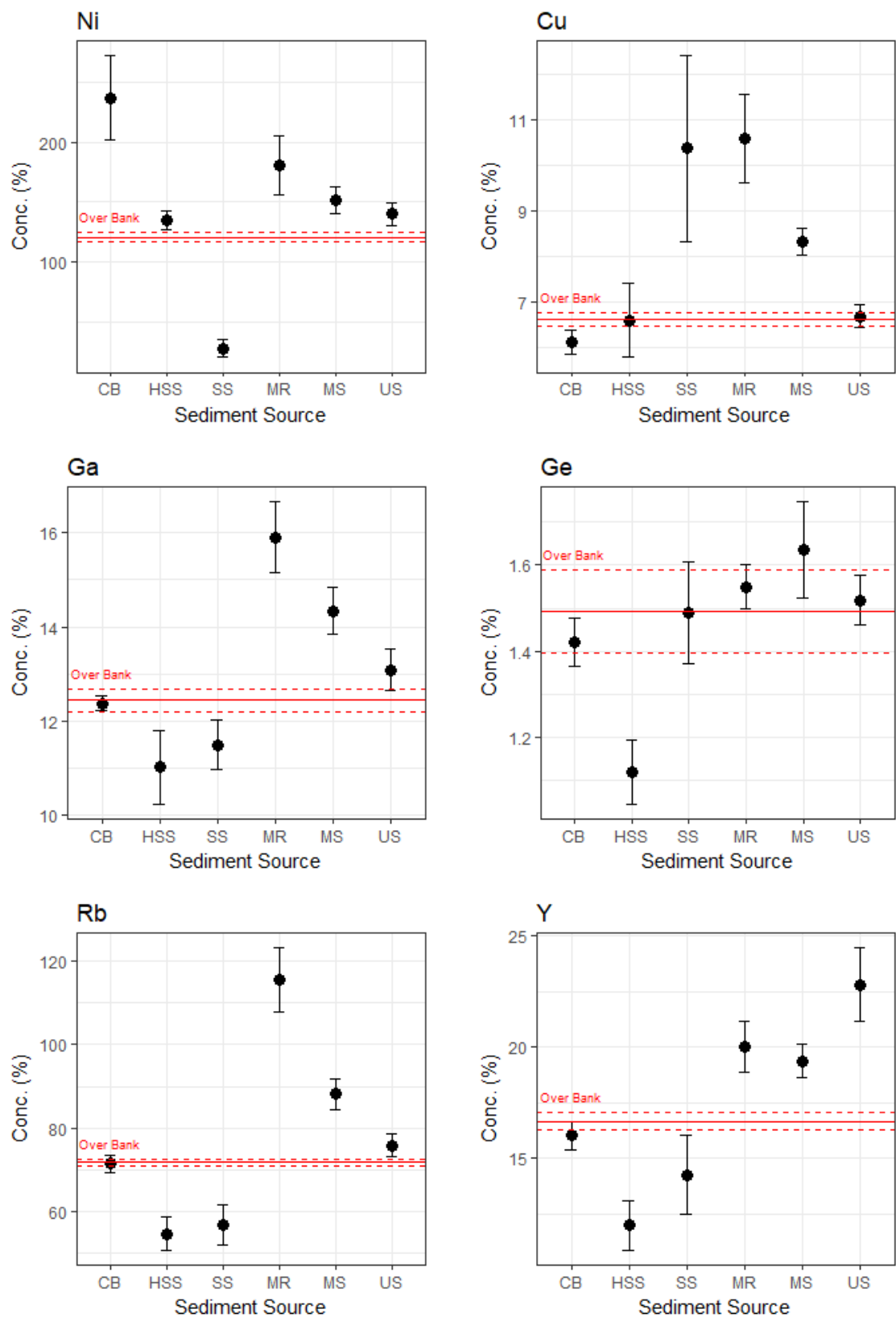


Figure 26. Geochemical plots of mean, minimum and maximum values for each sediment source group by individual tracer with Over Bank deposits overlaid in red for <63- μ m-size fraction.

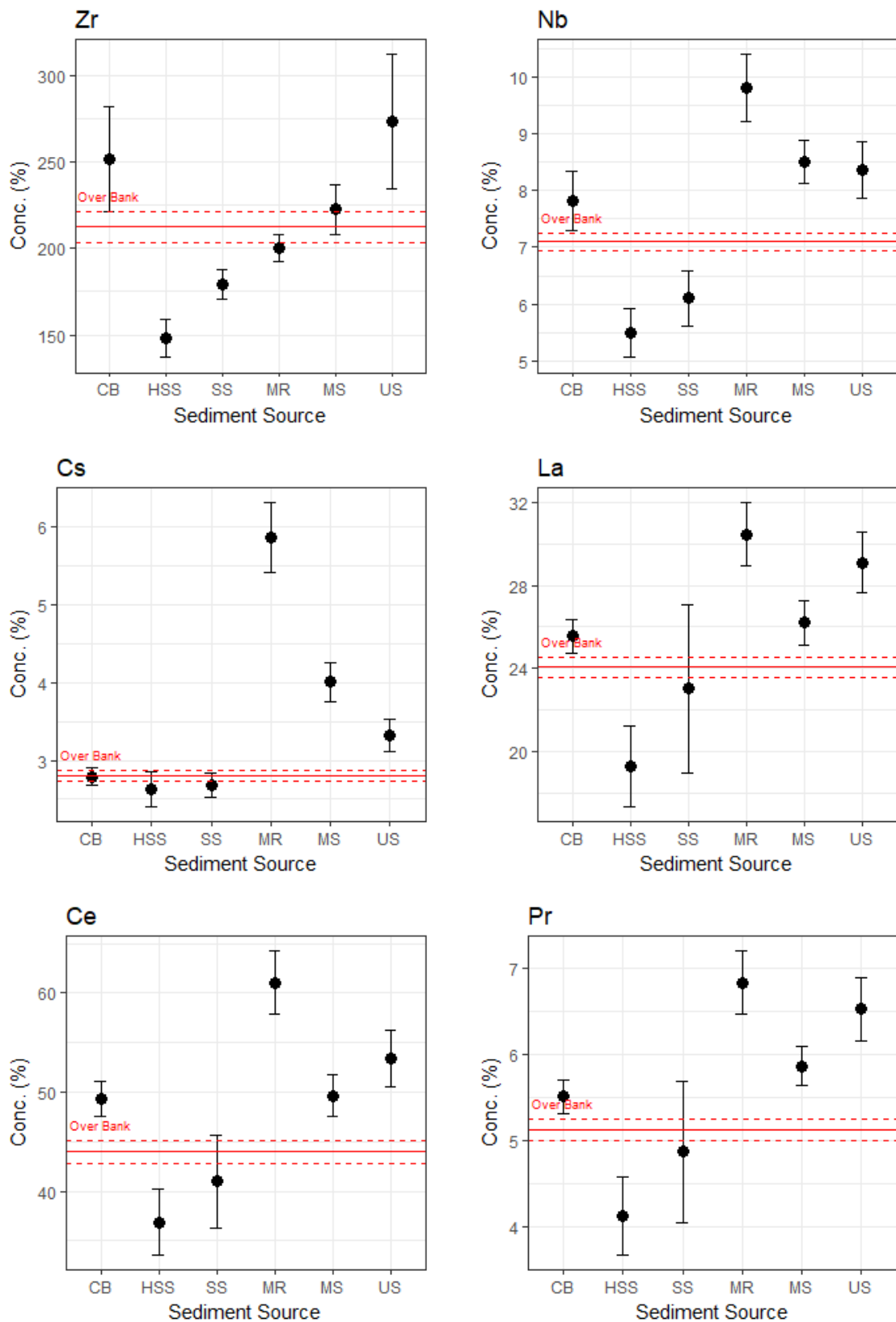


Figure 27. Geochemical plots of mean, minimum and maximum values for each sediment source group by individual tracer with Over Bank deposits overlaid in red for <63- μ m-size fraction.

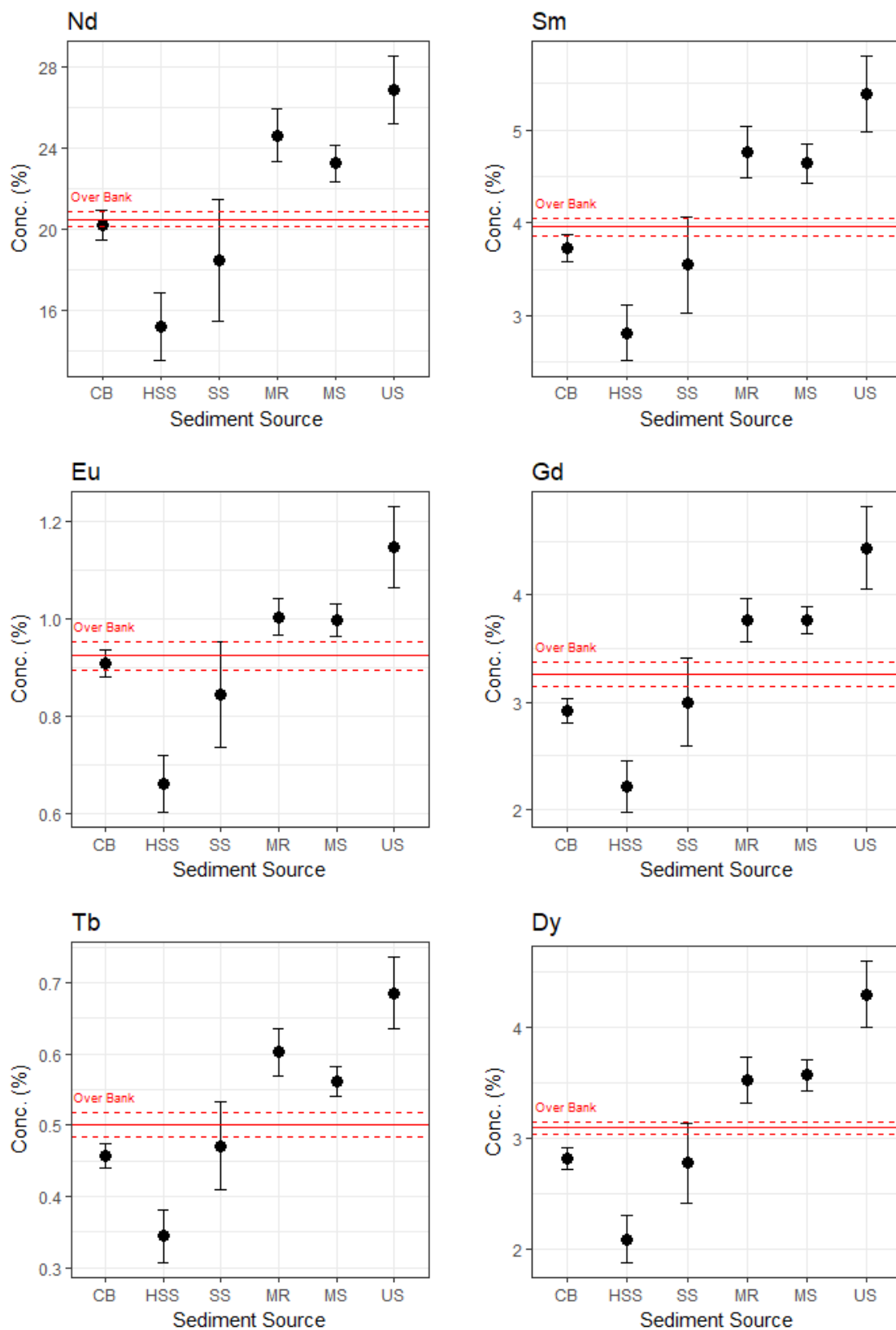


Figure 28. Geochemical plots of mean, minimum and maximum values for each sediment source group by individual tracer with Over Bank deposits overlaid in red for <63- μ m-size fraction.

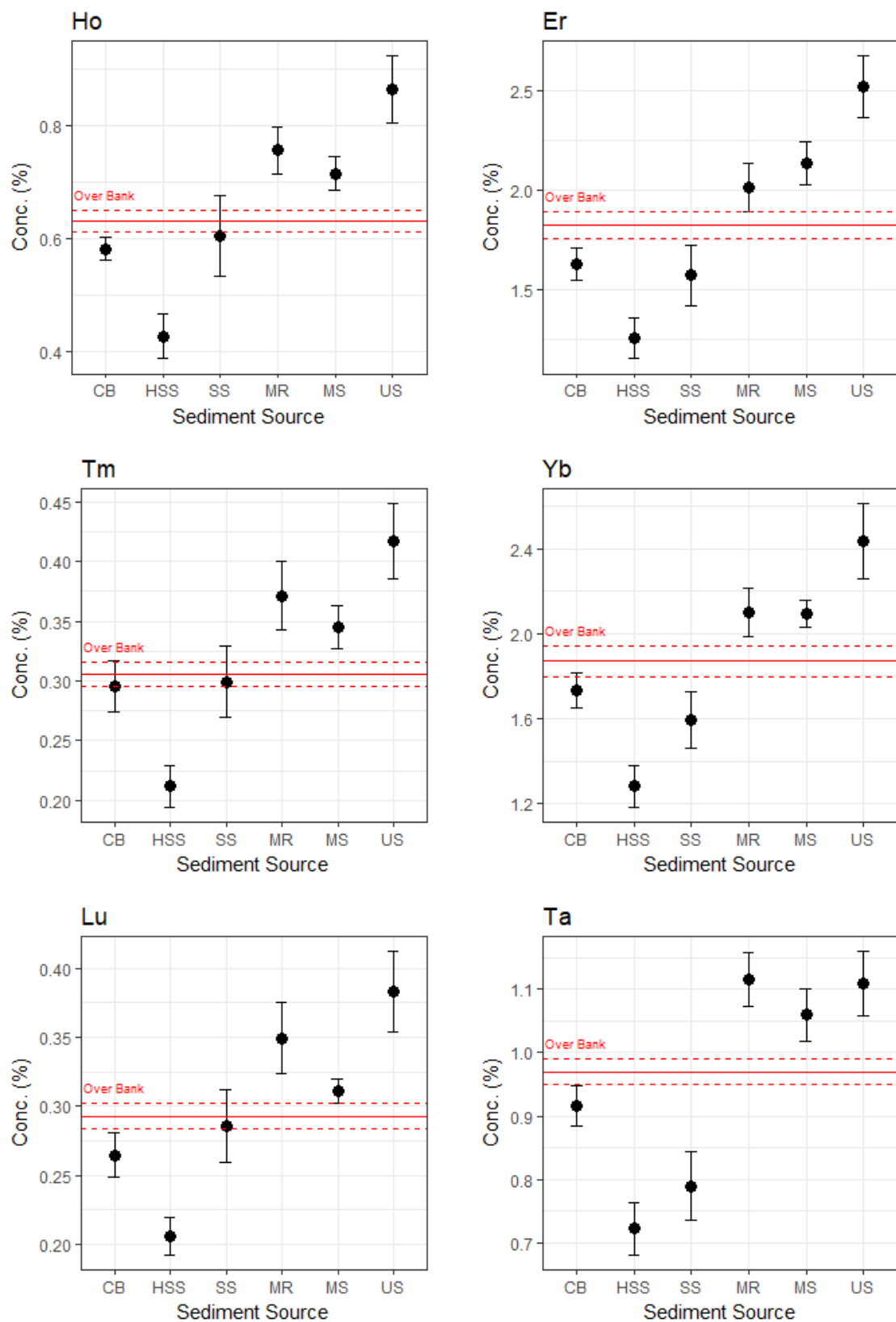


Figure 29. Geochemical plots of mean, minimum and maximum values for each sediment source group by individual tracer with Over Bank deposits overlaid in red for <63- μ m-size fraction.

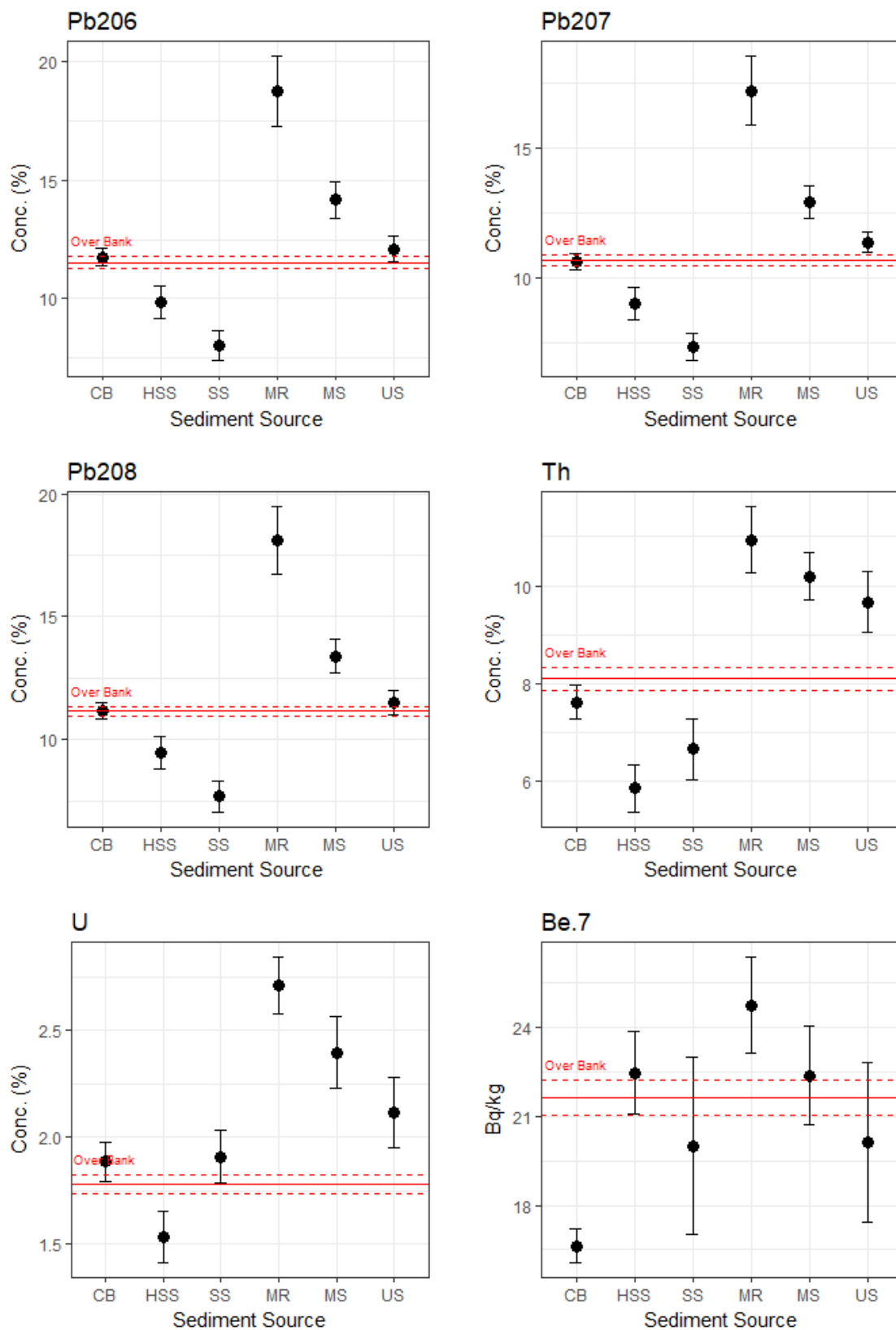


Figure 30. Geochemical plots of mean, minimum and maximum values for each sediment source group by individual tracer with Over Bank deposits overlaid in red for <63- μ m-size fraction.

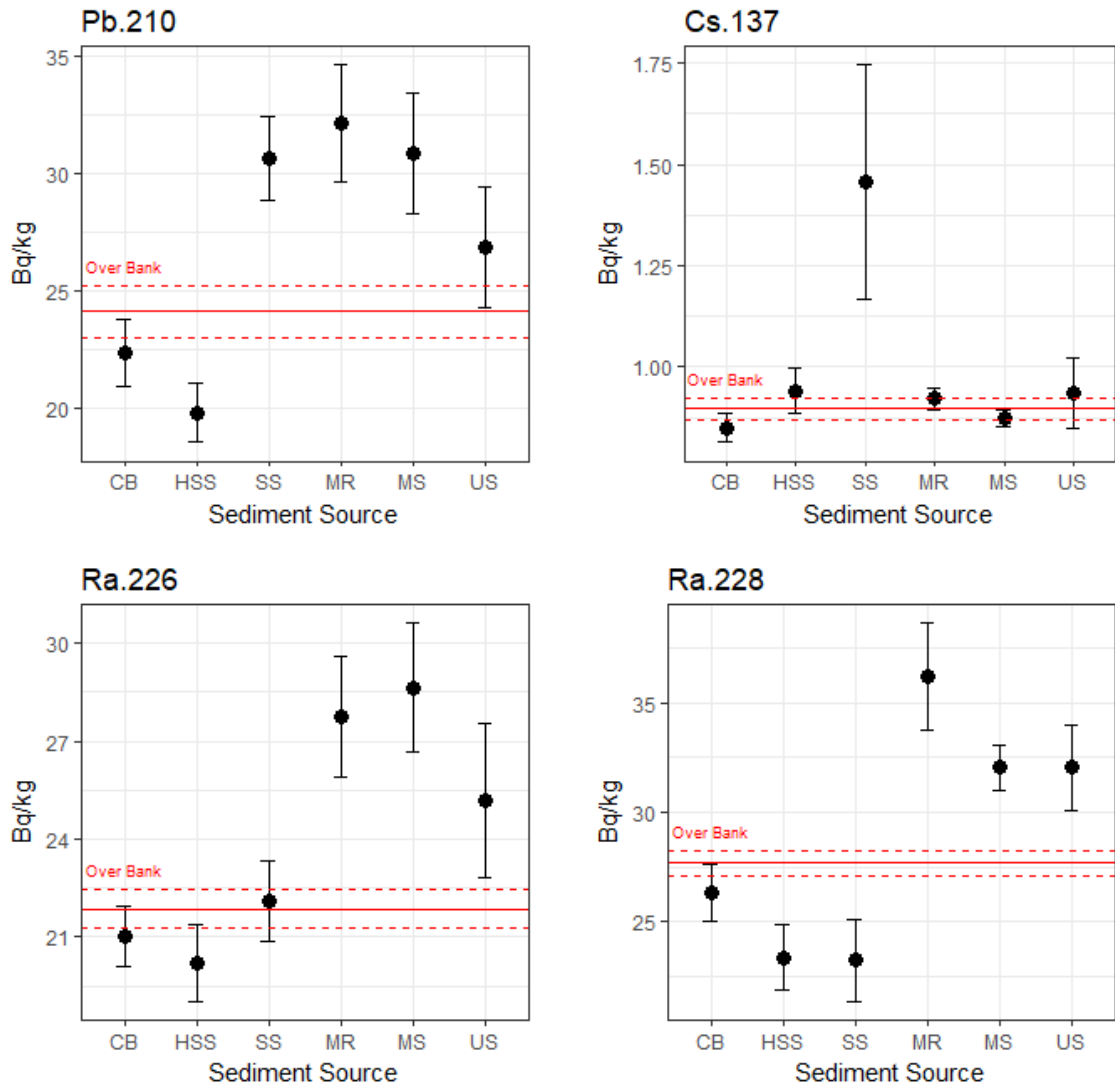


Figure 31. Geochemical plots of mean, minimum and maximum values for each sediment source group by individual tracer with Over Bank deposits overlaid in red for <math><63\text{-}\mu\text{m}</math> size fraction.

Appendix 2: Geochemical range plot for size fraction: 125–300 μm

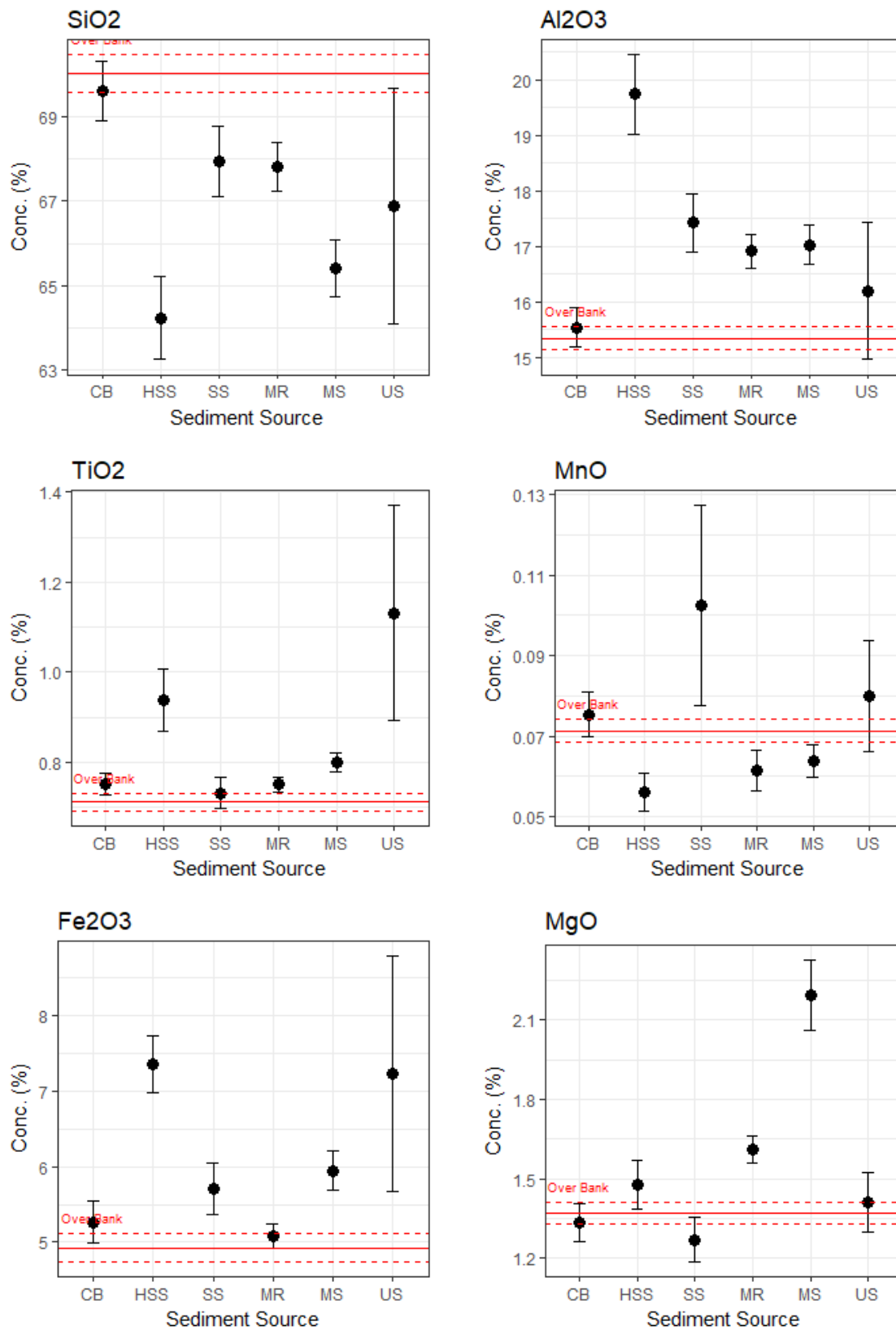


Figure 32. Geochemical plots of mean, minimum and maximum values for each sediment source group by individual tracer with Over Bank deposits overlaid in red for 125–300- μm size fraction.

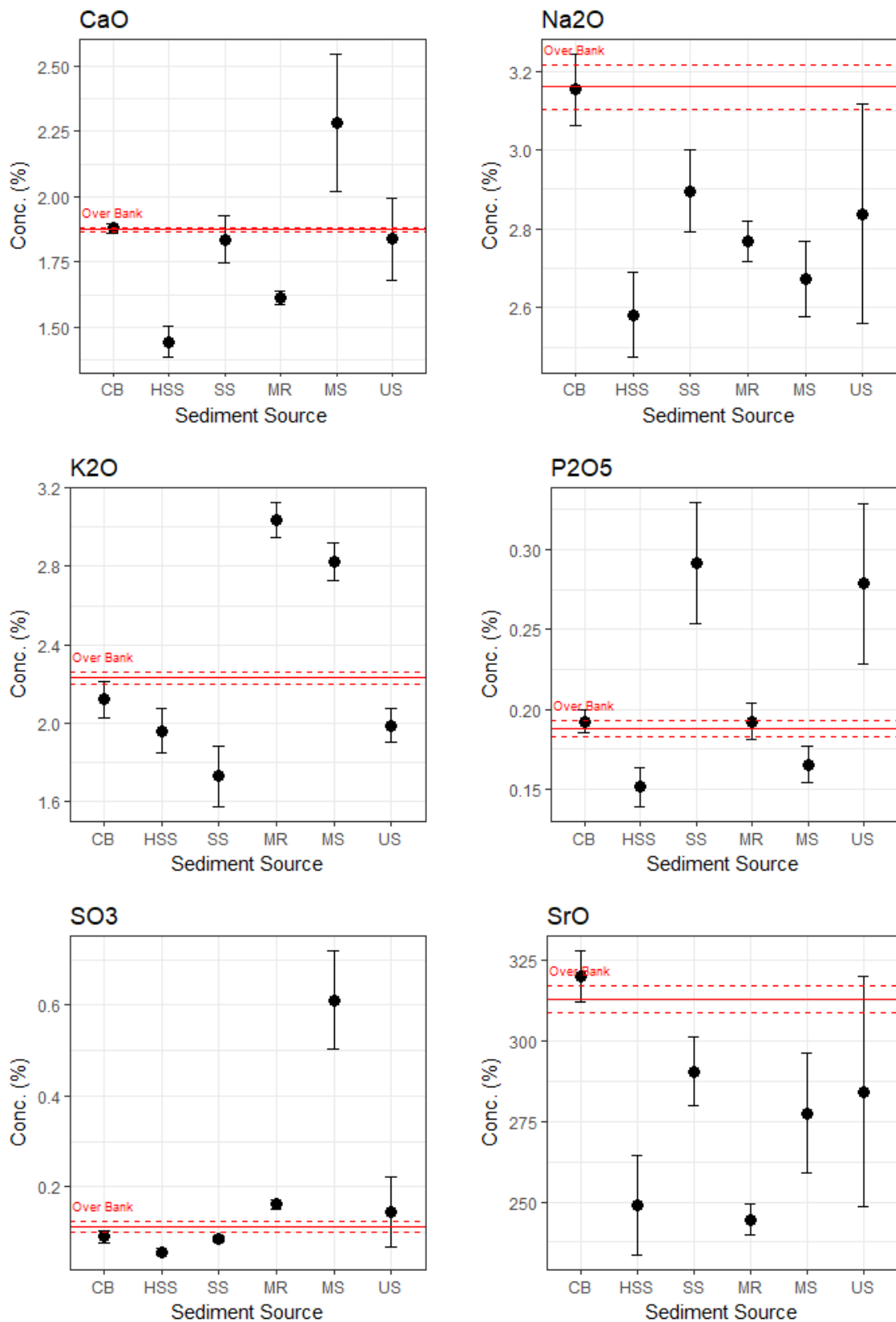


Figure 33. Geochemical plots of mean, minimum and maximum values for each sediment source group by individual tracer with Over Bank deposits overlaid in red for 125–300- μ m-size fraction.

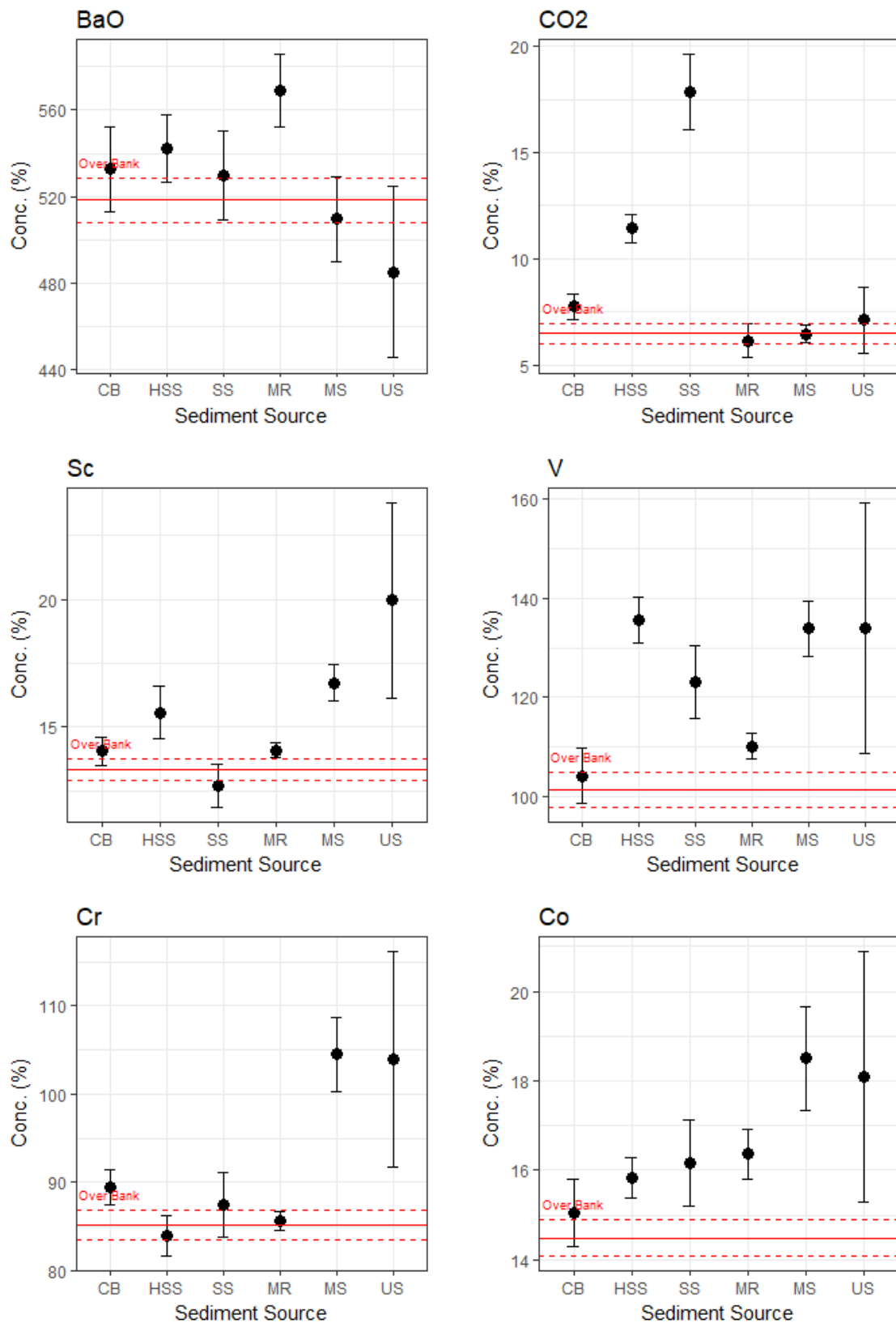


Figure 34. Geochemical plots of mean, minimum and maximum values for each sediment source group by individual tracer with Over Bank deposits overlaid in red for 125–300- μ m size fraction.

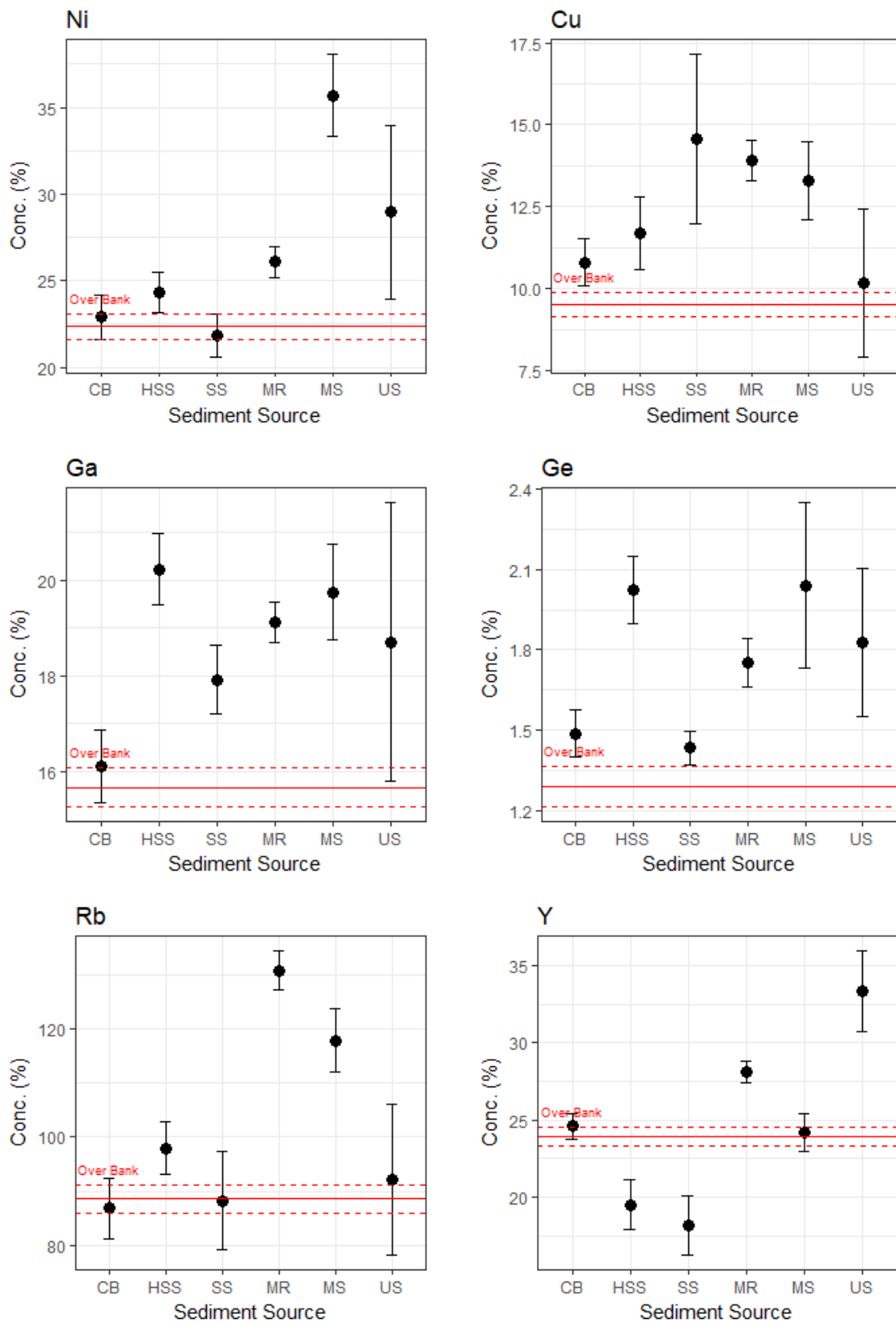


Figure 35. Geochemical plots of mean, minimum and maximum values for each sediment source group by individual tracer with Over Bank deposits overlaid in red for 125–300- μ m-size fraction.

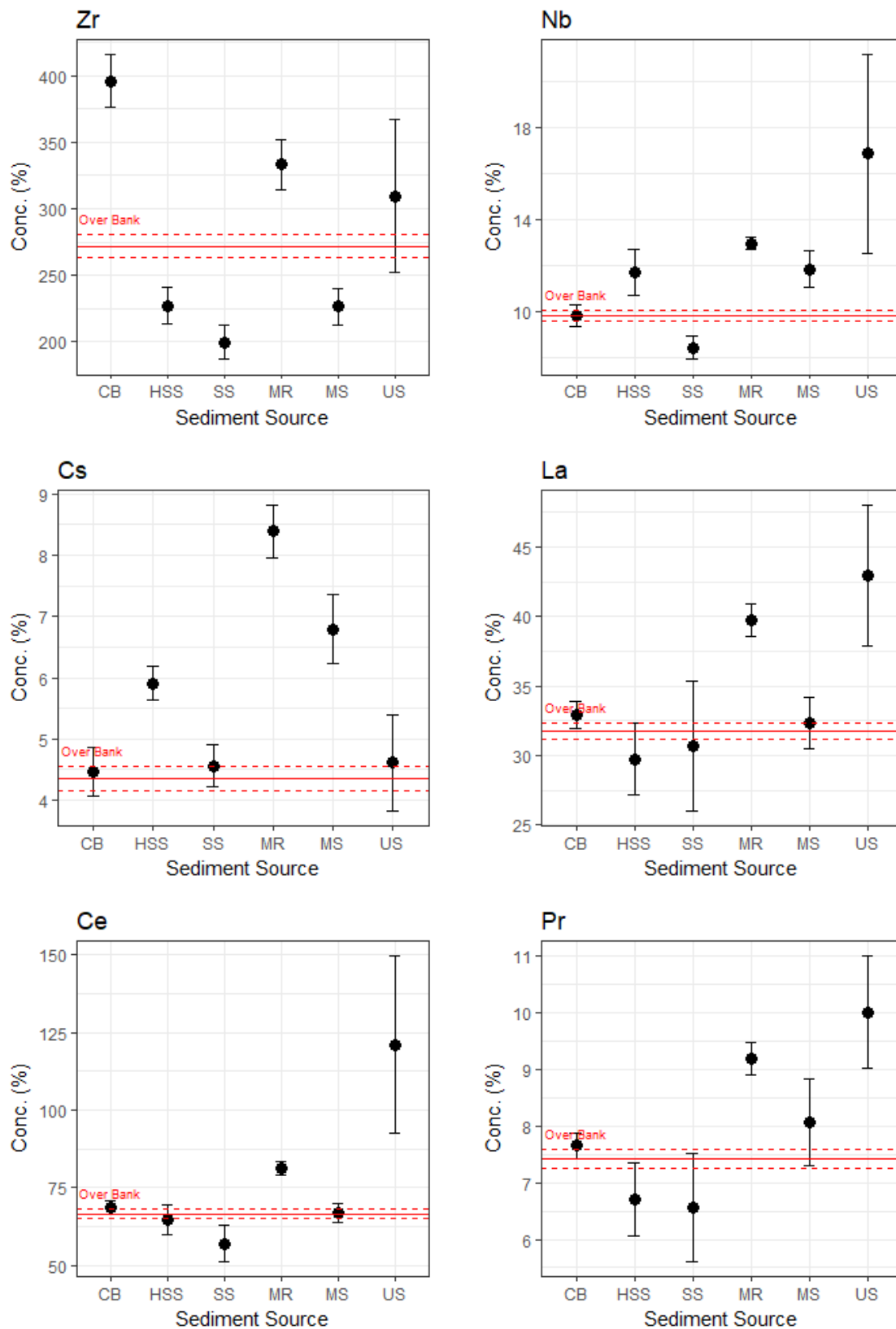


Figure 36. Geochemical plots of mean, minimum and maximum values for each sediment source group by individual tracer with Over Bank deposits overlaid in red for 125–300- μ m-size fraction.

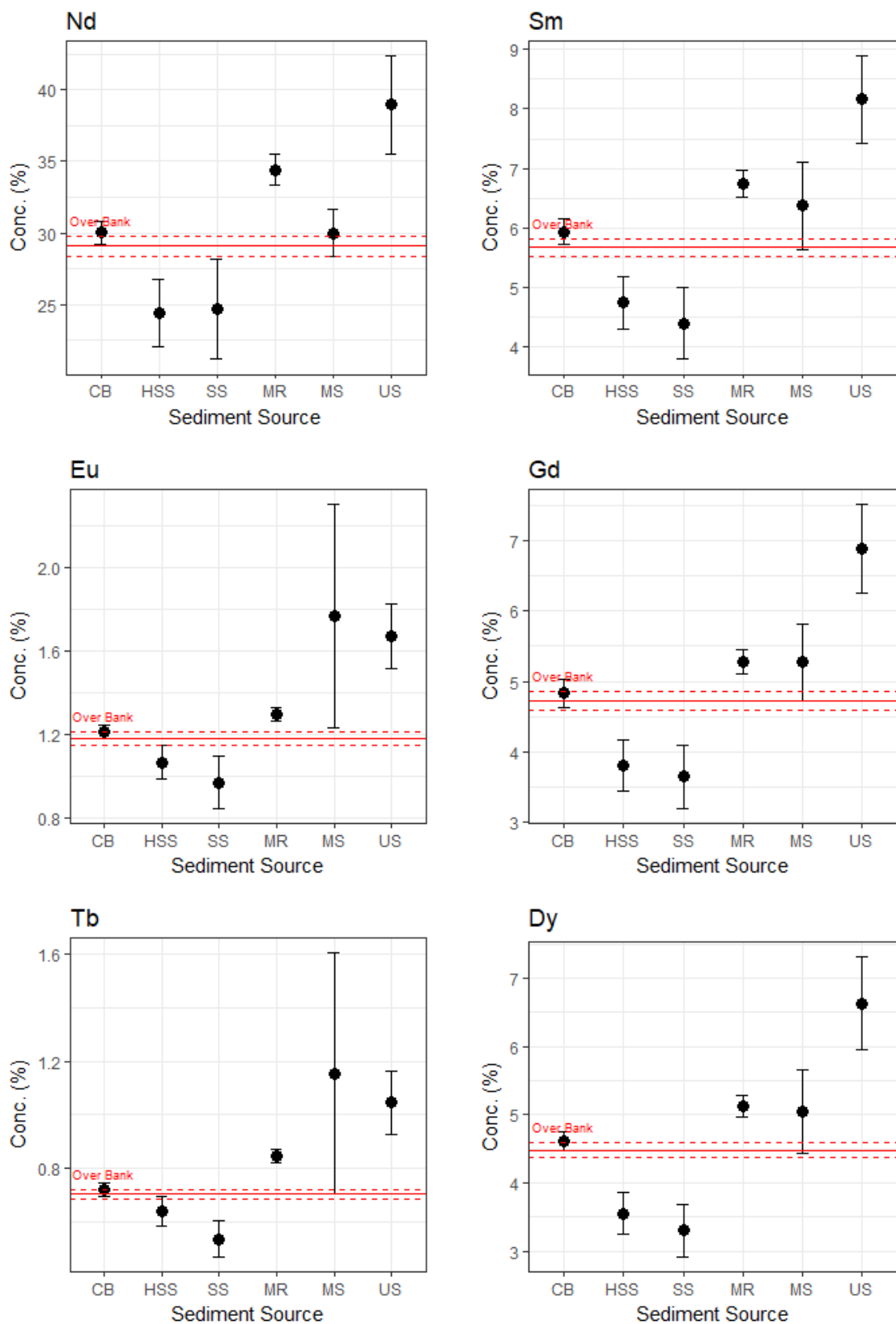


Figure 37. Geochemical plots of mean, minimum and maximum values for each sediment source group by individual tracer with Over Bank deposits overlaid in red for 125–300- μ m-size fraction.

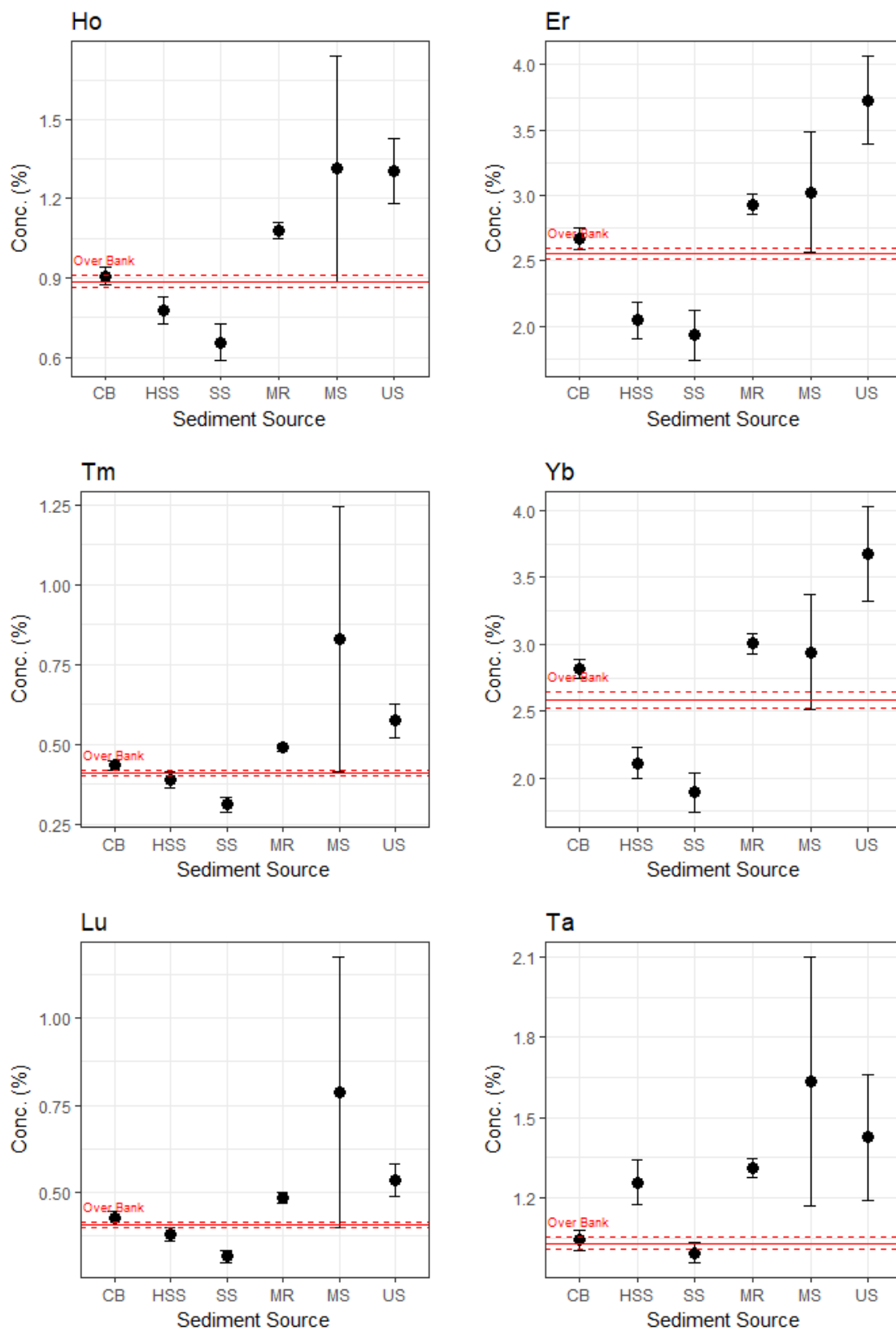


Figure 38. Geochemical plots of mean, minimum and maximum values for each sediment source group by individual tracer with Over Bank deposits overlaid in red for 125–300- μ m size fraction.

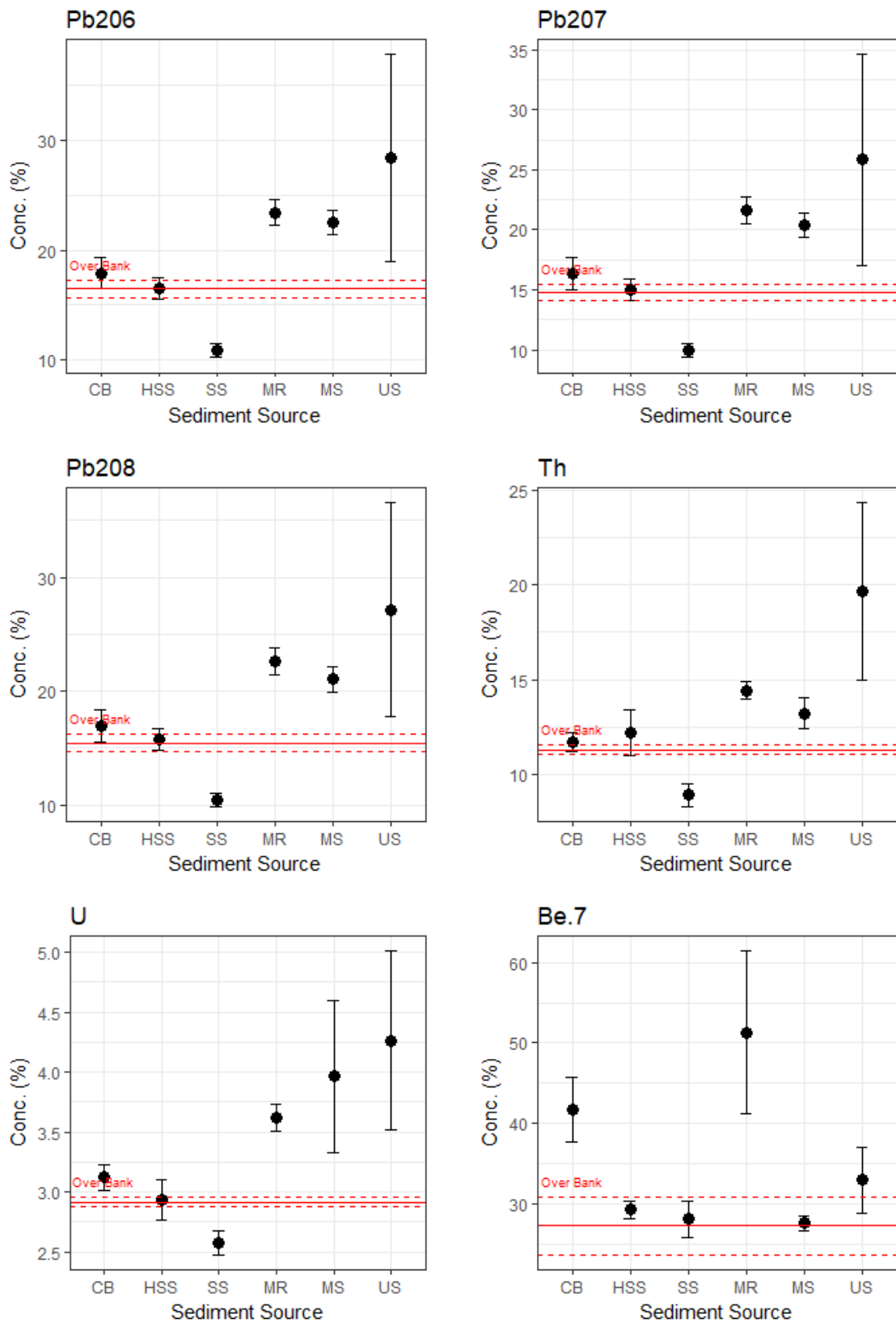


Figure 39. Geochemical plots of mean, minimum and maximum values for each sediment source group by individual tracer with Over Bank deposits overlaid in red for 125–300- μ m-size fraction.

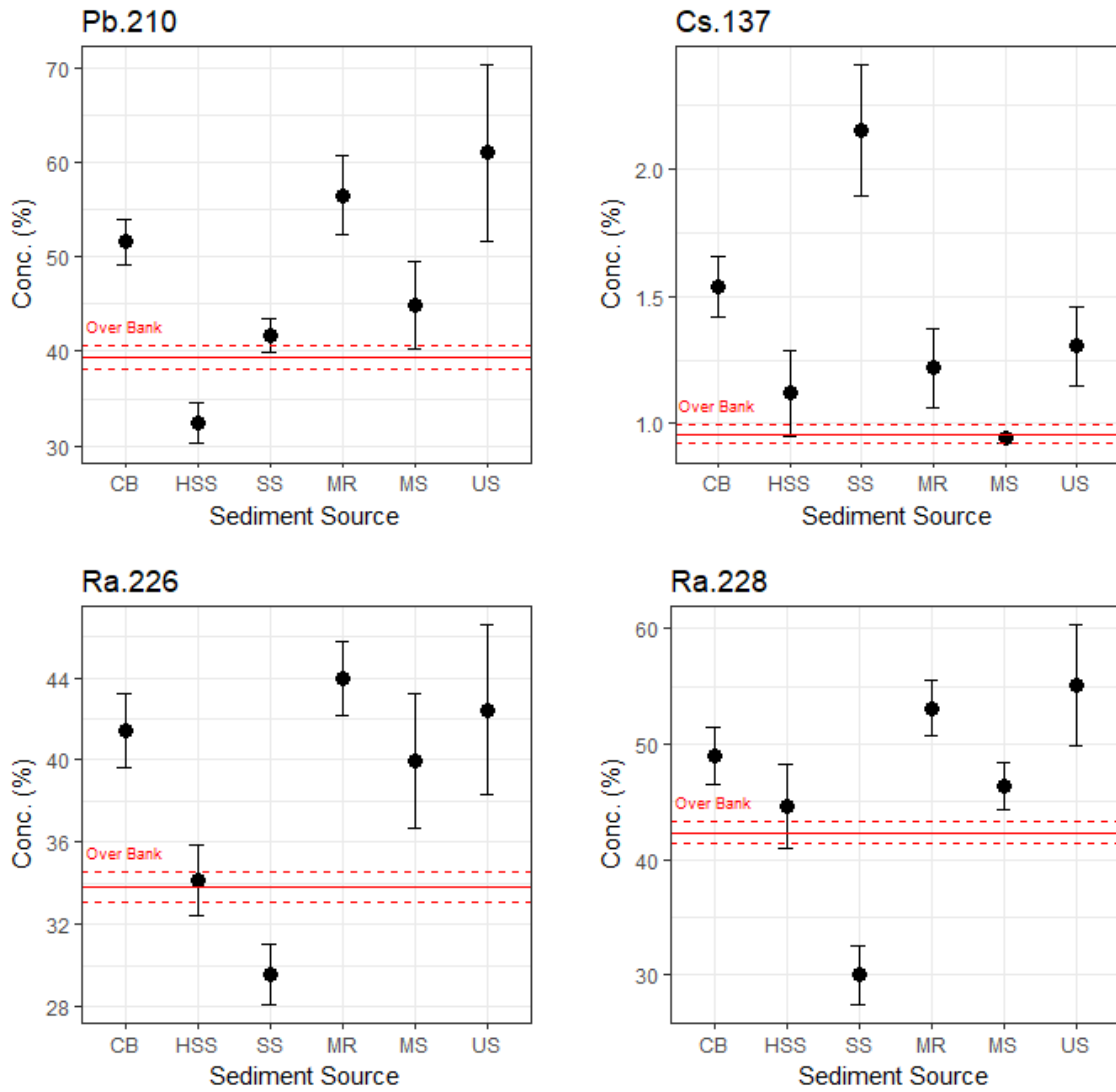


Figure 40. Geochemical plots of mean, minimum and maximum values for each sediment source group by individual tracer with Over Bank deposits overlaid in red for 125–300- μ m-size fraction.

Appendix 3: Mineralogy Summary Outputs

Table 23. Mineral assemblages from XRD analysis for Hill Surface sediment for each source sample for both particle size fractions

Hill Surface					
Sample	< 63 µm size		125–300 µm size		
	Compound Name	Chem. Formula	Sample	Compound Name	Chem. Formula
1	Silicon Oxide	SiO ₂	70	Silicon Oxide	SiO ₂
	Sodium Aluminium Silicate	NaAlSi ₃ O ₈		Sodium Aluminium Silicate	NaAlSi ₃ O ₈
	Potassium Aluminium Silicate Hydroxide	KAl ₂ (Si, Al) ₄ O ₁₀ (OH) ₂			
2	Silicon Oxide	SiO ₂	71	Silicon Oxide	SiO ₂
	Sodium Aluminium Silicate	NaAlSi ₃ O ₈		Sodium Aluminium Silicate	NaAlSi ₃ O ₈
3	Silicon Oxide	SiO ₂	72	Silicon Oxide	SiO ₂
	Sodium Calcium Aluminium Silicon Oxide	Na _{0.98} Ca _{0.02} Al _{1.02} Si _{2.98} O ₈		Sodium Aluminium Silicate	NaAlSi ₃ O ₈
4	Silicon Oxide	SiO ₂	73	Silicon Oxide	SiO ₂
	Sodium Aluminium Silicate	NaAlSi ₃ O ₈		Sodium Aluminium Silicate	NaAlSi ₃ O ₈
5	Silicon Oxide	SiO ₂	74	Silicon Oxide	SiO ₂
	Sodium Calcium Aluminium Silicon Oxide	Na _{0.98} Ca _{0.02} Al _{1.02} Si _{2.98} O ₈			
6	Silicon Oxide	SiO ₂	75	Silicon Oxide	SiO ₂
	Sodium Calcium Aluminium Silicon Oxide	Na _{0.98} Ca _{0.02} Al _{1.02} Si _{2.98} O ₈		Sodium Aluminium Silicate	NaAlSi ₃ O ₈
7	Silicon Oxide	SiO ₂	76	Silicon Oxide	SiO ₂
	Sodium Aluminium Silicate	NaAlSi ₃ O ₈		Sodium Aluminium Silicate	NaAlSi ₃ O ₈
8	Silicon Oxide	SiO ₂	77	Silicon Oxide	SiO ₂
	Sodium Aluminium Silicate	NaAlSi ₃ O ₈		Sodium Aluminium Silicate	NaAlSi ₃ O ₈

Table 24. Mineral assemblages from XRD analysis for Channel sediment for each source sample for both particle size fractions

Channel					
< 63 µm size			125–300 µm size		
Sample	Compound Name	Chem. Formula	Sample	Compound Name	Chem. Formula
9	Silicon Oxide	SiO ₂	78	Silicon Oxide	SiO ₂
	Sodium Aluminium Silicate	NaAlSi ₃ O ₈		Sodium Aluminium Silicate	NaAlSi ₃ O ₈
10	Silicon Oxide	SiO ₂	79	Silicon Oxide	SiO ₂
	Sodium Aluminium Silicate	NaAlSi ₃ O ₈		Sodium Aluminium Silicate	NaAlSi ₃ O ₈
11	Silicon Oxide	SiO ₂	80	Silicon Oxide	SiO ₂
	Sodium Aluminium Silicate	NaAlSi ₃ O ₈		Sodium Aluminium Silicate	NaAlSi ₃ O ₈
12	Silicon Oxide	SiO ₂	81	Silicon Oxide	SiO ₂
	Sodium Aluminium Silicate	NaAlSi ₃ O ₈		Sodium Aluminium Silicate	NaAlSi ₃ O ₈
13	Silicon Oxide	SiO ₂	82	Silicon Oxide	SiO ₂
	Sodium Aluminium Silicate	NaAlSi ₃ O ₈			
14	Silicon Oxide	SiO ₂	83	Silicon Oxide	SiO ₂
	Sodium Calcium Aluminium Silicon Oxide	Na _{0.98} Ca _{0.02} Al _{1.02} Si _{2.98} O ₈		Sodium Aluminium Silicate	NaAlSi ₃ O ₈
15	Silicon Oxide	SiO ₂	84	Silicon Oxide	SiO ₂
	Sodium Aluminium Silicate	NaAlSi ₃ O ₈		Sodium Aluminium Silicate	NaAlSi ₃ O ₈
16	Silicon Oxide	SiO ₂	85	Silicon Oxide	SiO ₂
	Sodium Aluminium Silicate	NaAlSi ₃ O ₈		Sodium Aluminium Silicate	NaAlSi ₃ O ₈

Table 25. Mineral assemblages from XRD analysis for Unconsolidated sediment for each source sample for both particle size fractions

Unconsolidated						
Sample	< 63 µm size		125–300 µm size			
	Compound Name	Chem. Formula	Sample	Compound Name	Chem. Formula	
17	Silicon Oxide	SiO ₂	86	Silicon Oxide	SiO ₂	
	Sodium Aluminium Silicate	NaAlSi ₃ O ₈		Sodium Aluminium Silicate	NaAlSi ₃ O ₈	
	Potassium Aluminium Silicate Hydroxide	KAl ₂ (Si, Al) ₄ O ₁₀ (OH) ₂				
18	Silicon Oxide	SiO ₂	87	Silicon Oxide	SiO ₂	
	Sodium Aluminium Silicate	NaAlSi ₃ O ₈		Sodium Aluminium Silicate	NaAlSi ₃ O ₈	
				Potassium Aluminium Silicate Hydroxide Hydrate	(K, H ₃₀) Al ₂ (Si ₃ Al) O ₁₀ (OH) ₂ · x H ₂ O	
19	Silicon Oxide	SiO ₂	88	Silicon Oxide	SiO ₂	
	Sodium Aluminium Silicate	NaAlSi ₃ O ₈		Sodium Aluminium Silicate	NaAlSi ₃ O ₈	
20	Silicon Oxide	SiO ₂	89	Silicon Oxide	SiO ₂	
	Sodium Aluminium Silicate	NaAlSi ₃ O ₈				
21	Silicon Oxide	SiO ₂	90	Silicon Oxide	SiO ₂	
	Sodium Aluminium Silicate	NaAlSi ₃ O ₈		Sodium Aluminium Silicate	NaAlSi ₃ O ₈	
22	Silicon Oxide	SiO ₂	91	Silicon Oxide	SiO ₂	
	Sodium Aluminium Silicate	NaAlSi ₃ O ₈		Sodium Aluminium Silicate	NaAlSi ₃ O ₈	
23	Silicon Oxide	SiO ₂	92	Silicon Oxide	SiO ₂	
	Sodium Aluminium Silicate	NaAlSi ₃ O ₈				
	Potassium Aluminium Silicate Hydroxide Hydrate	(K, H ₃₀) Al ₂ (Si ₃ Al) O ₁₀ (OH) ₂ · x H ₂ O		Sodium Aluminium Silicate	NaAlSi ₃ O ₈	
24	Silicon Oxide	SiO ₂	93	Silicon Oxide	SiO ₂	
	Sodium Aluminium Silicate	NaAlSi ₃ O ₈				
	Potassium Aluminium Silicate Hydroxide Hydrate	(K, H ₃₀) Al ₂ (Si ₃ Al) O ₁₀ (OH) ₂ · x H ₂ O				

Table 26. Mineral assemblages from XRD analysis for Overbank sediment for each source sample for both particle size fractions

Overbank					
< 63 µm size			125–300 µm size		
Sample	Compound Name	Chem. Formula	Sample	Compound Name	Chem. Formula
25	Silicon Oxide	SiO ₂	94	Silicon Oxide	SiO ₂
	Sodium Aluminium Silicate	NaAlSi ₃ O ₈		Sodium Aluminium Silicate	NaAlSi ₃ O ₈
26	Silicon Oxide	SiO ₂	95	Silicon Oxide	SiO ₂
	Sodium Aluminium Silicate	NaAlSi ₃ O ₈		Sodium Aluminium Silicate	NaAlSi ₃ O ₈
27	Silicon Oxide	SiO ₂	96	Silicon Oxide	SiO ₂
	Sodium Aluminium Silicate	NaAlSi ₃ O ₈		Sodium Aluminium Silicate	NaAlSi ₃ O ₈
28	Silicon Oxide	SiO ₂	97	Silicon Oxide	SiO ₂
	Sodium Aluminium Silicate	NaAlSi ₃ O ₈		Sodium Aluminium Silicate	NaAlSi ₃ O ₈
				Potassium Aluminium Silicate Hydroxide	KAl ₂ (Si, Al) ₄ O ₁₀ (OH) ₂
29	Silicon Oxide	SiO ₂	98	Silicon Oxide	SiO ₂
	Sodium Aluminium Silicate	NaAlSi ₃ O ₈		Sodium Aluminium Silicate	NaAlSi ₃ O ₈
30	Silicon Oxide	SiO ₂	99	Silicon Oxide	SiO ₂
	Sodium Aluminium Silicate	NaAlSi ₃ O ₈		Sodium Aluminium Silicate	NaAlSi ₃ O ₈
31	Silicon Oxide	SiO ₂	100	Silicon Oxide	SiO ₂
	Sodium Aluminium Silicate	NaAlSi ₃ O ₈		Sodium Aluminium Silicate	NaAlSi ₃ O ₈
32	Silicon Oxide	SiO ₂	101	Silicon Oxide	SiO ₂
	Sodium Aluminium Silicate	NaAlSi ₃ O ₈		Sodium Aluminium Silicate	NaAlSi ₃ O ₈

Table 27. Mineral assemblages from XRD analysis for Mudstone sediment for each source sample for both particle size fractions

Mudstone					
< 63 µm size			125–300 µm size		
Sample	Compound Name	Chem. Formula	Sample	Compound Name	Chem. Formula
33	Silicon Oxide	SiO ₂	102	Silicon Oxide	SiO ₂
	Sodium Aluminium Silicate	NaAlSi ₃ O ₈		Sodium Aluminium Silicate	NaAlSi ₃ O ₈
	Potassium Aluminium Silicate Hydroxide Hydrate	(K, H ₃ O) Al ₂ (Si ₃ Al) O ₁₀ (OH) ₂ ·x H ₂ O		Potassium Aluminium Silicate Hydroxide	KAl ₂ (Si, Al) ₄ O ₁₀ (OH) ₂
	Iron Magnesium Aluminium Silicate Hydroxide	(Mg, Fe) ₆ (Si, Al) ₄ O ₁₀ (OH) ₈			
34	Silicon Oxide	SiO ₂	103	Silicon Oxide	SiO ₂
	Sodium Aluminium Silicate	NaAlSi ₃ O ₈		Sodium Aluminium Silicate	NaAlSi ₃ O ₈
35	Silicon Oxide	SiO ₂	104	Silicon Oxide	SiO ₂
	Sodium Aluminium Silicate	NaAlSi ₃ O ₈		Sodium Aluminium Silicate	NaAlSi ₃ O ₈
				Potassium Sodium Iron Aluminium Magnesium Silicate Hydroxide	(K, Na) (Fe, Al, Mg) ₂ (Si, Al) ₄ O ₁₀ (OH) ₂
			Magnesium Iron Aluminium Silicate Hydroxide	(Mg, Fe, Al) ₆ (Si, Al) ₄ O ₁₀ (OH) ₈	
36	Silicon Oxide	SiO ₂	105	Silicon Oxide	SiO ₂
	Sodium Aluminium Silicate	NaAlSi ₃ O ₈		Sodium Aluminium Silicate	NaAlSi ₃ O ₈
37	Silicon Oxide	SiO ₂	106	Silicon Oxide	SiO ₂
	Sodium Aluminium Silicate	NaAlSi ₃ O ₈		Sodium Aluminium Silicate	NaAlSi ₃ O ₈
				Potassium Aluminium Silicate Hydroxide Hydrate	(K, H ₃ O) Al ₂ (Si ₃ Al) O ₁₀ (OH) ₂ ·x H ₂ O
			Iron Magnesium Aluminium Silicate Hydroxide	(Mg, Fe) ₆ (Si, Al) ₄ O ₁₀ (OH) ₈	

Mudstone					
< 63 µm size			125–300 µm size		
Sample	Compound Name	Chem. Formula	Sample	Compound Name	Chem. Formula
38	Silicon Oxide	SiO ₂	107	Silicon Oxide	SiO ₂
	Sodium Aluminium Silicate	NaAlSi ₃ O ₈		Potassium Aluminium Silicate Hydroxide Hydrate	(K, H ₃ O) Al ₂ (Si ₃ Al) O ₁₀ (OH) ₂ · x H ₂ O
	Potassium Aluminium Silicate Hydroxide	KAl ₂ (Si, Al) ₄ O ₁₀ (OH) ₂		Sodium Aluminium Silicate	NaAlSi ₃ O ₈
	Iron Magnesium Aluminium Silicate Hydroxide	(Mg, Fe) ₆ (Si, Al) ₄ O ₁₀ (OH) ₈		Iron Magnesium Aluminium Silicate Hydroxide	(Mg, Fe) ₆ (Si, Al) ₄ O ₁₀ (OH) ₈
39	Silicon Oxide	SiO ₂	108	Silicon Oxide	SiO ₂
	Sodium Aluminium Silicate	NaAlSi ₃ O ₈		Sodium Aluminium Silicate	NaAlSi ₃ O ₈
	Potassium Aluminium Silicate Hydroxide Hydrate	(K, H ₃ O) Al ₂ (Si ₃ Al) O ₁₀ (OH) ₂ · x H ₂ O		Potassium Aluminium Silicate Hydroxide	KAl ₂ (Si, Al) ₄ O ₁₀ (OH) ₂
				Iron Magnesium Aluminium Silicate Hydroxide	(Mg, Fe) ₆ (Si, Al) ₄ O ₁₀ (OH) ₈
40	Silicon Oxide	SiO ₂	109	Silicon Oxide	SiO ₂
	Sodium Aluminium Silicate	NaAlSi ₃ O ₈		Sodium Aluminium Silicate	NaAlSi ₃ O ₈
				Potassium Aluminium Silicate Hydroxide Hydrate	(K, H ₃ O) Al ₂ (Si ₃ Al) O ₁₀ (OH) ₂ · x H ₂ O

Table 28. Mineral assemblages from XRD analysis for Channel Bank sediment for each source sample for both particle size fractions

Channel Bank					
< 63 µm size			125–300 µm size		
Sample	Compound Name	Chem. Formula	Sample	Compound Name	Chem. Formula
41	Silicon Oxide	SiO ₂	110	Silicon Oxide	SiO ₂
	Sodium Aluminium Silicate	NaAlSi ₃ O ₈		Sodium Aluminium Silicate	NaAlSi ₃ O ₈
42	Silicon Oxide	SiO ₂	111	Silicon Oxide	SiO ₂
	Sodium Aluminium Silicate	NaAlSi ₃ O ₈		Sodium Aluminium Silicate	NaAlSi ₃ O ₈
43	Silicon Oxide	SiO ₂	112	Silicon Oxide	SiO ₂
	Sodium Aluminium Silicate	NaAlSi ₃ O ₈		Sodium Aluminium Silicate	NaAlSi ₃ O ₈
44	Silicon Oxide	SiO ₂	113	Silicon Oxide	SiO ₂
	Sodium Aluminium Silicate	NaAlSi ₃ O ₈		Sodium Aluminium Silicate	NaAlSi ₃ O ₈
45	Silicon Oxide	SiO ₂	114	Silicon Oxide	SiO ₂
	Sodium Aluminium Silicate	NaAlSi ₃ O ₈		Sodium Aluminium Silicate	NaAlSi ₃ O ₈
46	Silicon Oxide	SiO ₂	115	Silicon Oxide	SiO ₂
	Sodium Aluminium Silicate	NaAlSi ₃ O ₈		Sodium Aluminium Silicate	NaAlSi ₃ O ₈
47	Silicon Oxide	SiO ₂	116	Silicon Oxide	SiO ₂
	Sodium Aluminium Silicate	NaAlSi ₃ O ₈		Sodium Aluminium Silicate	NaAlSi ₃ O ₈
48	Silicon Oxide	SiO ₂	117	Silicon Oxide	SiO ₂
	Sodium Aluminium Silicate	NaAlSi ₃ O ₈		Sodium Aluminium Silicate	NaAlSi ₃ O ₈

Table 29. Mineral assemblages from XRD analysis for Mountain Range sediment for each source sample for both particle size fractions

Mountain Range					
< 63 µm size			125–300 µm size		
Sample	Compound Name	Chem. Formula	Sample	Compound Name	Chem. Formula
49	Silicon Oxide	SiO ₂	118	Silicon Oxide	SiO ₂
	Sodium Aluminium Silicate	NaAlSi ₃ O ₈		Sodium Aluminium Silicate	NaAlSi ₃ O ₈
50	Silicon Oxide	SiO ₂	119	Silicon Oxide	SiO ₂
	Sodium Aluminium Silicate	NaAlSi ₃ O ₈		Sodium Aluminium Silicate	NaAlSi ₃ O ₈
51	Silicon Oxide	SiO ₂	120	Silicon Oxide	SiO ₂
	Sodium Aluminium Silicate	NaAlSi ₃ O ₈		Sodium Aluminium Silicate	NaAlSi ₃ O ₈
52	Silicon Oxide	SiO ₂	121	Silicon Oxide	SiO ₂
	Sodium Aluminium Silicate	NaAlSi ₃ O ₈		Sodium Aluminium Silicate	NaAlSi ₃ O ₈
53	Silicon Oxide	SiO ₂	122	Silicon Oxide	SiO ₂
	Sodium Aluminium Silicate	NaAlSi ₃ O ₈		Sodium Aluminium Silicate	NaAlSi ₃ O ₈
54	Silicon Oxide	SiO ₂	123	Silicon Oxide	SiO ₂
	Sodium Aluminium Silicate	NaAlSi ₃ O ₈		Sodium Aluminium Silicate	NaAlSi ₃ O ₈
55	Silicon Oxide	SiO ₂	124	Silicon Oxide	SiO ₂
	Sodium Aluminium Silicate	NaAlSi ₃ O ₈		Sodium Aluminium Silicate	NaAlSi ₃ O ₈
56	Silicon Oxide	SiO ₂	125	Silicon Oxide	SiO ₂
	Sodium Aluminium Silicate	NaAlSi ₃ O ₈		Sodium Aluminium Silicate	NaAlSi ₃ O ₈

Table 30. Mineral assemblages from XRD analysis for Hill Subsurface sediment for each source sample for both particle size fractions

			Hill Subsurface		
< 63 µm size			125–300 µm size		
Sample	Compound Name	Chem. Formula	Sample	Compound Name	Chem. Formula
57	Silicon Oxide	SiO ₂	126	Silicon Oxide	SiO ₂
	Sodium Aluminium Silicate	NaAlSi ₃ O ₈		Sodium Aluminium Silicate	NaAlSi ₃ O ₈
58	Silicon Oxide	SiO ₂	127	Silicon Oxide	SiO ₂
	Sodium Aluminium Silicate	NaAlSi ₃ O ₈		Sodium Aluminium Silicate	NaAlSi ₃ O ₈
59	Silicon Oxide	SiO ₂	128	Silicon Oxide	SiO ₂
	Sodium Aluminium Silicate	NaAlSi ₃ O ₈		Sodium Aluminium Silicate	NaAlSi ₃ O ₈
60	Silicon Oxide	SiO ₂	129	Silicon Oxide	SiO ₂
	Sodium Aluminium Silicate	NaAlSi ₃ O ₈		Sodium Aluminium Silicate	NaAlSi ₃ O ₈
61	Silicon Oxide	SiO ₂	130	Silicon Oxide	SiO ₂
	Silicon Oxide	SiO ₂		Sodium Aluminium Silicate	NaAlSi ₃ O ₈
62	Silicon Oxide	SiO ₂	131	Potassium Aluminium Silicate Hydroxide	KAl ₂ (Si, Al) ₄ O ₁₀ (OH) ₂
	Sodium Aluminium Silicate	NaAlSi ₃ O ₈		Silicon Oxide	SiO ₂
63	Silicon Oxide	SiO ₂	132	Sodium Aluminium Silicate	NaAlSi ₃ O ₈
	Sodium Aluminium Silicate	NaAlSi ₃ O ₈		Sodium Aluminium Silicate	NaAlSi ₃ O ₈
64	Silicon Oxide	SiO ₂	133	Potassium Aluminium Silicate Hydroxide Hydrate	(K, H ₃₀) Al ₂ (Si ₃ Al) O ₁₀ (OH) ₂ · x H ₂ O
	Sodium Aluminium Silicate	NaAlSi ₃ O ₈		Silicon Oxide	SiO ₂
65	Silicon Oxide	SiO ₂	134	Sodium Aluminium Silicate	NaAlSi ₃ O ₈
	Sodium Aluminium Silicate	NaAlSi ₃ O ₈		Silicon Oxide	SiO ₂
				Sodium Aluminium Silicate	NaAlSi ₃ O ₈

			Hill Subsurface		
< 63 µm size			125–300 µm size		
Sample	Compound Name	Chem. Formula	Sample	Compound Name	Chem. Formula
66	Silicon Oxide	SiO ₂	135	Silicon Oxide	SiO ₂
	Sodium Aluminium Silicate	NaAlSi ₃ O ₈		Sodium Aluminium Silicate	NaAlSi ₃ O ₈
67	Silicon Oxide	SiO ₂	136	Silicon Oxide	SiO ₂
	Sodium Aluminium Silicate	NaAlSi ₃ O ₈		Sodium Aluminium Silicate	NaAlSi ₃ O ₈
68	Silicon Oxide	SiO ₂	137	Silicon Oxide	SiO ₂
	Sodium Aluminium Silicate	NaAlSi ₃ O ₈		Sodium Aluminium Silicate	NaAlSi ₃ O ₈
69	Silicon Oxide	SiO ₂	138	Silicon Oxide	SiO ₂
	Sodium Aluminium Silicate	NaAlSi ₃ O ₈		Sodium Aluminium Silicate	NaAlSi ₃ O ₈



11-15 Victoria Avenue
Private Bag 11 025
Manawatu Mail Centre
Palmerston North 4442

T 0508 800 800
F 06 952 2929
help@horizons.govt.nz
www.horizons.govt.nz